DOTTORATO DI RICERCA IN BIOINGEGNERIA
UNIVERSITÀ DEGLI STUDI DI BOLOGNA
XIX CICLO

PHD THESIS:
"NEW TECHNIQUES FOR THE PEDALLING PERFORMANCE ASSESSMENT IN CYCLING"

DANIELE BIBBO

Supervisore: Prof. Tommaso D'Alessio
Dipartimento di Elettronica Applicata
Università degli Studi di Roma Tre

Controrelatore: Prof. Angelo Cappello
Dipartimento di Elettronica
Informatica e Sistemistica
Università degli Studi di Bologna

Coordinatore: Prof. Angelo Cappello
Dipartimento di Elettronica
Informatica e Sistemistica
Università degli Studi di Bologna

Sede di ricerca: *Università degli Studi Roma TRE*

ROMA TRE
Università degli studi

“To my father, my mother and my brother.”

KEYWORDS

BIOENGINEERING
CYCLING
SPORT **S**CIENCE
PEDAL **F**ORCES **M**EASUREMENT
ELECTROMYOGRAPHY

INDEX

ACKNOWLEDGEMENTS **1**

INTRODUCTION **2**

1. THE DESIGN OF THE INSTRUMENTED PEDAL **6**

1.1 THE STATE OF THE ART 8
1.2 THE MECHANICAL DESIGN 12
1.3 STRAIN GAUGES BASED TRANSDUCERS 15
1.3.1. Theory of deformation *16*
1.3.2. Strain gauges theory *19*
1.4 THE LOAD CELL DESIGN 24
1.5 OTHER PEDAL COMPONENTS DESIGN 35
1.5.1. The stirrup design *36*
1.5.2. The spindle design *38*
1.5.3. Choice of strain gauges *39*
1.6 DESIGN OF THE ELECTRONICS FOR WHEATSTONE BRIDGES 42
1.7 PEDAL CALIBRATION 46
1.8 TEST OF FORCE MEASUREMENT WITH THE INSTRUMENTED PEDAL 53

2. COMBINING ELECTRICAL AND MECHANICAL DATA TO EVALUATE MUSCULAR ACTIVITIES DURING CYCLING **56**

2.1 MATERIALS AND METHODS 58
2.1.1. The biomechanical model *58*
2.1.1.1 The kinematic model 58
2.1.1.2 The Dynamic model 60
2.1.1.3 The muscle model 60
2.1.2. Experimental setup *61*
2.1.3. Signal Processing *62*
2.2 RESULTS AND DISCUSSION 64
2.3 CONCLUSIONS 71

3. MUSCULAR FATIGUE FROM ELECTROMYOGRAPHIC RECORDINGS: REAL-TIME MONITORING DURING EXERCISE TRAINING **72**

3.1 MATERIALS AND METHODS 74
3.2 RESULTS 77
3.3 DISCUSSION AND CONCLUSIONS 79

4. THE PEDAL FORCE MEASURE AS A MEAN TO RELIABLY ESTIMATE MAXIMAL MUSCLE POWER **80**

4.1 CONTEXT 80
4.2 MATERIALS AND METHODS 81
4.2.1. Participants *81*
4.2.2. Stereophotogrammetry *81*
4.2.3. Instrumented pedal *82*
4.2.4. Experimental procedure *82*
4.2.5. Data processing *83*
4.2.6. Data analysis and statistics *84*
4.3 EXPERIMENTAL RESULTS 86

5. PEDALLING EFFICIENCY EVALUATION USING PEDAL FORCE MEASURE **106**

5.1 CONTEXT AND IMPORTANCE OF THE STUDY 107
5.1.1. The Proposed Approaches *107*
5.2 THE PEDALLING MOVEMENT 109
5.2.1. The pedalling style *109*
5.2.2. The role of the foot *109*
5.3 THE BODY POSTURE OF THE CYCLING GESTURE: THE POSITION ON THE SADDLE 110
5.4 THE PEDALLING EFFICIENCY EVALUATION 113
5.4.1. Experimental Setup *113*

5.4.2. Instruments *114*
5.5 SIGNAL PROCESSING 115
5.5.1. The LabVIEW monitor *117*
5.6 RESULTS AND DISCUSSION 119
5.6.1. Pedal forces measures *119*
5.6.2. The efficiency index *122*
5.7 CONCLUSIONS 134

ACKNOWLEDGEMENTS

As probably it happened to many Phd students at the end of their course, one of the last night of working I asked myself how it was possible to do all this with the enthusiasm that every day I have waking up. The only answer is in the unique context I have found in my research group, the Biolab3. It is wonderful and amazing what we have built together in these years.

For this reason, I would like to thank my supervisor Prof. Tommaso D'Alessio for giving me the possibility of developing my ideas with the freedom that everybody should have in working and for his precious suggestions and guidance.

I would like to thank Dr. Claudio Gallozzi of the Sport Science Institute of the Italian Olympic committee for his collaboration in the development of this work.

I would like to thank Dr. Andrea Macaluso of the Strathclyde Institute of Pharmacy and Biological Sciences of the University of Strathclyde, Glasgow, for hosting me in the Sport Science Laboratory to develop together part of this work.

The great part of this work would not have been possible without the help and the guide of my mentors Silvia Conforto and Maurizio Schmid that guided and encouraged me since I was an engineering student.

I would like to thank Ivan Bernabucci, Michela Goffredo and Paolo Caselli, they are more than colleagues, which supported and helped me in difficulties and who shared with me many beautiful or mad moments in my life. Probably they are the best friends I have.

I would like to thank all the students that not only gave a contribution to this thesis, but also gave me great satisfactions in their professional growth during our work together.

I would also thank all the people who "lived" and still live with me in the lab in these years: Diego, Mauro, Rossana, Federica, Michela, Chiara, Anna Maria, Emanuele and Paolo C.

Last, I would like to thank my main sponsors: dear dad, thank you for giving me forces and motivations especially in the darkest moments; dear mum, thank you for your patience and for staying close to me everytime; thank you Dario.

Introduction

The analysis of sport performance is the general framework containing the research contribution offered by this work, where by “sport performance” it is meant the ensemble of the final result and the sequence of the motor actions producing the result itself. In this sense, the study deals with the biomechanical analysis of the motor actions, in terms of kinematics, kinetics and electrophysiology, and with the understanding of the motor efficiency, that is the relation between task’s execution and result.

The sequence of motor tasks characterizing the athlete's performance is strictly dependent on the practiced sport discipline. The correct execution of motor tasks needs a proper knowledge, in both conscious and proprioceptive ways, of the technique, the timing, the force to be applied and the multi-segmental coordination. In every discipline it is therefore identifiable a sport “gesture” that represents a motor signature and that the athlete continually tries to refine through the practice and the training. Practice and training reinforce the automatic procedures underlying the gesture execution by refining the intervention of the neuro-muscular control system.

Usually sport disciplines are classified on the basis of the motor gesture to be performed [1], and the most famous classification is that based on “open skill” and “closed skill” sports.

The motor gesture of an “open skill” sport discipline is composed of different and subjective motor tasks. For this reason it results very difficult to identify some parameters to analyze and quantitatively assess the performance. Most of the team sports, such as football, volley or basket, characterized by continuous interactions between the athletes belong to this category. Moreover, even sport disciplines where motor gestures are driven by the context, such as tennis, can be classified as “open skill”.

The “closed skill” sport disciplines are characterized by the repetition as accurate as possible of a well known gesture which, after a learning phase, is executed in an almost automatic way. The information provided from the environment is constant and expectable but is very important the role of the proprioceptive system which filters the information and makes the athlete know exactly and automatically how perform the motor task, that can be interpreted as an almost fixed pattern. Under this category it is possible to classify all the sports characterized by periodic movements as for example rowing, running or cycling, but also sports that need an extreme precision and accuracy in the execution of the gesture as the ones requiring a bow.

Since in these sport disciplines the motor gesture is always the same, it is possible to extract some parameters from motion data and to use them to assess the performance. It is possible to do it because the gesture is expectable and repetitive so using techniques that give information about the kinematics, the kinetics or the muscular activity it is feasible to understand "how" the gesture is performed.

The cycling, which is the sport discipline studied in this work, belongs to the "closed skill" class. The athlete continuously repeats the act of pedalling; different environments, such as the slopes of the path, can modify the execution of the gesture in terms of timing, applied forces and muscles involved, but not the gesture itself. It becomes important to identify the proper parameters that can give information related to the performance. This choice is not obvious because the cycling performance is affected by several variables as it is documented by some studies which describe the problem from different points of view, as biomechanical, bioenergetic, aerodynamic etc.[2]

First of all in cycling it is very important to evaluate the relationship among the athlete and the "instrument" used to perform the motor gesture. The athlete's posture on the bicycle that is the relative distances among the points of contact of the athlete and the bicycle (saddle, pedals, handlebar) produce notable changes to the kinematic chain of the lower limbs, bringing variations to the performance. Particular importance has to be given to the variations of height and the fore-aft position of the saddle: in previous studies it has been assessed that excursions of some millimetres in professional athletes bring to an adoption of a different strategy of pedalling [3]. For instance the fore-aft position of the saddle is different among the climbers and the sprinters. The first ones assume a backward position that allows a greater angular excursion of the knee articulation and a distribution of the force on a wider part of the pedalling cycle. On the other hand sprinters tend to apply an impulsive force on a smaller part of the pedalling cycle, in order to be as fast as possible.

Secondly the study of the pedalling dynamics, relying on the evaluation of the resistances to the motion, can give insights on parameters definition. The dynamic evaluation can be expressed in terms of resistant torques to the axle of rotation of the chain driver of the bicycle, as already introduced in literature [2]. In the same work it was assessed that in the execution of the gesture, the athlete has to win the components of rolling resistance related to the friction between the wheel and the road, as well as those connected with the friction among all the mechanical components between the wheel and the point of application of the force to the pedal. Besides, in the case of a sloped circuit, it was underlined the importance of the weight force component in the direction opposed to the advancement and of the

dissipated force component related to the resistance of the air, that can be simulated by an equivalent resistance to the wheel proportional to the speed of the bicycle.

The effects of these resistances can be esteemed however in terms of resistant torque to the wheel that it has to be overcome from the torque applied to the system chain driver-cranks-pedals.

Finally, from the energetic point of view, it has been valued that the unitary path work during the progression in plain is proportional to the square of the speed according to:

$$W_c = a + b \cdot v^2$$

where ν represents the speed respect to the air, while *a* and *b* they are constant for determined boundary conditions. The correspondent energetic waste is function both of the global efficiency of the progression and of the mechanical work according to:

$$C_c = W_c \eta^{-1}.$$

The efficiency therefore is expressed as the ratio among the unitary path work and energetic cost of the physical exercise. In numerous studies it has been assessed that its maximum value is about 0.25 and besides it has been shown that it depends on the frequency of pedalling and from the mechanical power to which the exercise is performed [4,5].

In the quoted works, however, the efficiency of pedalling results related to bioenergetic evaluation and therefore it could be integrated from further indexes of efficiency used to asses the performance of the gesture related to the mechanical characteristics of it, obtained using measures of the force applied to the pedal and from the estimation of the kinematic parameters.

In this study the performance has been evaluated on the basis of some dynamic and kinematic parameters measurable during the execution of every single cycle of pedalling. Besides, it has been thought about monitoring the muscular activity through the analysis of the surface electromyography signals of the muscles of the lower limbs involved in the gesture, with the intent to prevent phenomena related to the muscular fatigue. Therefore, in this work the act of “cycling” has been studied by considering and integrating kinematics, kinetics and electrophysiology related to the motor task.

The summary of the thesis is reported in the following lines, where the contents of each chapter have been outlined. Literature analysis has been inserted at the begin of each

chapter in order to underline the state of the art and the contribution provided by this work to the single topics.

Chapter 1 deals with the design and the development of an instrumented pedal that has been realized to measure the dynamic loads exerted by the athletes during the execution of the gesture. This chapter reports: project and dimensioning of the mechanical components; the realization of the electronic circuit; the procedure of calibration; experimental test for instrument validation.

Chapter 2 presents a modelling approach to understand how the muscles of the lower limb contribute to the execution of the gesture of pedalling, with the special aim of understanding the muscular synergies and their modifications. An eight muscles model is used to estimate the muscular forces by using an inverse dynamic approach, and then a comparison with myoelectric signal envelopes has been carried on to analyze the relation between force production and muscular electrical activity.

Chapter 3 describes methods for the evaluation of the surface electromyography signal (sEMG) recorded in dynamic conditions in order to monitor the muscular activity of the lower limbs during the execution of the gesture. In particular, muscular activity has been codified by using the simultaneous variations of the envelope and the mean spectral frequency of the signal so giving raise to a four states muscular code. Experimental tests have been designed and implemented to validate the proposal of the muscular status coding.

Chapter 4 presents an application of using the instrumented pedal to assess the maximal muscle power compared with the estimation done using a stereophotogrammetry technique, that is based on the measure the acceleration of a flywheel of a friction braked cycle ergometer.

The availability of an instrumented pedal to measure forces exerted by the athlete at the foot level, unveils the possibility to measure maximal muscle power from the force information. Following this end, the purpose of the work was to test the reliability and validity of this new method based on a direct measure of power, and comparing it against a kinematic based indirect estimation based un stereophotogrammetric recordings.

Chapter 5 presents the biomechanical analysis of the gesture and discuss how the athlete's performance can depend on both the body posture and the execution of the movement (that is, how the force is applied to the pedal). Some indexes have been proposed and validate in order to assess the efficiency of the motor task. These indexes can be provided on-line to the athlete by using a dedicated device that has been designed and implemented for monitoring purposes.

1. The design of the instrumented pedal

In order to analyse pedalling dynamics, an instrumented pedal has been designed and realized, to measure the forces that are applied during the execution of the gesture. The pedal makes it possible to measure the time series of these forces, based on load cell technology. The realization of the device has been thought to be mounted on bicycles also in on field tests (outside roads, velodromes).

During pedalling, the action exerted by the foot on the pedal determines a distribution of the pressures that can be modelled as the action of a resultant force applied in a point. In general, this force will have a direction that doesn't necessarily lie in one of the planes defined by the pedal or by the crank, and can be therefore decomposed in three components according to a generic reference system.

It is possible to define different reference systems (RS) that refer to either the pedal, the crank, or the laboratory. In particular (Figure 1.1):

- the reference system RSp is related to the pedal: considering the crank at the top dead centre and the pedal parallel to the ground, this reference systems has the origin in the centre of the load plain of the pedal, the X_p axis directed forward along the antero-posterior direction, the Y_p axis directed outside from the bicycle along the medio-lateral direction and the Z_p axis directed to the bottom along the perpendicular to the ground;
- the reference system RSc refers to the crank: considering the crank at the top dead centre and the pedal parallel to the ground, this reference systems has the origin in the centre of the upper extremity of the crank on the line that identify Y_p and the three axes coinciding with the RSp ones.

- the reference system RSl refers to the laboratory: considering the crank at the top dead centre and the pedal parallel to the ground, this reference systems has the origin in the centre of the chain driver on the lower extremity of the crank and the three axes with the same direction of the previous system but translated along the crank itself.

Moreover are defined with θ_p the relative angle between the directions identified by X_p and X_c and with θ_c the relative angle between the between the directions identified by Z_c and Z_l.

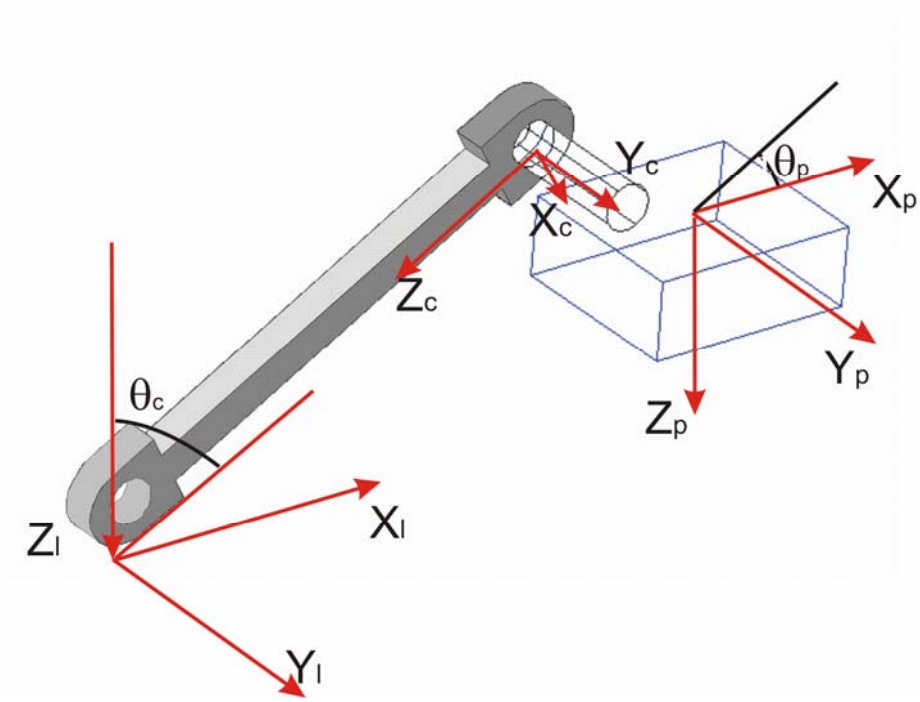

Figure 1.1: *Pedal, crank and laboratory reference systems*

The force applied to the pedal can be thus decomposed into its three components F_x, F_y, F_z related to the three different axes of RSp: each of these determines a reaction in terms of forces and torques applied both on the pedal spindle and on the crank. These forces cause deformations for compression-traction and for bending.

The realized instrumented pedal measures 2 components of the force applied to the pedal: the component perpendicular to the plane F_z and the component parallel to the plane and direct along the direction antero-posterior F_x. The medio-lateral component is negligible in comparison to these two. The two measured components represent the action exerted by the foot to overcome resistances to the progression.

1.1 The state of the art

In the scientific literature on sport science, different are the approaches that are undertaken in the analysis of cycling. In particular, this sport is analyzed from three different perspectives: the aerodynamics, the bioenergetics and the biomechanics.

In the analysis of a closed skill gesture such as the pedalling in cycling, the study of the biomechanics is extremely relevant, because kinematic and kinetic data extraction makes it possible to extract reliable parameters to evaluate the athlete's performance.

In the evaluation of parameters that can be correlated to biomechanical aspects of pedalling, several research works aim to the realization of acquisition systems to obtain dynamic data.

Among them, Soden and co-workers in the 1979 [6] pioneered this area, by developing a system for the simultaneous estimation of both the kinematics and the force applied to the pedal. The system was constituted by an instrumented pedal for the measure of the dynamic data, combined with photogrammetric devices aiming at the estimation of the following kinematic parameters:

- the variation of the angle of the bicycle oscillation during pedalling;
- the medio-lateral pose of the cyclist during the simulation of a climbing on a slope;
- the medio-lateral pose of the bicycle (tilt angle) during the phase of slope climbing;
- the vertical position of a marker fixed on the back of the athlete during the phase of slope climbing;
- the overall pose of the pedal during the execution of the gesture.

By solving a direct dynamic problem, from the kinematics the force applied to the pedal was estimated. These one was compared to the force measured by the developed device that probably can be identified as the first instrumented pedal in the analysis of cycling. Then in this work, by evaluating the forces applied to the bicycle frame to assess the sport performance, a feasibility study on measurements of forces by an instrumented pedal was carried on. The authors showed that during simulated conditions of start, climb or sprint the differences between estimated and measured values were less than 20%.

In successive studies [7,8], in order to measure the loads applied during pedalling, a multi-component instrumented pedal was developed. This pedal measured three-dimensional

force and torque in a reference system fixed to the pedal, and the angles of both crank and pedal. In this way the effective force, which is the one perpendicular to the crank, was estimated; furthermore the contribution of the effective force to the resultant, calculated on a plane parallel to the sagittal plane of the bicycle, was used to evaluate the efficiency of pedalling. Also an index of performance (P.I.) was defined as the ratio between the mean effective and the maximum forces in a pedalling cycle. Since P.I was found to depend on the position of the foot, the pedalling technique was interpreted as influencing the whole performance. The use of a different technique based on the adoption of a different position of the foot on the pedal, showed an increased energetic cost but a simultaneous increase of the P.I. with advantages in the performance. P.I., suggested as an indicative index of the performance, was then related to the applied force and consequently to the muscular work. In that way it was demonstrated that the measure of forces provided by the instrumented pedal can give useful and reliable information in the assessment of the performance.

However in these studies some fundamental aspects of performance evaluation were missing. First of all, the relationship between the applied force and the muscular activity, as evaluated for example by electromyography techniques, was not analysed. In fact, the analysis of myoelectrical activity is necessary to correctly interpret the motor gesture. The measure of the force alone can not provide an exhaustive interpretation, since the same force can be obtained as the result of different combinations of muscular synergies that can be influenced by several factors ranging from the pedalling technique to the physical condition of the athlete.

Moreover, even if a biomechanical index to asses the performance has been introduced, it was obtained by post-processing of data recorded in a laboratory and it was not used to provide the cyclist with direct information on the gesture execution. Moreover in these work no direct correlation between the index of performance and variations in the geometry of the bicycle was taken into account. As a matter of fact, changing the geometry of the bicycle has been demonstrated to influence the performance [3].

In similar works the authors use the same pedal to provide information on the loads applied on the bicycle during the exercise. In particular, in [9] the authors studied the stress applied to the mechanical elements of the bicycle in relation with the weight of the athlete. The test was done with different values of resistance using a cycloergometer to measure the resistant power. In [10] the same authors confirmed the instrumented pedal as the most accurate and reliable device in describing the gesture of pedalling from a biomechanical

point of view. The performance was studied by overloading the pedal in different conditions; the whole load applied by the cyclist was reconstructed by using an instrumented pedal based on a combination of seven load cells that could be used to measure six components (3 forces and 3 torques). The results showed the importance of the two components on the sagittal plane in the evaluation of the performance during the execution of the gesture.

In other works, aiming at reducing the dimensions of the measuring devices (that is the instrumented pedals) new geometries of load cells were experimented. In particular, in [11] a load cell with an octagonal ring shape was realized; it was equipped with a peculiar combination of strain gauges to measure decoupled force components on the pedal.

In more recent studies [12], efficiency indexes were used to demonstrate how prolonged cycling modifies the patterns of force measured at the pedal: an increase of the maximum peak in the force's curve, evaluated as the average over the pedalling cycle is associated to a simultaneous increase in the negative direction of the minimum in the second phase of the cycle, that is identified as the phase of pulling. The proposed explanation supposed that the muscular fatigue induces the athlete to concentrate his effort on the first phase of the gesture, the pushing, neglecting the second phase, the pulling. Some limitations of this study relate to the definition of fatigue expressed in terms of athlete's exhaustion, to the design of a laboratory device rather than an instrument to be used on the field and to the acquisition of kinematic information provided by photogrammetic devices.

The tendency to develop systems to be used in tests on the field, using a bicycle rather than a simulator, is outlined by very recent papers [13,14] devoted to structural analysis of the frame and the mechanical elements of the bicycle. The common limit of these works was once again that all the system, also if was equipped with a telemetric system for the transmission of data, was studied and fitted on a specific bicycle that was modified in some elements, so that it was not possible to move all the system on the bicycle of each athlete to use it for biomechanical consideration on them. In a successive work by the same authors [15], the instrumented pedal was used to make considerations on the posture of the athlete during cycling. This represents one of the great challenges in the study of this sport, and it needs instruments and techniques that could be used on t each athlete's bicycle, to directly perform the correct regulation and give them the possibility of training, after the assessment of the regulation of the geometries of the bicycle, in the best way.

In literature there are other studies that rely on the use of an instrumented pedal, but most of them did not realize instruments to be used in field test contexts or those need of further instruments to evaluate other parameters as the kinematic data [12,16,17].

In conclusion, most of these projects have been developed realizing devices that allowed the execution of tests in laboratory, working therefore on simulators of the specific gesture, or application on bicycles to perform tests on the field using especially designed bicycle. One if the limitation of this approach is that the performance is strictly related to the regulation of the bicycle's geometries as well as the posture of the athlete on the bike. So the best way to make a test on a cyclist is to let him using his own bicycle, still modifying as less as possible the conditions in which the gesture is performed during a normal training or competition. Changing the bicycle or introducing external objects, such as bags or belts to carry the instruments necessary to acquire and/or process data, introduces limitation in the execution of the task, which is modified in its natural way of performing. So the aim of this work has been the design and the development of a new instrumented pedal that could be fitted on the bicycle of each athlete without modifying the geometry of a commercial pedal and without introducing differences in the posture. Moreover, the acquired data can be processed and on-line fed back to the athlete, with the intend of providing him with the information about the way the gesture is executed, and about his performance.

1.2 The mechanical design

In the realization of the pedal particular attention has been set to guarantee minimal impact in terms of changing geometry and masses of the commercial pedals. As a matter of fact, it is not possible to modify over certain limits (< 1mm) the position of the fastener of the shoe along the three spatial directions. More in detail, the design of the instrumented pedal needed to preserve the original measures of the pedal, with fastening clipless system, as the distance of the plan of fastening from the axle of rotation, the distance of the middle of the fastening system from the crank and the antero-posterior distance from the pedal bolt.

The structure of the instrumented pedal has been realized on the base of a pedal equipped with the type Shimano® Pedalling Dynamics (SPD) clipless fastening system, making a new design of the whole structure with the purpose to measure the forces above described. In Figure 1.2 it is possible to notice the different components between the instrumented pedal and a commercial one. The clipless fastening system (1) is connected through two spacer screws to an especially designed load cell (2), which has been fixed to a "U" shape stirrup (3), which presents two circular holes to its extremities. In these holes two ball bearings were fitted that allow the relative rotation among the stirrup and a transmission-shaft (4), fixed to the crank of the bicycle.

The measure of the angle θp is made through a smart encoder (5) positioned between the stirrup, using another stirrup of smaller dimensions, and the spindle, which has a cylindrical hole at the corresponding extremity.

The technological innovation of this instrument consists of displacing the load cell among the SPD fastening system and the spindle used to connect the pedal to the crank. In fact the SPD fastener is directly connected to the load cell in such a way that the applied force is transmitted first to the cell, then to the stirrup and finally to the spindle.

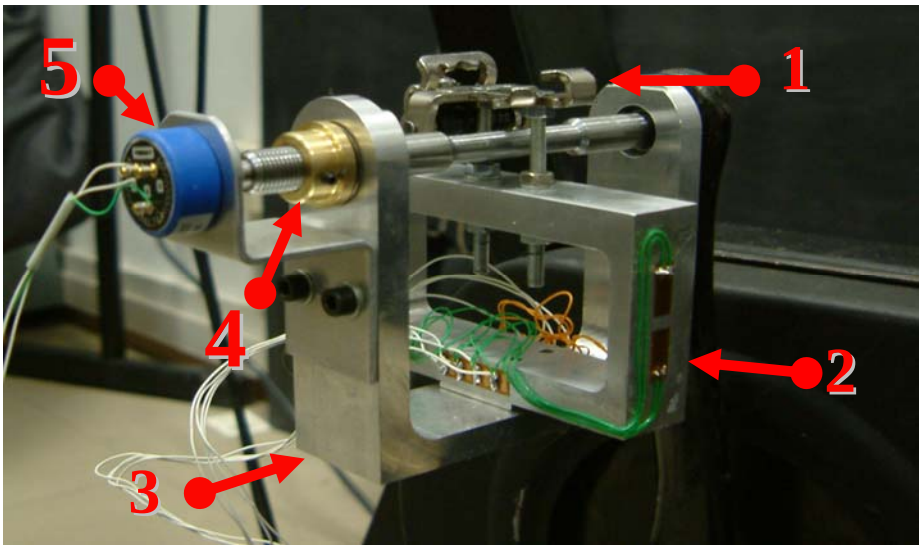

Figure 1.2: *The instrumented pedal.*

In the design phase, which was done through the use of CAD/CAM (Computer Aided Design/Computer Aided Manufacturing) software, the pedal has been dimensioned considering the maximum predicted loads applied during fatiguing exercises, increased according to a safety factor so that the criterions of structural verification were satisfied. Particular attention has been set in the design of the load cell that was realized as the other components in an aluminium alloy. The structure of the load cell is rectangular so that it has allowed identifying the deformations resulting from the application of the two force components to be measured.

In Figure 1.3 the simulation of the assembled structure is shown: in the picture, it is also possible to identify the three main components of the pedal.

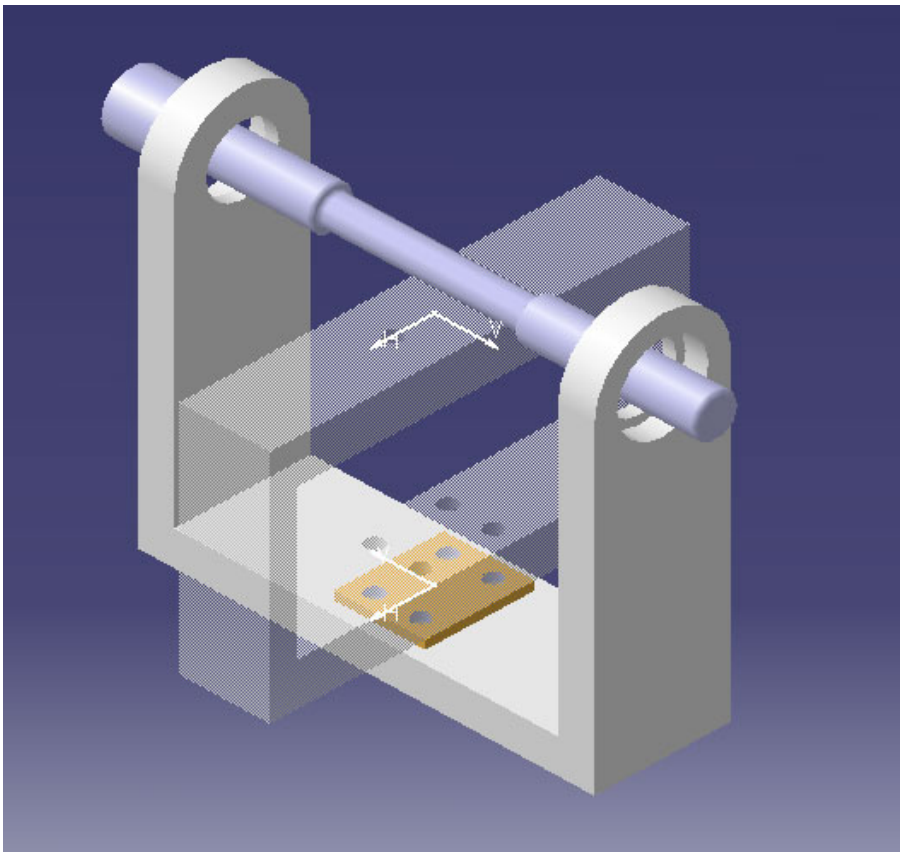

Figure 1.3: *CAD/CAM simulation of the pedal structure.*

All the components were designed in order to resist to maximum loads applied during the exercise. In fact every component was verified to be resistant to each component of the force applied by the athlete, considering its shape, its dimensions and the material used to make it. The values Fz=1000N e Fx=1000N were chosen as design loads, considering previous studies of literature about estimation of those [7].

In general terms, forces can be measured using mechanical or electromechanical devices. The latter ones are more commonly used in the realm of human movement analysis, because they allow acquiring signal used to make elaborations on data, while the firsts are in generally used to have a quick measure of a dynamic parameter when it's not needed an acquisition. The two main classes of force transducers are piezoelectric based devices and strain gauges based ones.

The main component of the instrumented pedal is the load cell that is based on the use of strain gauges. In fact with these kinds of transducers it is possible to develop a device that

is useful to measure forces with a digital system of acquisition. In the development of the design of the load cell, the aim has been to build a device useful to transduce in a simply way the two pedal force components in electric signal, introducing as few as possible noise and cross-talk effects.

1.3 Strain gauges based transducers

The strain gauges based devices are generally the most used in the field of force measurement. The basis of the strain gauges theory relies on the relationship between the deformation of the material's structure and its electrical features. A percent deformation of the strain gauges, due to a force applied to the structure it's fixed, corresponds to a percent variation of its electrical resistance that is proportional to the force. The electrical resistance is much higher of its variation that could be considered linearly proportional to the deformation, as it'll be described below. The sensitivity to the deformation of a strain gauge is generally maximum along a mean direction that depends on the shape of it.

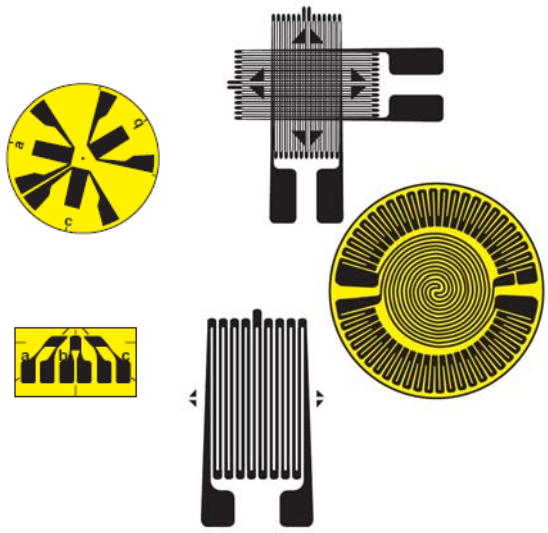

Figure 1.4: Different kinds of commercial strain gauges.

Generally it is possible to find, as commercial device, sheets with single or multiple strain gauges photoengraved and already assembled in a particular configuration, with different mechanical dimensional or electrical details (Figure 1.4).

In order to measure low variation of electrical resistance, usually strain gauges are assembled in an electric circuit in a "Wheatstone bridge" configuration (Figure 1.5). This

circuit combines the electrical resistance variation of each element composing the bridge. Strain gauges are connected on a Wheatstone bridge in different ways depending on the kind of measurement that has to be done.

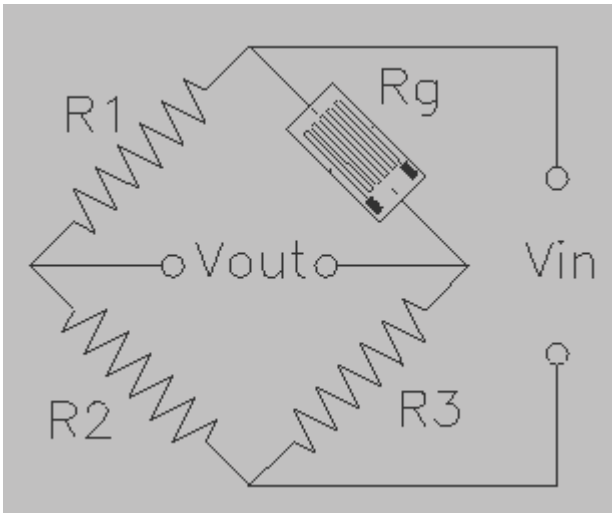

Figure 1.5: The Wheatstone bridge.

1.3.1. Theory of deformation

The deformation of a body is related to the variation of its shape due to the application of a force. In particular the percent deformation ε is defined as the ratio between the increase of the length and the original length. It is an adimensional parameter but it is usually expressed in terms of [μm/m], because the value of the variation of the length is not comparable with the original dimension (Figure 1.6).

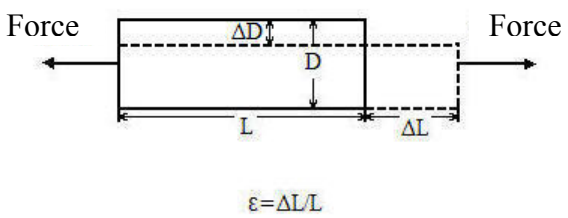

Figure 1.6: Deformation of a body.

Generally a material, to which a force is applied, changes its shape not in a permanent, and if the force is removed it returns to its initial shape. This behaviour is defined as “elastic” so the deformation is called “elastic deformation”.

When a one-dimensional force is applied to an elastic structure, this changes its shape principally along the direction of the force application and than along the two perpendicular directions to the force itself. This is due to a physical phenomenon called “Poisson’s deformation”. The magnitude of these deformations depends on the material’s behaviour and it’s expressed using the “Poisson coefficient”ν. This is expressed as the opposite of the ratio between the transversal (perpendicular to the applied force direction) and axial (along the applied force direction) deformations:

$$\nu = -\frac{\varepsilon_t}{\varepsilon_a} \qquad \textbf{1.1}$$

with:

$$\varepsilon_t = \frac{\Delta D}{D} \quad \text{e} \quad \varepsilon_a = \frac{\Delta L}{L}. \qquad \textbf{1.2}$$

Using the relative deformation ε it is possible to know the stress of the material, called strain, related to the applied force using the Hooke’s law:

$$\sigma = \varepsilon \cdot E = \frac{F}{A} \qquad 1.3$$

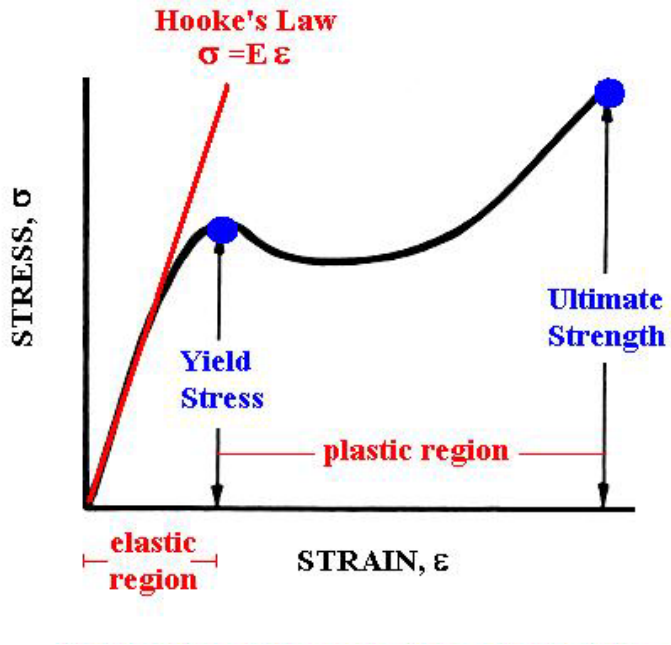

Figure 1.7: Typical trend of a stress-strain curve.

with E Young's modulus of the material, F the applied force and A section to which the force is applied. This relationship is valid in the first part of the strain-stress curve of a material that represents the elastic behaviour of the structure (Figure 1.7). The relationship between strain and deformation is given by the modulus of elasticity of the considered material (steel 210.000 N/mm^2, aluminium 70.000 N/mm^2).

In Figure 1.7 a typical trend of a strain-deformation curve for steel is represented. There is a value of the strain called "elastic limit", which defines the border between two different behaviours. If a force that corresponds to a strain lower than this limit is applied to a test piece of a material, when it is removed the test piece recovers its original shape, while if the force corresponds to a strain greater than the elastic limit the test piece is not able to recover its original shape. These behaviours are called "elastic" and "plastic", respectively. Moreover, for every material there is a particular load that represents the breaking point.

It is possible to take advantage of the material's elastic features in order to have a measure of the force applied to the test piece, using the strain gauges. A strain gauge consists of an insulating flexible backing which supports a metallic foil pattern. The gauge is attached to the surface of the metallic structure to which the force is applied by an appropriate adhesive (e.g. cyanoacrylate). As the structure is deformed, the foil is deformed, causing its electrical resistance to change. the deformation of the structure has to be in the range of the

elastic behaviour. The electric resistance change is usually measured using a Wheatstone bridge.

1.3.2. Strain gauges theory

A strain gauge is normally obtained by photo-engraving on a metallic foil in a particular shape depending on the application. Usually, to measure a deformation, multiple strain gauges assembled in a particular configuration are used.

The most common shape of a strain gauge is a grid. The grid could have a different pattern depending on the class of deformation the strain gauge is designed to. The most common kinds are the unidirectional strain gauges which are suitable to detect deformations of a structure along an axis. To this purpose, the grid has two different sections in its shape: some thick lines parallel to the axis of deformation are connected with bold lines perpendicular to the axis of deformation. In this way the strain gauges presents a greater sensitivity in one direction respect to the other.

Usually strain gauges are available with electrical resistance values in the range 30Ω to 3000Ω; the most common values used in design of load cells being 120Ω, 350Ω and 1000Ω. A strain gauge should be fitted as well as possible; it means that for example it is important to accurately align the strain gauge according to the deformation's direction and to paste it correctly. In this way, the electrical resistance should change consequently to the strain applied. However strain gauges are also influenced by the variation of temperature and it is possible to define a parameter that describes this phenomenon:

$$\alpha = \frac{\frac{\Delta R}{R}}{T}. \qquad \textbf{1.4}$$

In commercial strain gauges the sensitivity to the temperature is reduced using particular techniques, but has to be taken in account in assembling strain gauges in a load cell.

To understand how a strain gauge works, it is important to underline that the electrical resistance of a conducting wire is:

$$R = \rho \cdot \frac{l}{S} \qquad \textbf{1.5}$$

with ρ resistivity of the material, l and S respectively length and section of the conductor. If the wire is stretched along its main direction, there is an increase of l and a decrease of S, so the resistance increases. Moreover, for most materials the resistivity increases with the deformation, coherently with the increasing described.

Applying the natural log to the previous equation:

$$\ln(\mathrm{R}) = \ln(\rho) + \ln(l) - \ln(\mathrm{S}) \qquad \textbf{1.6}$$

and applying the derivative:

$$\frac{\Delta \mathrm{R}}{\mathrm{R}} = \frac{\Delta\rho}{\rho} + \frac{\Delta l}{\mathrm{l}} - \frac{\Delta \mathrm{S}}{\mathrm{S}} = \frac{\Delta\rho}{\rho} + \frac{\Delta l}{\mathrm{l}} - \left(\frac{\Delta b}{b} + \frac{\Delta h}{h}\right) = \frac{\Delta\rho}{\rho} + \frac{\Delta l}{\mathrm{l}}(1+2\nu) \qquad \textbf{1.7}$$

From the $\frac{\Delta \mathrm{R}}{\mathrm{R}} = \frac{\Delta\rho}{\rho} + \frac{\Delta l}{\mathrm{l}} - \frac{\Delta \mathrm{S}}{\mathrm{S}} = \frac{\Delta\rho}{\rho} + \frac{\Delta l}{\mathrm{l}} - \left(\frac{\Delta b}{b} + \frac{\Delta h}{h}\right) = \frac{\Delta\rho}{\rho} + \frac{\Delta l}{\mathrm{l}}(1+2\nu)$ 1.7 it is possible to obtain:

$$\frac{\frac{\Delta \mathrm{R}}{\mathrm{R}}}{\frac{\Delta l}{l}} = \frac{\frac{\Delta\rho}{\rho}}{\frac{\Delta l}{\mathrm{l}}} + (1+2\nu) = K_1 + K_2 = K \qquad \textbf{1.8}$$

K represents a parameter that is related to physical properties of the material and it's called "gauge factor". The value of this for metal is typically equal to 2.

So it is possible to obtain:

$$\frac{\Delta \mathrm{R}}{\mathrm{R}};\ \mathrm{K} \cdot \frac{\Delta l}{l} = \mathrm{K} \cdot \varepsilon \qquad \textbf{1.9}$$

and using

$$\sigma = \varepsilon \cdot \mathrm{E} = \frac{\mathrm{F}}{\mathrm{A}} \qquad \textbf{1.3}$$

$$\frac{\Delta \mathrm{R}}{\mathrm{R}} = \mathrm{K} \cdot \frac{\sigma}{\mathrm{E}} = \mathrm{K} \cdot \frac{\mathrm{F}}{\mathrm{A} \cdot \mathrm{E}}.$$

In this way, the electrical resistance is proportional to the force applied.

Typical values of deformation ε are in the range $10^{-6} \div 10^{-4}$ $\mu\mathrm{m/m}$, so the percent variation of resistance is:

$$\left(\frac{\Delta R}{R}\right)_{Max} = K \cdot \varepsilon \; ; \; 0.0002 \qquad \textbf{1.10}$$

The most common way to measure these small resistance variations is to use a Wheatstone bridge. This is a particular configuration used to connect resistors and it also permits to compensate temperature effects.

As in Figure 1.8, a Wheatstone bridge is a circuit that presents 4 resistive branches and it is supplied with a voltage V_{in}.

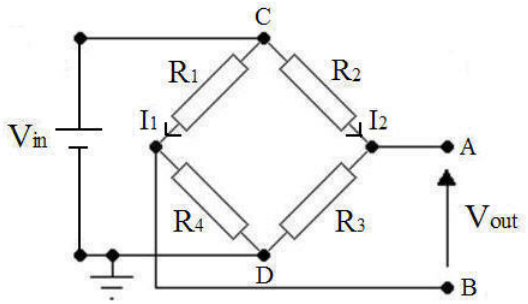

Figure 1.8: Wheatstone bridge.

The bridge is balanced when the output voltage is V_{out}=0. Considering that if the bridge is balanced, the following equations hold:

$$\begin{cases} R_1 I_1 = R_2 I_2 \\ R_4 I_1 = R_3 I_2 \end{cases} \qquad \textbf{1.11}$$

Consequently:

$$\frac{R_1}{R_4} = \frac{R_2}{R_3} \qquad \textbf{1.12}$$

So the condition to obtain a balanced bridge is given by:

$$R_1 R_3 = R_2 R_4 . \quad 1.13$$

A strain gauges' bridge is commonly used in the nearby of the equilibrium point. Imposing this as initial condition:

$$V_{out} = V_{AB} = (V_C - V_B) - (V_C - V_A) = R_1 I_1 - R_2 I_2 = V_{in} \cdot \frac{R_1}{R_1 + R_4} - V_{in} \cdot \frac{R_2}{R_2 + R_3} \qquad \textbf{1.14}$$

Considering that:

$$I_1 = \frac{V_{in}}{R_1 + R_4} \quad \text{e} \quad I_2 = \frac{V_{in}}{R_2 + R_3} \qquad \textbf{1.15}$$

So the expression yields:

$$V_{out} = V_{in} \cdot \left(\frac{R_1}{R_1 + R_4} - \frac{R_2}{R_2 + R_3} \right) = V_{in} \cdot \frac{R_1 R_3 - R_2 R_4}{(R_1 + R_4)(R_2 + R_3)} \qquad 1.16$$

Considering the variation of the electrical resistance R_1, there is a consequently unbalancing of the bridge, so the new value of V_{out}, due to the new value of the resistance $R_1 + \Delta R_1$, becomes:

$$\frac{V_{out} + \Delta V_{out}}{V_{in}} = \frac{(R_1 + \Delta R_1)R_3 - R_2 R_4}{(R_1 + \Delta R_1 + R_4)(R_2 + R_3)} = \frac{R_1 R_3 + \Delta R_1 R_3 - R_2 R_4}{(R_1 + \Delta R_1 + R_4)(R_2 + R_3)}. \qquad \textbf{1.17}$$

If the bridge was originally balanced, $V_{out} = 0$ and $R_1 R_3 - R_2 R_4 = 0$, so:

$$\frac{\Delta V_{out}}{V_{in}} = \frac{\Delta R_1 R_3}{(R_1 + \Delta R_1 + R_4)(R_2 + R_3)} \qquad \textbf{1.18}$$

Considering:

$$\alpha = \frac{R_3}{R_2 + R_3} \quad \text{e} \quad R_m = R_1 + R_4 \qquad \textbf{1.19}$$

finally:

$$\frac{\Delta V_{out}}{V_{in}} = \alpha \cdot \frac{\Delta R_1}{\Delta R_1 + R_m} = \frac{\alpha}{R_m} \cdot \frac{\Delta R_1}{1 + \frac{\Delta R_1}{R_m}}. \qquad \textbf{1.20}$$

If the variation of electrical resistance is very low as compared to the original value $\left(\frac{\Delta R_1}{R_1} = 1 \right)$, the terms $\frac{\Delta R_1}{R_m}$ could be neglected and considering that $R_1 = R_2 = R_3 = R_4$, the expression becomes:

$$\frac{\Delta V_{out}}{V_{in}} = \frac{\alpha}{R_m} \cdot \Delta R_1 = \frac{1}{2} \cdot \frac{1}{2R_1} \cdot \Delta R_1 = \frac{1}{4} \cdot \frac{\Delta R_1}{R_1}. \qquad \textbf{1.21}$$

Considering the contribution of each strain gauge:

$$\frac{\Delta V_{out}}{V_{in}} = \frac{1}{4} \left(\frac{\Delta R_1}{R_1} - \frac{\Delta R_2}{R_2} + \frac{\Delta R_3}{R_3} - \frac{\Delta R_4}{R_4} \right). \qquad \textbf{1.22}$$

This last expression gives a direct relationship between the variation of the electrical resistance of each strain gauges and the output of the Wheatstone bridge. The contributions

of opposite branches are summed while the ones of adjacent branches are subtracted. This is the most important feature of the Wheatstone bridge that has to be considered in assembling strain gauges of a load cell. Finally, the variation of resistance due to temperature gives equal variations on all the resistors, so it is compensated directly by the bridge.

In the design of the load cell used on the pedal all these features were considered, as described in the following.

1.4 The load cell design

The load cell presents a particular shape chosen to have a compact structure that permits to measure the two pedal force's components. It is a parallelepiped 92×55×20mm with a rectangular hole 80×35mm in the middle, so it can also be considered as a 4 fixed beams of different length and width. The rationale is to use the property of a rectangular fixed beam to associate the applied force to the deformation of the structure. The load cell presents also 2 threaded holes on the top to fix it with screws to the connection for the shoe and 4 threaded holes on the bottom to fix it to a flask, which will be described below.

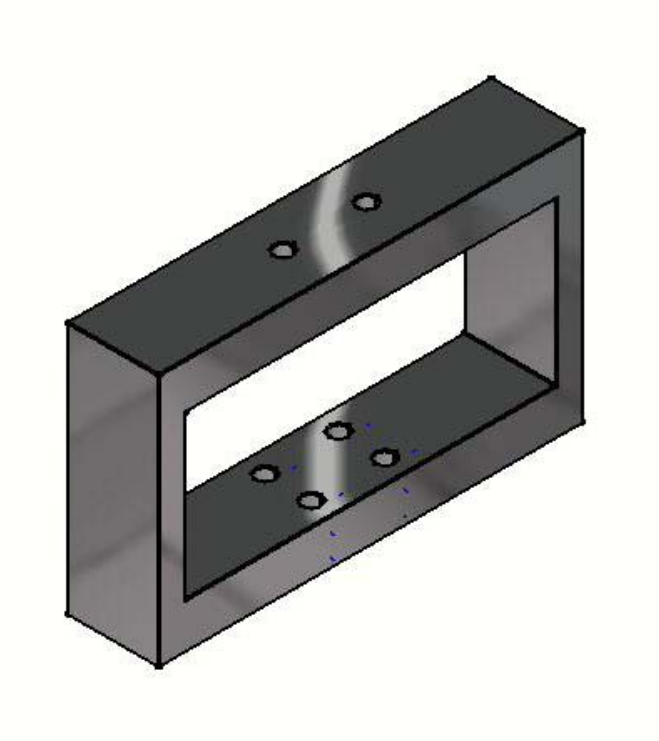

Figure 1.9: The load cell structure.

To understand how the load cell is deformed under the action of the pedal force, a simulation has been performed, by applying the two components Fz and Fx. The deformations of the load due the components Fz and Fx are respectively shown in Figure 1.10 and Figure 1.11. It is possible to consider the two effects separately to analyse how to position the strain gauges.

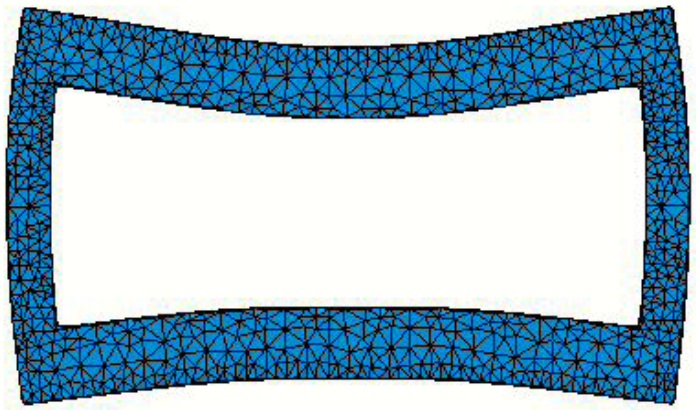

Figure 1.10: deformation of the load cell under the action of Fz component

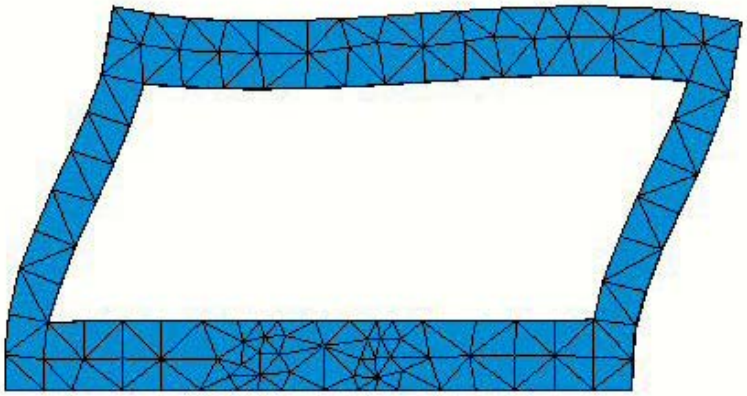

Figure 1.11: deformation of the load cell under the action of Fx component

The strain gauges were placed on the load cell in the positions shown in Figure 1.12. The strain gauges for the measure of the Fx component were placed on the external lateral surfaces of the load cell (AD and BC sides), while the ones for the measure of the Fz component were placed on the external bottom surface (DH and CH sides).

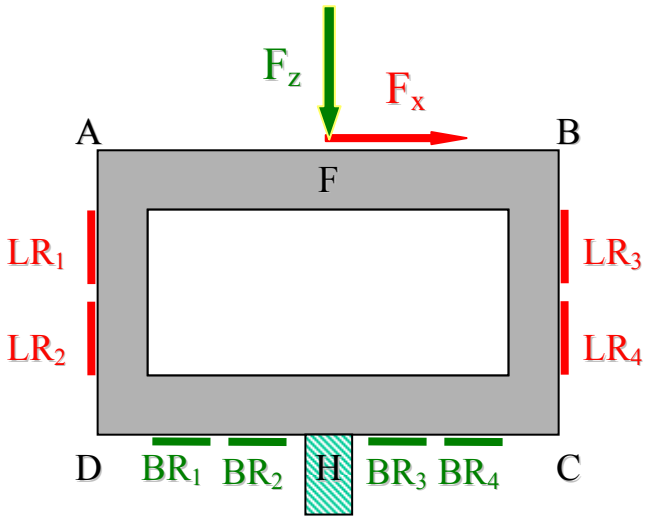

Figure 1.12: Strain gauges disposition on the load cell.

The load cell, as shown in Figure 1.13, can be divided in segments as if it is composed of 4 fixed beams. Each beam is subject to the action of forces and torques and it is consequently deformed. The strain gauges were fixed on the lateral sides of the load cell and on the bottom side. In fact, it is possible to consider the deformation of the equivalent beam AD and of the beam BC to measure the component Fx, while, for the component Fz, the deformation of DC can be divided in DH and CH. The two couples of beams present mirrored deformations when forces are applied and this has to be taken into account during the connection of strain gauges in the Wheatstone bridge configuration.

Under the action of Fx, on each equivalent beam of the load cell internal forces and torques are applied because of rigid constraints, as shown in the free body diagram in the Figure 1.13.

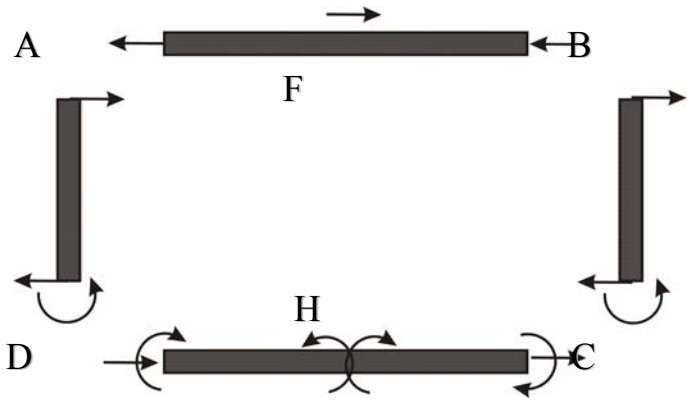

Figure 1.13: Free body diagram of the load cell under the Fx action.

Considering at first the equivalent beam AD deformed under the action of the component Fx, it presents a deformation that is similar to a saddle point, as shown in Figure 1.14. It is possible to fix a strain gauge on the external surface in the position LR1 and a second one in LR2. In this way while the first one is compressed, the second one is stretched. Putting these on two adjacent branches of a Wheatstone bridge, the two contributes are summed.

The same situation, though mirrored, occurs on the beam BC, where the strain gauge LR3 is deformed as the strain gauge LR2 while the strain gauge LR4 is deformed as LR1.

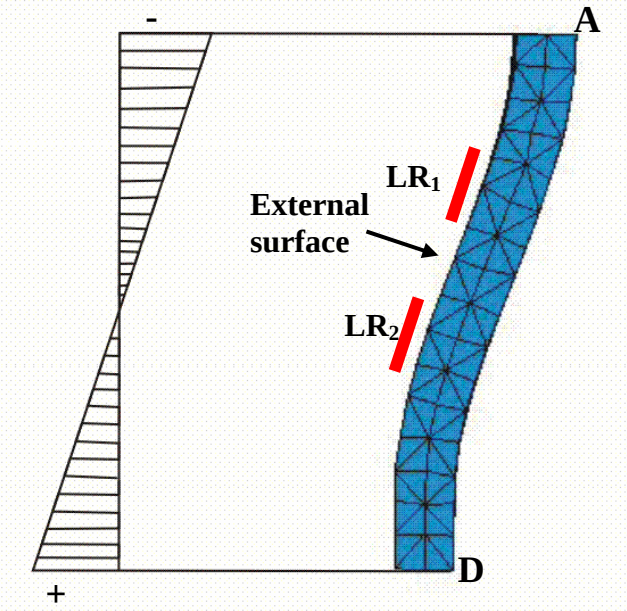

Figure 1.14: Deformation of the equivalent beam AD under the action of the Fx component.

These 4 strain gauges are assembled on the Wheatstone bridge. As described above the strain gauge LR1 and LR2 have to be displaced on adjacent branches of the bridge, such as LR3 and LR4. At the same time, the strain gauges LR1 and LR4 have to be displaced on opposite branches as LR2 and LR3.

The corresponding sections are deformed according to the equation:

$$\sigma = E\varepsilon \qquad \text{where} \quad \varepsilon_{LR1} = -\varepsilon_{LR2} = -\varepsilon_{LR3} = \varepsilon_{LR4} = \varepsilon$$

with E Young modulus of the material.

By positioning the strain gauges as in Figure 1.15 on the Wheatstone bridge, the output signal is:

$$\frac{\Delta V}{V_{in}} = k\left(\frac{\Delta LR1}{LR1} - \frac{\Delta LR2}{LR2} - \frac{\Delta LR3}{LR3} + \frac{\Delta LR4}{LR4}\right) = kG\left(\varepsilon_{LR1} - \varepsilon_{LR2} - \varepsilon_{LR3} + \varepsilon_{LR4}\right) = 4kG\varepsilon \qquad \textbf{1.23}$$

where G is the Gauge Factor, ε is the percent deformation in one of the section and k a constant. With this configuration, it is possible to obtain the measure of Fx, independently from the other components applied on the load cell, as it'll be described in the following.

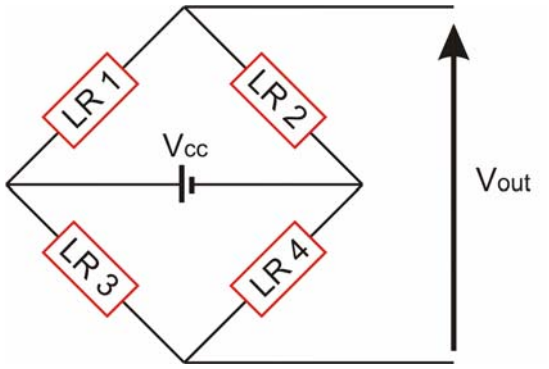

Figure 1.15: The Wheatstone bridge for strain gauges related to Fx measure.

The deformation caused by the load applied during the normal use of the load cell has to be such that the structure is not damaged, so a correct dimensioning of the elements is necessary, to verify that the applied strain is less than the maximum admissible by the used material. The dimensioning has to be done considering the maximum bending moment that is expressed by:

$$\sigma_{Max} = \frac{\mathrm{M}_{fMax}}{\mathrm{W}} \qquad \textbf{1.24}$$

were σ_{Max} is the maximum resistance of the material to the axial strain, expressed in N/mm^2, M_{fMax} is the maximum bending moment in $\mathrm{N}\cdot\mathrm{mm}$ and W is the modulus of resistance to the flexion, that is the capacity of the beam to oppose resistance to stresses, expressed in mm^3. For beams with rectangular section this is:

$$\mathrm{W} = \frac{1}{6}\cdot b \cdot h^2 \quad \textbf{1.25}$$

with *b* and *h* respectively length and width of the beam.

Ideally the beam is deformed, as shown in Figure 1.14 according to a course described by the flex that connects the lines parallel to the axis of the undeformed beam passing through the points A and D. The deformation diagram is shown in figure 9: on each faces of the load cell the fibres of the material become, in static conditions, from stretched to compress. So in the middle, the beam results not submitted to a condition of tension. Therefore the bending moment is maximum to the border (points A and D) and null in the middle. It is expressed by the equation:

$$\mathrm{M}_{fMax} = \mathrm{F}\cdot\frac{l}{2} = 27.5\cdot\mathrm{F} \qquad \textbf{1.26}$$

because the load cell has $l = 55$.

From the equation $\mathrm{M}_{fMax} = \mathrm{F} \cdot \frac{l}{2} = 27.5 \cdot \mathrm{F}$ 1.26:

$$\mathrm{W} = \frac{1}{6} \cdot 20 \cdot 6^2 = 120 \text{ mm}^3 \quad \textbf{1.27}$$

so the maximum strain is:

$$\sigma_{Max} = \frac{\mathrm{M}_{fMax}}{\mathrm{W}} = \frac{27.5 \cdot \mathrm{F}}{120} ; \frac{1}{4.36} \cdot \mathrm{F} \quad \textbf{1.28}$$

Considering a maximum peak of the Fz of 1000 N equally distributed on each side of the load cell, the actual value yields:

$$\sigma_{Max} ; 115 \text{ N/mm}^2 \quad \textbf{1.29}$$

The condition to be respected is $\sigma_{Max} < \sigma_{ADM}$, with σ_{ADM} maximum strain admissible by the considered material. For the load cell was chosen the aluminium Anticorodal 60 alloy, an alloy typically used in the field of cycling structure with a good elasticity and an elevated value of resistance to bending, that has $\sigma_{ADM} = 160 \text{N/mm}^2$, so the condition is verified.

It has also to be outlined that, in this procedure, the effect of the other resultant force's component has not been taken into account on this side of the load cell. If on the load cell is applied the Fz component the effect on the beam AD is as if are applied on it a couple of force, which makes a compression of the beam, and two torques, that make the beam to be flexed. Both these solicitations deform it on the external surface in such a way that the two strain gauges are equally stretched or compressed, so if these are connected on the bridge as described above these contributions are not measured (Figure 1.16).

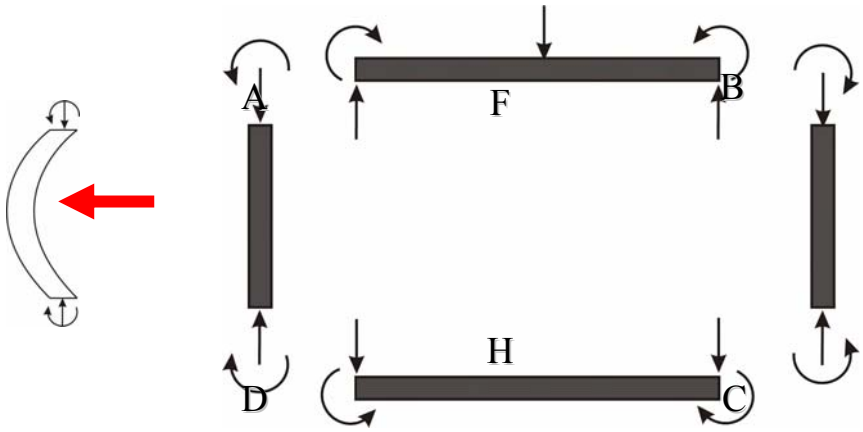

Figure 1.16: Free body diagram of the load cell under the Fz action.

For the measure of the component Fz similar considerations apply: the equivalent beam DH deformed under the action of the component Fz presents a deformation of flexion as if a shear stress is applied, as shown in Figure 1.17. It is possible to fix a strain gauge on the external surface in the position BR1 and a second one in BR2. In this way both strain gauges are compressed, but in a different way.

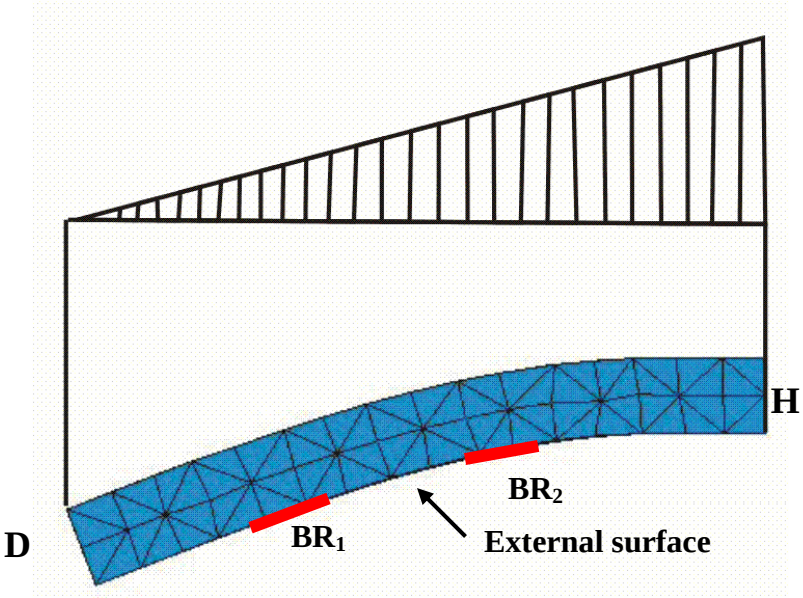

Figure 1.17: Deformation of the equivalent beam AD under the action of the Fx component.

With this configuration, the measurement of the tangential force that deforms an inserted beam is the most sensitive.

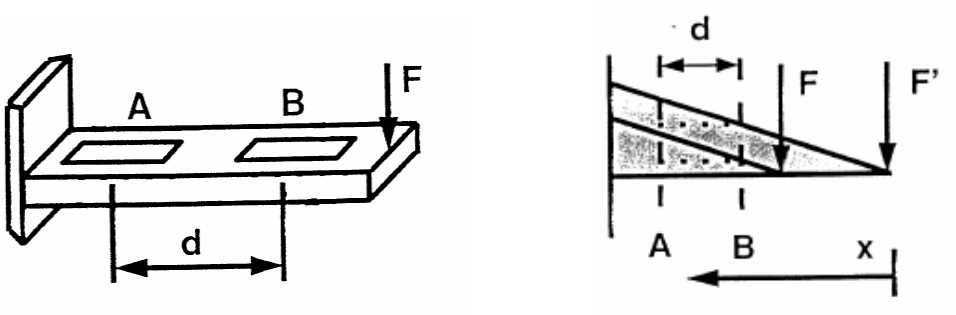

Figure 1.18: Strain gauges displacement for the measure of a generic shear force.

Considering the beam in Figure 1.18, in a generic section the deformation is function of the force F, according to the equation:

$$\sigma = E\varepsilon = \frac{M_f}{W} \qquad \textbf{1.30}$$

Where

$$\varepsilon_A = \frac{M_A}{EW} = \frac{Fx_A}{EW}$$
$$\varepsilon_B = \frac{M_B}{EW} = \frac{Fx_B}{EW} \qquad \textbf{1.31}$$

with Mn is the bending momentum in the generic section n, xn is the force arm, E is the Young's modulus of the material and W is the modulus of resistance to the bending.

By positioning the strain gauges A and B on adjacent branches of the Wheatstone bridge, the output signal is:

$$\frac{\Delta V}{V_{in}} = k\left(\frac{\Delta R_A}{R_A} - \frac{\Delta R_B}{R_B}\right) = kG\left(\varepsilon_A - \varepsilon_B\right) = \frac{kG}{EW}\left(x_A - x_B\right)F = \frac{kG}{EW}dF \qquad 1.32$$

where G is the Gauge Factor, d is the distance between the strain gauges and k is a constant. With this configurations, it is possible to obtain the measure of F, independently of its application point on the beam.

On the basis of these considerations, the strain gauges were mounted as shown in Figure 1.19.

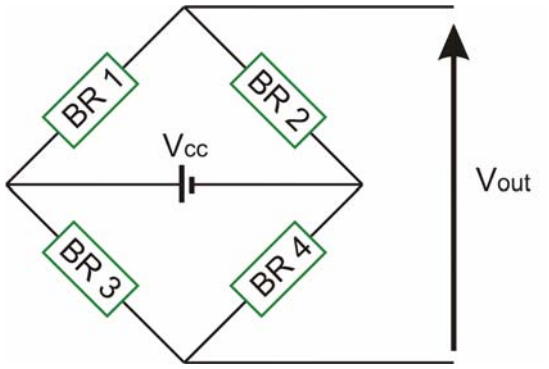

Figure 1.19: The Wheatstone bridge for strain gauges related to Fz measure.

Considering this configuration the following equation is valid:

$$\frac{\Delta V}{V_{in}} = k'G\left(\varepsilon_{BR1} + \varepsilon_{BR4}\right) - \left(\varepsilon_{BR2} + \varepsilon_{BR3}\right) \quad \textbf{1.33}$$

Considering the force applied in the point F of the load cell, the deformations of the strain gauges BR1 and BR4 are the same, as are BR2 and BR3, so if Fz is constant:

$$\begin{cases} \varepsilon_{BR1} + \varepsilon_{BR4} = k_1 \\ \varepsilon_{BR2} + \varepsilon_{BR3} = k_2 \end{cases} \qquad \text{with k1, k2 constant values.}$$

If Fz is applied in a different point of the top surface of the load cell, the deformation could be for example:

$$\begin{cases} \varepsilon_{BR1} > \varepsilon_{BR4} \\ \varepsilon_{BR2} > \varepsilon_{BR3} \end{cases} \quad \text{with the yielding condition} \quad \begin{cases} \varepsilon_{BR1} + \varepsilon_{BR4} = k_1 \\ \varepsilon_{BR2} + \varepsilon_{BR3} = k_2 \end{cases}$$

and in this case the output is the same as in the previous case.

Also in this case the deformation caused by the load applied during the normal use of the load cell has to be that the structure is not damaged, so a correct dimensioning of this part of the load cell is necessary. The maximum bending moment that is still expressed by:

$$\sigma_{Max} = \frac{\mathrm{M}_{fMax}}{\mathrm{W}} \quad 1.34$$

where M_{fMax} is the maximum bending moment allocated in the point H and the modulus of resistance to the flexion W has the same expression used above.

Ideally the beam is deformed, as shown in Figure 1.17 according to a second order polynomial that connects the points A and D. The deformation diagram is shown in figure 9: on the bottom surface the fibres of the material are, in static conditions, compressed. The bending moment is maximum in the point H and it is expressed by the equation:

$$\mathrm{M}_{fMax} = \mathrm{F} \cdot l = 38 \cdot \mathrm{F} \quad \textbf{1.35}$$

because l is the distance between the point D and the holes where the screws fix the load cell to the structure of the pedal.

From the equation $\mathrm{W} = \frac{1}{6} \cdot b \cdot h^2$ 1.25:

$$\mathrm{W} = \frac{1}{6} \cdot 38 \cdot 10^2 = 3800 \text{ mm}^3 \quad \textbf{1.36}$$

so the maximum strain is:

$$\sigma_{Max} = \frac{\mathrm{M}_{fMax}}{\mathrm{W}} = \frac{38 \cdot \mathrm{F}}{3800} ; \frac{1}{100} \cdot \mathrm{F} \quad \textbf{1.37}$$

If a maximum peak of 1000 N for Fz equally distributed on each side of the load cell, is applied, it becomes:

$$\sigma_{Max} ; 10 \text{ N/mm}^2 \quad \textbf{1.38}$$

The condition $\sigma_{Max} < \sigma_{ADM}$, remembering that $\sigma_{ADM} = 160 \text{N/mm}^2$ for Anticorodal aluminium alloy, is easily verified.

If the Fx component is applied on the load cell, the strain gauges BR1 and BR2, as BR3 andBR4, are deformed in the same way. The configuration used to assemble them on the Wheatstone bridge is such that only the differences between the two strain gauges can be measured. As a result, the effect of every other force or momentum but the shear force, is not measured.

1.5 Other pedal components design

In the same way as it has been done for the load cell's structure, it is necessary to dimension the other elements of the pedal, in order to verify that the whole structure is resistant to the applied loads. In particular the "U" shaped stirrup and the spindle are subject to the same force that is applied on the load cell, but in a different way. Both these components were dimensioned as it has be done for the load cell, verifying that the applied loads determine a state of tension compatible with the maximum one accepted for the used material. For the stirrup the same alloy used for the pedal was chosen, while for the spindle a carbon steel C40 was used, because this last material has mechanical features that permit to have a great resistance with reduced dimensions of the spindle itself.

1.5.1. The stirrup design

The “U” shape stirrup is the element that connects the load cell with the spindle. It presents four threaded holes to connect it to the load cell and two lateral sockets to mount the ball bearing, to couple it with the spindle.

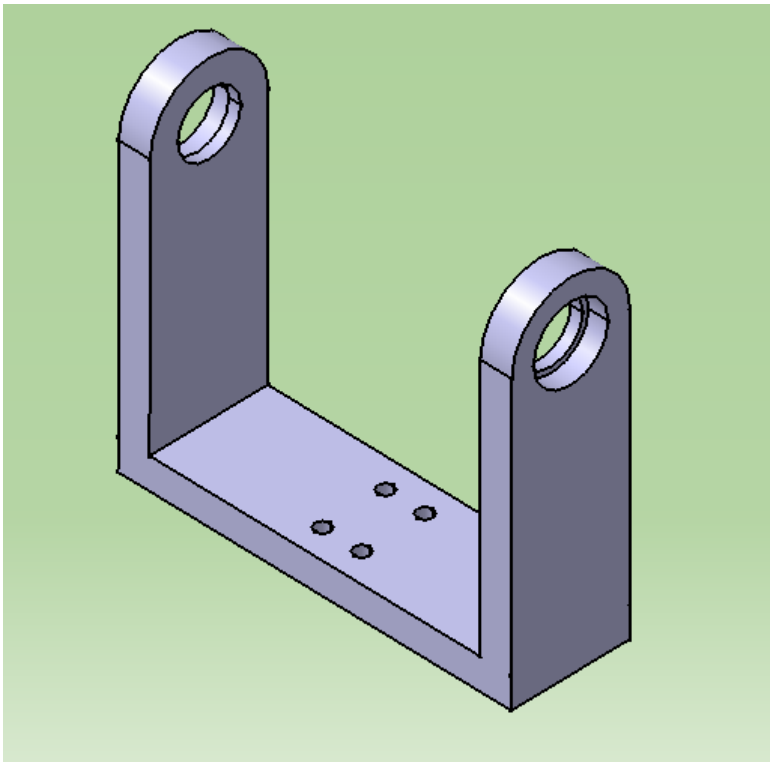

Figure 1.20: The stirrup structure.

Also the stirrup can be schematized as composed of 3 beams. It is possible to consider forces applied on each beam under the action of the two components Fx and Fz applied on the load cell. The load cell and the stirrup are rigidly fixed through 4 screws, so forces applied on the first element are directly transmitted to the second one.

As in the load cell case, it is possible to assume that each beam is subject to the action of forces and torques and it is consequently deformed.

Under the action of Fz, on each equivalent beam of the stirrup internal forces and torques are applied because of rigid constraints, as shown in the free body diagram in the Figure 1.21.

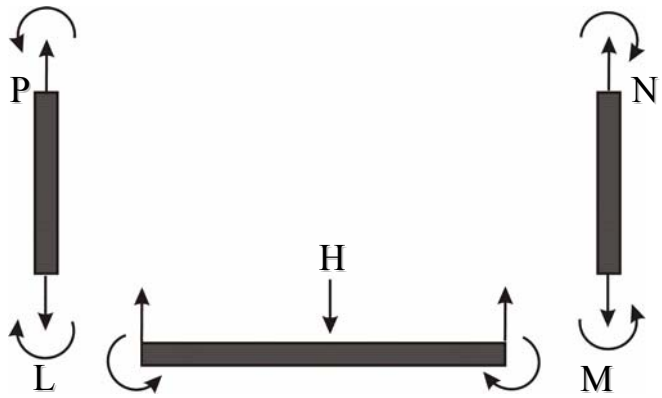

Figure 1.21: Free body diagram of the stirrup under the Fz action.

Considering at first the equivalent beam LM under the action of the component Fz, it presents a maximum bending moment in the points L and M.

The dimensioning has to be done considering the maximum bending moment that is expressed by:

$$\sigma_{Max} = \frac{M_{fMax}}{W} \quad \textbf{1.39}$$

With $M_{fMax} = 50 \cdot F \ N \cdot mm$ and W=320 mm^3 already defined above. So the numerical value yields:

$$\sigma_{Max} = \frac{M_{fMax}}{W} = \frac{50 \cdot F}{320} \ ; \ \frac{1}{6.4} \cdot F \qquad \textbf{1.40}$$

Considering a maximum peak of the Fz of 1000 N equally distributed on each side of the load cell, it becomes:

$$\sigma_{Max} \ ; \ 78 \ N/mm^2 \qquad \textbf{1.41}$$

The condition to be respected is $\sigma_{Max} < \sigma_{ADM}$, with σ_{ADM} maximum strain admissible by the considered material. Also for the stirrup was chosen the aluminium Anticorodal 60 alloy and remembering that has $\sigma_{ADM} = 160 N/mm^2$ the condition is verified.

The beams LP and MN are subject to the same σ_{Max} so these are verified in the same way. It is important to remember that on these beams two holes for the ball bearings are present, but the presence of the spindle justify the hypothesis of having a beam without holes that could be considered as a continuous structure.

If the Fx component is applied on the load cell, the beam LM will be subject to forces that produce a bending moment similar to the case of Fz above described (Figure 1.22). The only difference is the value of W that is higher, because b and h are inverted, so it is W=1200 mm^3. It means that the beam is more resistant to solicitation and considering also in this case Fx=1000N shared on the two sides, the resistance of the structure is verified.

Finally two twisting moments are applied on the beams LP and MN, each with the same value of the bending moment that is applied in the case of Fz. Because it was verified that the two beams are resistant to Fz, those are resistant also to a twisting moment of the same value.

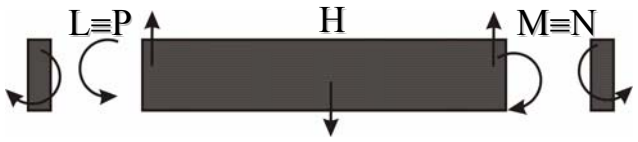

Figure 1.22: Free body diagram of the stirrup under the Fx action (top view).

1.5.2. The spindle design

The pedal spindle represents the element of connection between the stirrup and the crank. It was designed to have a thread that could be fitted in a standard crank. For its realization, carbon steel C40 was chosen, because it grants a good resistance to the bending moment. The shape of the spindle presents a minimum section in the middle, because this part has to pass through the two elements that connect the load cell with the SPD fastening system.

Figure 1.23: the pedal spindle structure.

On the spindle, two forces in the points that connect this with the stirrup through the ball bearings are applied, as consequence of the forces applied on the load cell. These forces determine a bending moment on the spindle. This moment is maximum in the point CR that connects it with the crank (Figure 1.23). In fact, since it is rigidly fitted on the stirrup through the ball bearings, the part PN that is between these last two is subject to a force of compression-extension.

There is a minimum dimension that the spindle must have to resist to this bending moment, which is expressed by the equation:

$$d_{\lim} = 2{,}17 \cdot \sqrt[3]{\frac{M_f}{\sigma_{adm}}} \qquad 1.42$$

Considering that for the carbon steel C40 $\sigma_{adm} = 350 N/mm^2$ and that $M_{fMax} = 50 \cdot F \ N \cdot mm$ it results:

$$d_{\lim} \cong 11mm$$

On the basis of this dimensioning it was chosen a diameter for the section CR d=12mm.

1.5.3. Choice of strain gauges

An important step in the design of the load cell was the choice of the best strain gauges for this application [9]. As a matter of fact, choosing the features and the parameters

of a strain gauge is critical to optimize the performances under specific environment conditions and operational and to get accurate and reliable measures.

The installation and the operation of the strain gauge are influenced by the choice of some parameters, as the features of the material of which it is composed, the material of the support, or the length and the configuration of its grid.

In practice, the process of selection of the strain gauge consists in the determination of a particular combination of parameters with the maximum compatibility with the environment and operational conditions. At the same time they will need to satisfy a set of specifications in terms of installation and operation. Among them, the most important are the precision, the stability, the durability and the smallest possible variations of its features with the temperature. The cost of the strain gauge is generally not significantly relevant, relative to the total cost of the load cell.

The principal factor that determines the characteristics of operation of the strain gauge is the alloy used for the grate. The available alloys from the Vishay Measurements Group, from which the strain gauges used in this project were bought, are: constantan auto-compensated in temperature, isoelasic constantan and karma.

The foil support has important functions: it allows the manipulation during the installation, it furnishes surface to bond the strain gauge to the material and it is an electric isolation between the metallic sheet and the load cell. The materials of support furnished by the Vishay Measurements Group are of two types: the polyimide and the resin epoxide-phenolic, reinforced with fibre of glass.

The length of a strain gauge is the active or sensitive length of the grate, as shown in the Figure 1.24. The length of the strain gauge is often an important factor for the determination of the performance of the strain gauge.

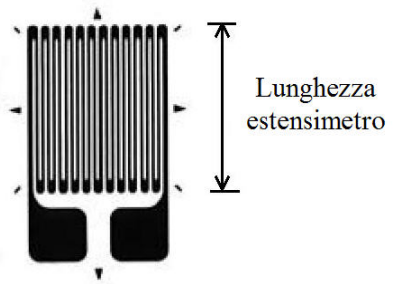

Figure 1.24: Strain gauge active length.

The configuration of the strain gauge refers to the form of the grid, to the number and the direction of grids in multi grid ones, to the configuration of the terminals and various constructive characteristics.

For a single grate strain gauge, the predisposition for a particular application depends from:

- Platforms to be soldered that have to be compatible in dimension and orientation with the available space to the point of installation.
- Width of the grid. If a strong gradient of perpendicular deformation to the strain gauge axis is present, a narrower grid is preferred, but a wider one improves the thermal dissipation and the stability.
- Resistance of the strain gauge. In certain cases the only difference among two available configurations in the same series is the electric resistance, typically 120 and 350 Ω.

On the basis of these considerations, the same strain gauges for the two Wheatstone bridges were chosen. Those are the Vishay CAE-06-240UZ-120 that are strain gauges with a single grid configuration and are constituted by an alloy of constantan with ultra fine support, rolled in polyamide. For both the bridges the strain gauges chosen have an electrical resistance of 120Ω.

1.6 Design of the electronics for Wheatstone bridges

The Wheatstone bridge circuit for the measure of the variation of electrical resistance of the strain gauges associated with deformations of the load cell is shown in Figure 1.25.

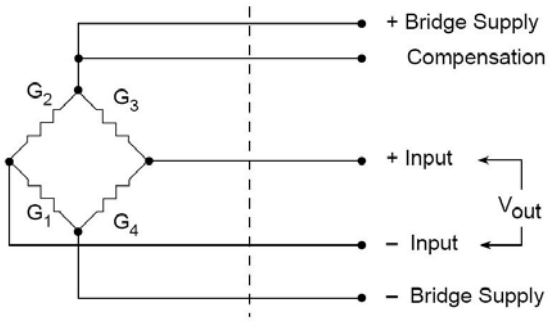

Figure 1.25: Wheatstone bridge channels configuration.

It is possible to notice that the bridge presents five pins of connection: two for the output in presence of bridge unbalancing, two for the power supply and a fifth used to compensate the positive voltage supply of the bridge and to reduce the noise.

Considering the two bridges on the load cell related to the measure of the force components, a commercial integrated device especially designed for strain gauges applications and characterized by low noise, low drift and linear amplification was used.

Generally it could also be possible to have voltage output smaller than 1 mV: in this case, the CMRR needed would be extremely high, and cannot be furnished by a conventional amplifier. This problem has been fixed with an amplifier that removes the common mode voltage, checking the negative tension of reference of the bridge in such a way that the tension to the terminal of negative input pin is always null. Then, for a symmetrical bridge configuration, an equal and opposite negative reference to the positive one is produced, therefore cancelling the common mode voltage.

The advantages of the realized system are:

- No floating supply is necessary.
- Possibility to vary the supply of the bridge from remote, if necessary.
- Independence from the effects of common mode voltage.

- Raised stability of the amplification in DC, which allows realizing many configurations.
- Low noise.
- High speed (for low gains).

The connections of the pins of the strain gauges amplifier are shown in Figure 1.26.

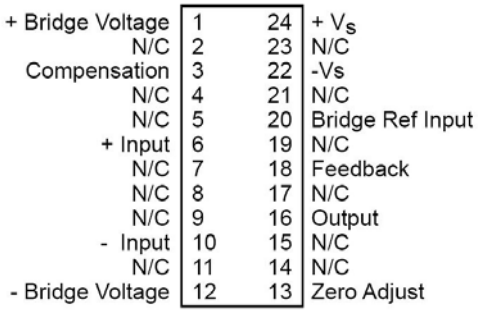

Figure 1.26: Pin map of the strain gauges amplifier.

For the realization of the general circuit of the strain gauge amplifier, a printed circuit was used, conceived and furnished by the RS-Components (code RS: 435-692). On this printed board it is possible to mount the strain gauge amplifier and all the additional components, thus realizing an amplifier/decoder for sensors in resistive bridge configuration. The printed circuit electrical scheme and its layout are shown in Figure 1.27 and in Figure 1.28.

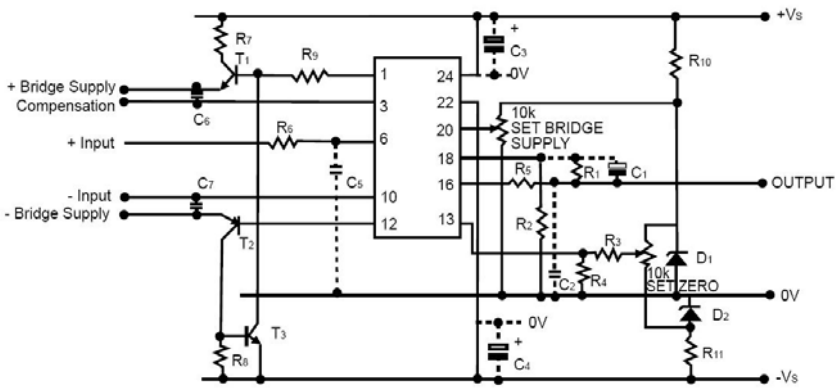

Figure 1.27: Electrical scheme of the circuit for the strain gauges amplifier.

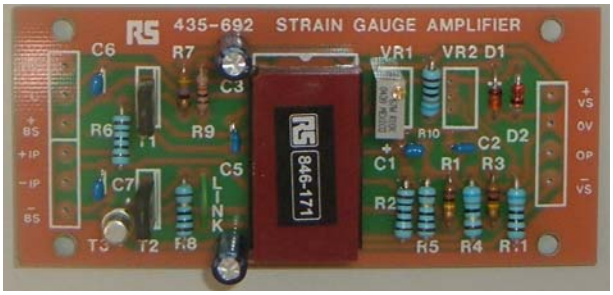

Figure 1.28 Layout of the circuit for the strain gauges amplifier.

The dimensions of each of the 2 assembled cards used for the Wheatstone bridges are 46×98 mm and the position of every component it is marked on them. The nominal values of each component shown in the previous figure are explained in the following chart:

$R_1 = 100\ K\Omega$	$R_{10} = 680\ \Omega$
$R_2 = 100\Omega$	$R_{11} = 680\ \Omega$
$R_3 = 100K\Omega$	$C_1 = C_6 = C_7 = 100\ nF$
$R_4 = 68\Omega$	$C_2 = C_5 = 10\ nF$
$R_5 = 10\ \Omega$	$C_3 = C_4 = 10\ \mu F$
$R_6 = 100\ \Omega$	$T_1 = BD135$
$R_7 = 47\ \Omega$	$T_2 = BD136$
$R_8 = 10\ \Omega$	$T_3 = BC109$
$R_9 = 1\ K\Omega$	$D_1 = D_2 = BZX85 - 6.2\ V$

The values of R1 and R2 give a gain G=1000, according to the following equation:

$$G=1+\frac{R_1}{R_2} \qquad \textbf{1.43}$$

The capacitors C5, C6, and C7 are used to reduce the noise and to slow down the output answer. As it is shown in Figure 1.27, the amplifier is directly fed with the fixed voltage, which is regulated in this case to 9V and has been obtained with two batteries. The bridge is not connected directly to the power supply, but through the two transistors T1 and T2 that drive the necessary current to each bridge, up to a maximum of 60mA and they make it independent from the amplifier. The total feeding of the bridge is equal to twice the reference input (that corresponds to the pin 20).

The two trimmers Vr1 and Vr2 are used, respectively, to regulate the supply of the bridge and to regulate the zero of reference, whose range is:

$$\pm 6.2 \cdot \frac{R_4}{R_3 + R_4} \text{ V.}$$

The strain gauges amplifier used is a good component because it introduces a very low level of noise and it has a ready answer to the exit. The white noise, intrinsic in the amplifier, has been reduced to the minimum using resistors of high quality; it can be reduced with the capacitors C1 and C2, which reduce the bandwidth of operation. The capacitors C3 and C4 mounted in a parallel configuration on the power supply inputs of the amplifier allow to reduce the interferences possibly coming from the power supply itself.

1.7 Pedal Calibration

In order to obtain the measure of force it is necessary to calibrate the instrumented pedal. This operation, that is the same used for force plates used in movement analysis, consists on the assessment of to relationship between electrical signals measured and forces applied to the pedal, moreover it has to be verified if there is cross talk between the two channels of force, that is the presence of signal on channel two due to the action on the other channel. If a pure vertical force is applied on the load plane of the pedal, there is a voltage output on the vertical channel but also on the channel of the horizontal force due to the interaction between the electro-magnetic fields of all the electronic components and the strain gauges positioning inaccuracies.

Ideally, forces should result in a proportional way to the measured electric parameters, but because of the cross talk due to the causes described above the recorded signals on different channels macaws not uncoupled, knows it is therefore necessary to make to calibration procedures. This consists in determining the calibration matrix, that gives the relationship between the vector of electrical measures V=(Vx,Vz) and the vector of the mechanical values F=(Fx,Fz).

In the calibration of the pedal the objective is to determine the coefficients of the calibration matrix [C] that yields the equation:

$$\underline{F} = \underline{\underline{C}} \times \underline{V} \qquad 1.44$$

The matrix of calibration C of the pedal is a 2x2 matrix that is composed of coefficients of direct and cross sensibility.

For the calculation of the coefficients of cross talk the pedal has been rigidly fixed on a plane, during the whole execution of the calibration procedures. Two series of known solicitations were applied along the x (parallel to the plan of the pedal) and z (orthogonal to the plan of the pedal) directions, and monitoring the two outputs of the instrument in order to acquire the correspondence among the forces applied on the pedal and the signals coming from the load cell.

The calibration of the signal related to the channel of the component of the vertical force has been done loading the plan of support with known loads of different values (Figure 3.10).

This operation has been realized starting from the unloaded pedal and, after reading the output in this condition, loading the pedal with a known weight along the axis z (force direction normal to the plan of the pedal).

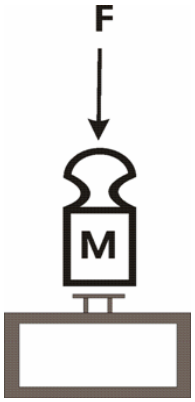

Figure 1.29: Calibration channel related to the vertical component to the pedal

Then the force component has been varied with increasing weights, measuring at every step the outputs of the pedal on both the channels (Chart 1.1: Voltage readings under the different conditions of Fz applying.). In a second phase, the response of the system has been analysed in the following way: a static mass weighting about 200N, and representative of a “new zero” has been loaded on the pedal, and the same set of known forces has been again applied, thus obtaining the difference between the recorded signals. In this way it has been verified that the variation of voltage related to the application of a known force, measured to the output of the Wheatstone bridges, is the same around the two points of work, with the purpose of verifying the linearity of the curve of work load-voltage of the load cell.

Calibration of Fz channel				
Load [N]	Vz [mV]	Vx [mV]	Difference from zero [mV]	
Zero reading.	0,2	-0,2		
+15	15,3	-2,2	15,1	-2
+15	14,7	-1,5	14,5	-1,3
+15	14,6	-1	14,4	-0,8
+15	14,4	-1,7	14,2	-1,5
zero reading with additional load	91	-2,4		
additional load +15N	106,1	-2,5	15,1	-0,1
0	-1	-2,3		
+15	14,3	-2,5	15,3	-0,1
Mean value of the two channels				
			14,77 [mV]	-0,97 [mV]

Chart 1.1: Voltage readings under the different conditions of Fz applying.

The same procedure has been performed for the calibration of the signal of the second channel related to the component of the force applied in parallel direction to the plan of the pedal (Chart 1.2: Readings under the different conditions of load of cut), with the difference that the calibrating force has been applied to the cell of load with the use of a pulley (Figure 1.30).

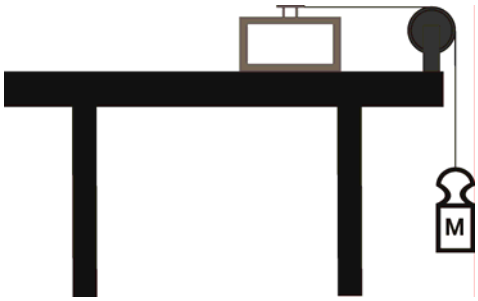

Figure 1.30: Procedure to calibrate the channel related to the horizontal component to the pedal

Fx				
Load [N]	Vx [mV]	Vz [mV]	Difference from zero [mV]	
0	-0,2	-1,2		
+15	53	-2,3	53,2	-1,1
0	-1,3	-2,9		
-15	-64	-2,3	62,7	0,6
0	-1,6	-3,6		
+15	56,7	-3,6	58,3	0
0	-2,4	-4,4		
-15	-63	-4,2	60,6	0,2

with additional load

0	287,5	1,3		
+15	341	2,5	53,5	1,2
0	-301	1,4		
-15	-342	1,7	41	0,3
0	306	1,8		
+15	351	2,4	45	0,6
0	-323	2,2		
-15	-374	2,6	51	0,4
			Mean value of the two channels	
			53,16 [mV]	0,27 [mV]

Chart 1.2: Readings under the different conditions of load of cut

For every measure and for each channel, the mean value of the output voltage has been calculated.

In the case of application of the Fx component on the load plane of the pedal, the outputs on the two channels are:

$$\begin{matrix} Fx = 15N \\ Fz = 0N \end{matrix} \Rightarrow \begin{cases} Vx = 53{,}16mV \\ Vz = 0{,}27mV \end{cases}$$

while in the case of application of the Fz component on the load plane of the pedal, the outputs on the two channels are:

$$\begin{matrix} Fz = 15N \\ Fx = 0N \end{matrix} \Rightarrow \begin{cases} Vz = 14{,}77mV \\ Vx = -0{,}97mV \end{cases}$$

From these results it is possible to observe that the mean value of the signal related to the component that is measured is greater than the one of the other channel, as expected, but also that the mean value of this last is not void, caused by the cross-talk.

A matrix of cross sensibility [CS] has been defined to describe the effects of the loads applied on every output channel. In the matrix every component attributes the sensibility of a channel towards the other:

$$[CS] = \begin{bmatrix} F_x csF_x & F_x csF_z \\ F_z csF_x & F_z csF_z \end{bmatrix} \qquad 1.45$$

Every term on the main diagonal of the matrix refers to the effect of a force on its channel, while the other terms refer to the effect of the cross talk of a channel on the other. FxcsFz for instance refers to the effect that the force Fz has on the channel related to Fx. Knowing these coefficients, it is possible to apply some equations of calibration that allow to calculate the loads applied using the recorded signals on each channels:

$$\begin{cases} F_x = \left(V_x - \dfrac{V_z \times F_x csF_z}{F_z csF_z} \right) \times \dfrac{1}{F_x csF_x} \\ F_z = \left(V_z - \dfrac{V_x \times F_z csF_x}{F_x csF_x} \right) \times \dfrac{1}{F_z csF_z} \end{cases} \qquad 1.46$$

The coefficients of the matrix of sensibility have been obtained simply as the ratio between the mean values obtained on each output and the value of the corresponding calibrating load, so the results are:

$$\begin{cases} F_x csF_x = \dfrac{53{,}16}{15000} = 3{,}54 \times 10^{-3} \left[\dfrac{V}{N} \right] \\ F_x csF_z = \dfrac{-0{,}97}{15000} = -6{,}47 \times 10^{-5} \left[\dfrac{V}{N} \right] \\ F_z csF_z = \dfrac{14{,}77}{15000} = 9{,}85 \times 10^{-4} \left[\dfrac{V}{N} \right] \\ F_z csF_x = \dfrac{0{,}27}{15000} = 1{,}8 \times 10^{-5} \left[\dfrac{V}{N} \right] \end{cases} \qquad 1.47$$

$$[CS] = \begin{bmatrix} 3{,}54 \times 10^{-3} & -6{,}47 \times 10^{-5} \\ 1{,}80 \times 10^{-5} & 9{,}85 \times 10^{-4} \end{bmatrix} \qquad 1.48$$

Replacing these values in the equations of calibration it is possible to evaluate the forces applied to the pedal using the matrix of calibration [C], such that result:

$$\underline{F} = \underline{\underline{C}} \times \underline{V} \qquad 1.49$$

$$\begin{bmatrix} F_x \\ F_z \end{bmatrix} = \begin{bmatrix} C_x & -C_{xz} \\ -C_{zx} & C_z \end{bmatrix} \times \begin{bmatrix} V_x \\ V_z \end{bmatrix} \qquad 1.50$$

$$\begin{cases} F_x = C_x \times V_x - C_{xz} \times V_z \\ F_z = C_z \times V_z - C_{zx} \times V_x \end{cases} \qquad 1.51$$

$$[C] = \begin{bmatrix} C_x & -C_{xz} \\ -C_{zx} & C_z \end{bmatrix} = \begin{bmatrix} \dfrac{1}{F_x csF_x} & -\dfrac{F_x csF_z}{F_x csF_x \times F_z csF_z} \\ -\dfrac{F_z csF_x}{F_x csF_x \times F_z csF_z} & \dfrac{1}{F_z csF_z} \end{bmatrix} \qquad 1.52$$

The matrix of calibration is finally:

$$[C] = \begin{bmatrix} 282{,}17 & 18{,}53 \\ -5{,}16 & 1015{,}23 \end{bmatrix} \qquad 1.53$$

From which the equations of calibration are:

$$\begin{cases} F_x = 282{,}17 \times V_x + 18{,}53 \times V_z \\ F_z = 1015{,}23 \times V_z - 5{,}16 \times V_x \end{cases} \qquad 1.54$$

1.8 Test of force measurement with the instrumented pedal

In this paragraph some samples corresponding to the time series of the angle and of the forces measured with the pedal during a test session are shown. In particular, considering the cycle of pedalling as composed of a phase of pushing with $0°<\theta p<180°$ and a phase of pulling with $180°<\theta p<360°$ (this analysis will be detailed in the following chapters of this thesis) it is possible to provide some insights on the acquired signal and of the possible application of this instrument.

At first, it has been observed that the force profiles and the time series of the pedal angle are in accordance with literature data [6,7,8,13,14], obtained by using different kind of devices. The time series of the pedal angle during each cycle presents some oscillatory variations from the ramp (Figure 1.31). A pure linear time course would indicate a pure translation motion of the pedal reference systems with respect to the laboratory reference system. The oscillations occur because of the movement of flex-extension of the ankle with which the cyclist during pedalling tries to maximize the crank-tangential component of force, which is the one used for the motion, opportunely inclining the foot.

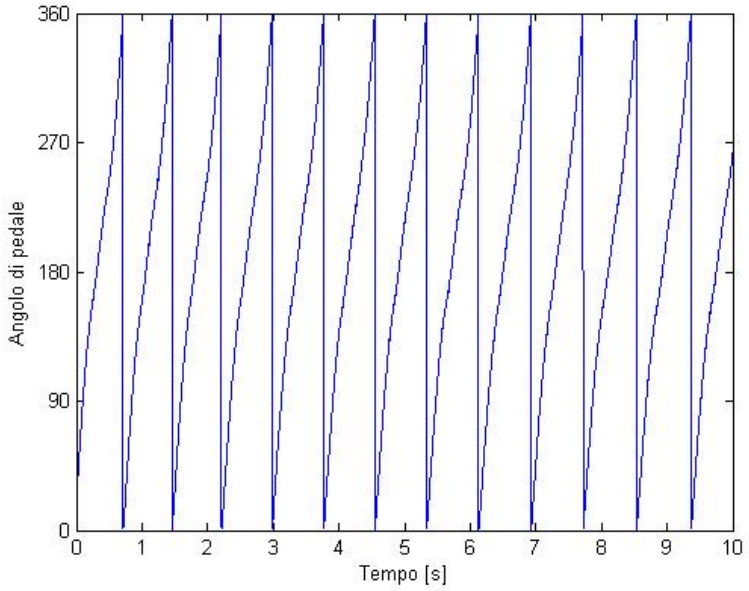

Figure 1.31: Time trend of the pedal angle.

In the following figures, the time trends of the two force components acquired synchronously with the angle are shown.

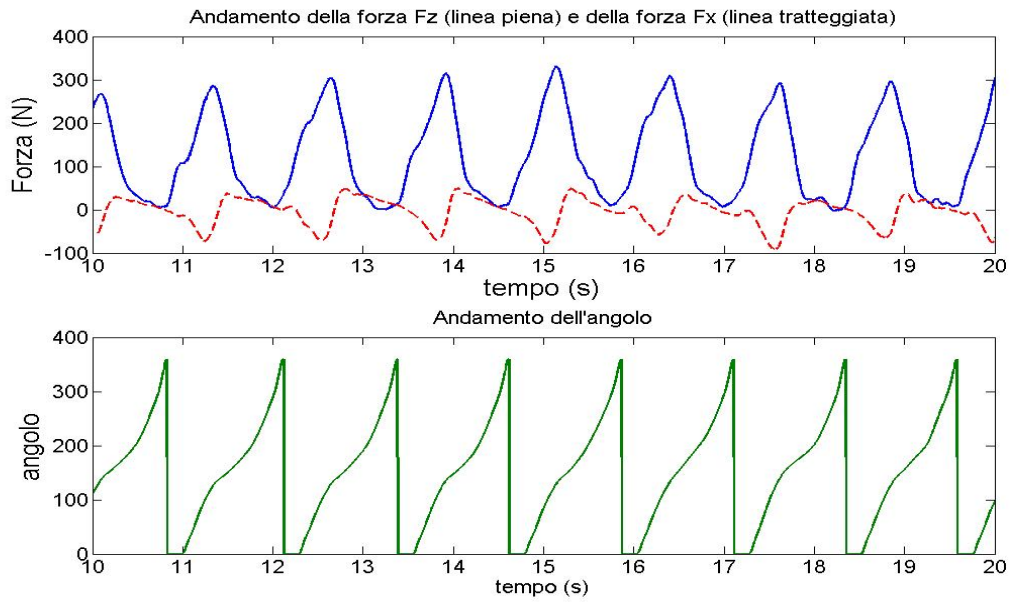

Figure 1.32: Time trends of the force components acquired synchronously with θ_p.

It is possible to notice that the two force components have similar time trends for each pedalling cycle, but the trend of each component is different respect to the other one. The Fz component has a higher peak value than Fx. Its maximum is allocated in the pushing phase, as expected. Regarding the Fx component, it has an alternate trend around the zero, because of the different way of application of the force during the whole cycle. To move the crank, a force along x in both the positive and negative direction of Xp, referring to the RSp, is applied on the load cell.

Using the measures of Fz, Fx, and θp it is possible to obtain the time series of the force components Ft and Fn, respectively tangent and parallel to the crank, using the equations:

$$\begin{cases} F_t = F_z \sin\theta_p + F_x \cos\theta_p \\ F_n = F_z \cos\theta_p + F_x \sin\theta_p \end{cases} \qquad 1.55$$

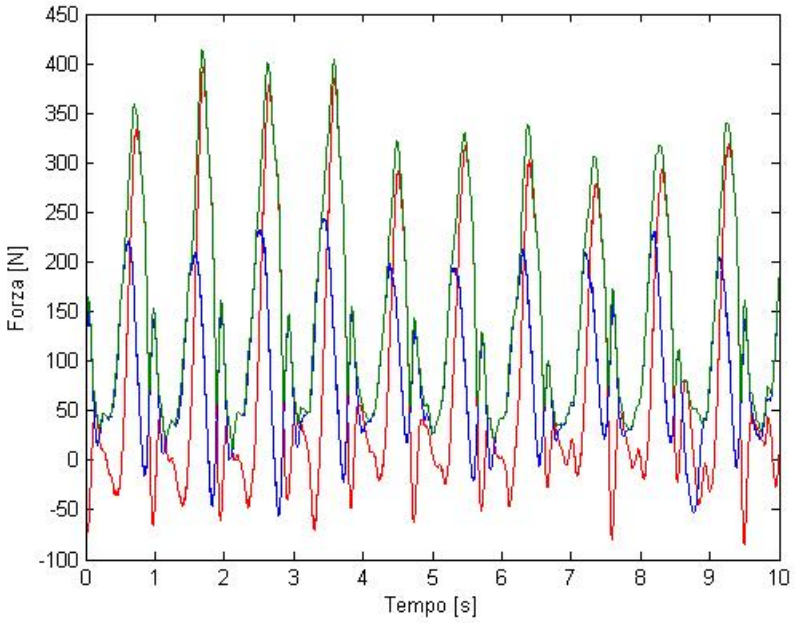

Figure 1.33: Time trends of the force components Ftot (green line), Ft (blue line) and Fn (red line).

Moreover using through the information obtained from the time trend of the pedal angle it is possible to obtain the mean force profiles in the cycle of pedalling.

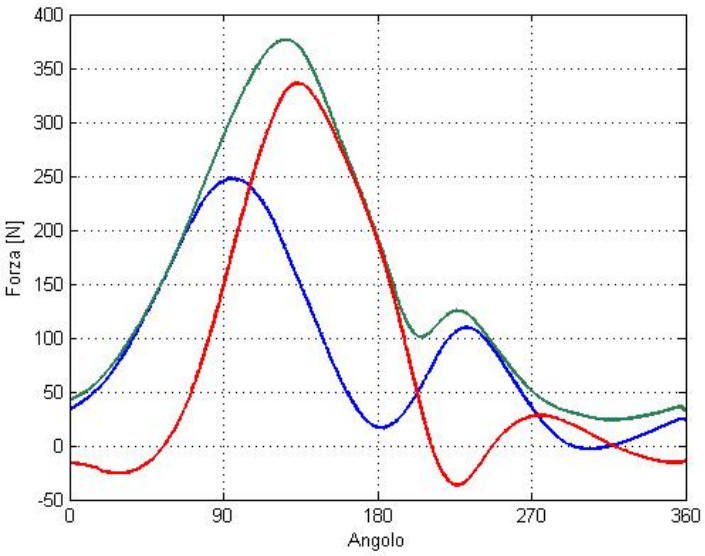

Figure 1.34: mean force profiles in the cycle of pedalling.

With these profiles it is possible to obtain information about the way the gesture is executed, and about the efficiency of pedalling, as it will be described in the following chapters.

2. Combining electrical and mechanical data to evaluate muscular activities during cycling

The quantitative assessment of muscular activity helps in describing the muscular synergies underlying motor tasks' execution through time. A thorough understanding of these synergies correspondingly implies the analysis and the comprehension of the relationships between muscular activity, provided by proper processing of surface ElectroMyoGraphy (sEMG) signals, and biomechanics of cycling, i.e. kinematic and dynamic variables.

In the literature there are many studies that study the relationship between sEMG and force exerted, finding a good correlation in static conditions [18]. However, it is generally acknowledged that this correlation is much more difficult to be established in dynamic conditions, thus preventing a correct assessment of the force contribution of single muscles to the global movement. Therefore, the need for studies on the relationship between sEMG and muscular force is to be stressed.

The present work is intended to deal with this problem, and is part of a wider project aiming at the study of athletes' performance during cycling. In a previous work [19] the authors examined muscular activity of rectus femoris during cycling, and showed how using a pair of electrical indicators, such as mean frequency and amplitude of sEMG signal, it is possible to monitor the instantaneous muscular status in real-time. In particular, the muscular status is represented by a four status code (i.e. force increase, force decrease, fatigue and recovery from fatigue) by considering simultaneously fatigue and force production conditions. Special attention has been devoted to the algorithms used to estimate the electrical indicators [20,21] properly designed to work adaptively on the statistical characteristics of the signals. The proposed monitor can be used to work in real time in order to prevent muscle failure due to fatigue, and thus to examine the loss of force altering the precision of the movement; at the same time, this monitor would allow the motor activity to be continued. Applications in sport, in particular for the analysis of performance and for the improvement of training procedure, should benefit from this approach.

The effective application of the monitor to cycling needs further improvements such as the integrated analysis of several muscles in order to exploit the muscular synergies applied for exercise execution; the measurement of the exerted force in order to predict the muscular force patterns by using an inverse dynamic approach.

Several studies defined muscular synergies by examining either the correlation between muscular activation patterns of pairs of muscles at a given time [22,23] or the order of recruitment within a muscle group [24]. In this sense the synergies were defined and then identified by the correlated changes in certain performance variables: kinematic, dynamic or electromyographic [25,26,27,28].

More recently, muscular synergies have been defined operationally and from a motor control point of view as a task-specific group of muscles that stabilizes specific performance variables [29]. In this direction, it is interesting to identify them as activity patterns of muscles involved in the movement that can change for both biomechanical (e.g. cadence change during pedalling) and physiological modifications (e.g. muscular fatigue).

The sport performance can be improved by learning the proper muscular synergies.

What does it mean to improve the performance in cycling? In cycling, the task efficiency can be evaluated from either a bio-energetic or a biomechanical (i.e. measurement of force applied on the pedal and estimation of the kinematics) [7,13] point of view. Neglecting the bio-energetic interpretation, a good performance is characterized by high values of the effective force exerted on the pedal for a large part of the pedalling cycle. The performance can be modified by several factors (i.e. kinematics, dynamic, physiological): position of the foot on the pedal , application of a different force profile driven by different patterns of muscular activity, muscular fatigue.

An inverse dynamics approach [30] can be used to predict the patterns of muscular force by the measurement of the force exerted on the pedal. The correlation with the muscle activity can be provided by comparing the predicted force pattern to the sEMG signal envelope.

Several studies on muscular force prediction presented in the literature [31,32] neglect the time-varying nature of cycling and consider the exercise as a static task. As a result, they provide single patterns of predicted muscular force and single sEMG envelope obtained by using rectification and low-pass filtering with fixed cut-off frequency. In this way, the necessary modifications of the sEMG processing techniques connected to the changes in the velocity of the execution of gesture (e.g. the length of the low pass filter for the envelope estimation) are not taken into account, thus biasing data processing and hindering actual changes in kinematics, dynamics or physiology. As a result, the interpretation of the results can be even more difficult to undertake.

This work deals with the study of the contribution of lower limb muscles to cycling with particular attention to the changes in muscular synergies due to kinematic, kinetic and physiological modifications. This will be carried on by implementing a classical inverse

dynamics approach to estimate muscular force to be correlated with the electrical indicators on muscular status. In conclusion, the aim is to provide preliminary insights on the possibility of using surface electromyography for the assessment of muscular contributions to motor tasks.

2.1 Materials and Methods

In this work the electrical muscular activity evaluated by processing sEMG signals will be compared to muscular force estimated by a suitable biomechanical model.

This section will be divided into three main sub-sections referring respectively to the biomechanical model, the experimental set-up and the signal processing.

2.1.1. The biomechanical model

The biomechanical model used for the evaluation of muscular forces was built in three steps:

- definition of a kinematic model to evaluate the position of every segment of the leg involved in the gesture;
- definition of a model based on inverse dynamics approach to evaluate the muscular torque for every joint;
- calculation of muscular forces through the data obtained with the two previous steps.

Using an optimization algorithm, a cost function based on a physiological criterion was minimized to predict muscular force patterns.

2.1.1.1 The kinematic model

The kinematic model of the lower limb is composed of constrained rigid elements and mechanical elements of the bicycle, used to transmit the motion to the wheel. By modelling each body segment and each mechanical element as a segment (Fig. 1) it is possible to define a kinematic chain composed by the thigh (segment DE), the shank (segment CD), the foot-pedal (segment BC), the crank (segment AB) and the cycle-frame. The pelvis (point E) was assumed to be fixed to the bicycle frame (point A).

In the sagittal plane, the kinematic chain defines a hinge joint model where the trunk is fixed to the frame and the centre of rotation of the thigh segment is on the seat. The foot and the pedal can be considered as a single element because they are fixed with a clipless pedal

system. The centre of rotation of the crank is fixed on the bicycle frame so that the whole system represents a closed kinematic chain.

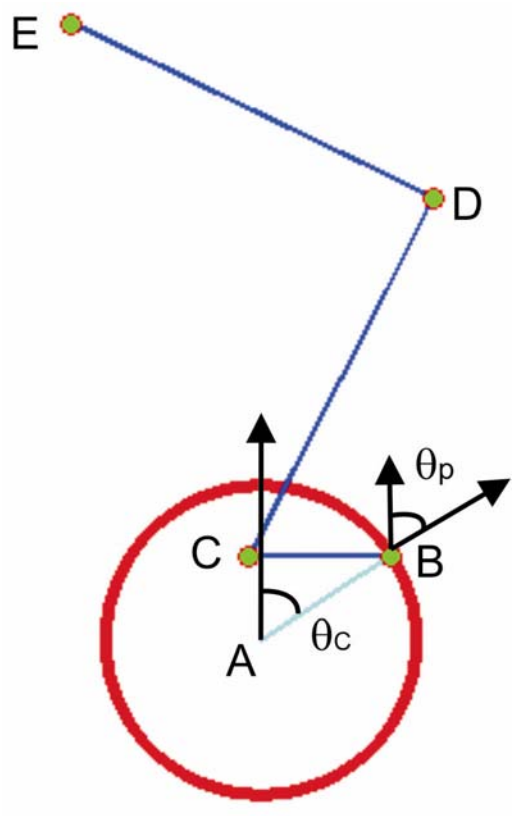

Fig.1: Kinematic chain of the lower limb during pedalling.

The number of degrees of freedom (d.o.f.) is given by:

$$d.o.f.=3(n-1)-2h=2 \qquad (1)$$

where n=5 is the number of chain members each having 3 d.o.f. The bicycle-frame is fixed and then the number of members is reduced to n-1. Each hinge joint (h=number of hinge joints) is a constraint that subtracts 2 d.o.f. to the kinematic chain.

The position of each member in the sagittal plane is determined by the length of each segment together with two angles:

1) the relative rotational angle between the frame of the bicycle and the crank, θ_C;

2) the relative rotational angle between the crank and the pedal, θ_P.

The length of each segment of the model was determined by measuring directly the body segments, the length of the crank, and the distance between the centre of rotation of the crank and the seat.

2.1.1.2 The Dynamic model

The kinematic data obtained in the previous analysis and the forces exerted on the pedal during pedalling (measured as explained in the following paragraph 2.2) were used in an inverse dynamic analysis to obtain the joint moments at ankle, knee and hip. In particular, a free body diagram approach was used. The moment of inertia, the location of the centre of mass and the mass of each segment, needed for the calculations of the joint moments, were estimated from height and mass of the athletes by using equations defined in the literature [33,34].

2.1.1.3 The muscle model

The muscular model considers nine muscles of the leg: tibialis anterior (TA, ankle flexor), soleus (SO, ankle extensor), gastrocnemius (GA, ankle extensor, knee flexor), vastii (VA, knee extensor), rectus femoris (RF, knee extensor, hip flexor), short head of biceps femoris (BFs, knee flexor), long head of biceps femoris (BF, knee flexor, hip extensor), iliacus (IL, hip flexor), and gluteus maximum (GLM, hip extensor).

The number of equations is not sufficient to calculate muscular force values. However, the number of the muscles can not be reduced because they are all needed to describe the biomechanics of the gesture. By considering the gesture as a sequence of simple motor tasks, each of the modelled muscles is responsible for a single motor task. In the real gesture this motor task is performed by several muscles, called synergists, which are all represented by the "equivalent" muscle of the model. The reason for this modelling is that all synergists for the respective "equivalent" muscle of the model have the same activation patterns in cycling as reported in the literature [30].

The relation between muscular moments and muscular forces for every joint considered in the model is given by the equation:

$$\sum F_i \cdot d_{ij} = M_j \qquad (2)$$

where Mj represents the muscular moment for the j-th joint, Fi is the muscular force exerted by the i-th muscle and dij is the effective moment arm of the i-th muscle from the j-th joint. The values of muscular moment arms were calculated as a function of the joint angle on the basis of the equation reported in [35].

The muscular forces implied were calculated by minimizing the cost function:

$$U = \sum_{i=1}^{9} \left(\frac{F_i}{PCSA_i} \right)^3 \qquad (3)$$

with the equality constraints given by the equation (2), and with the following inequality constraints:

$$0 < F_i < F_{iMAX} \qquad (4)$$

where F_i is the unknown force of the i-th muscle, $PCSA_i$ is the physiological cross sectional area of the i-th muscle, F_{iMAX} is the maximum force of the i-th muscle, and M_j and d_{ij} have yet been defined.

The cost function was chosen from the literature [36,37], as the one that best predicts muscular forces considering co-activation of all the muscles involved in the gesture. The exponent used in the equation (3) is based on the relationship between the endurance and the force of the muscles and depends on the specific subject. The cubic exponent guarantees the best tradeoff between the muscular contractile force and the maximum duration of the contraction.

The optimization problem was solved by a routine for the minimization of constrained functions present in the Optimization ToolBox of MATLAB (@The Mathworks, Inc.). Muscular forces were estimated on the basis of the signals acquired in the experimental tests.

2.1.2. Experimental setup

The experimental protocol consisted of pedalling on a cycling simulator for sessions about 50 minutes long. The pedalling cadence was fixed at 70 rounds per minute (rpm). The session ended with a sprint followed by a recovery phase. The cycling simulator is equipped with an aerodynamic brake at the wheel, in order to provide a linear relationship between the pedalling frequency and the resistance offered during exercise.

Acquisition of sEMG signals from RF, BF, TA and SO of the dominant leg was carried on by using circular sEMG electrodes (6 mm diameter and 20 mm electrode spacing, centre-to-centre) and double differential probes.

Simultaneous acquisition of dynamic data was allowed by a the instrumented pedal desribed in Chapter 1 [38] designed to be compliant with a commercial pedal (i.e. Shimano

Pedalling Dynamics SPD™ cleats) and mounted on the cycling simulator. The strain gauge load cells mounted on the pedal allow the measurement of force components exerted on the pedal. Moreover the angular displacement of the pedal, θ_P, was measured by a linear single-turn precision potentiometer placed between the pedal frame and the pedal spindle, while the angular displacement of the crank, θ_C, was measured by an encoder that uses the bicycle transmission gear.

Mechanical and sEMG signals were recorded by a movement analysis system (StepPC©, DEM-Italy) with a 2000 samples/s sampling rate and 12 bit A/D converter.

2.1.3. Signal Processing

Recorded signals were processed for different phases of the training session. In particular, the following five one-minute long different phases were considered: the warm-up, two standard situations respectively after 10 and 20 minutes of exercise, the sprint phase, the final phase.

sEMG signals were processed in order to obtain envelope and mean spectral frequency. Adaptive and automatic algorithms, already developed by some of the authors, were used in this analysis. In particular, for each h-th sEMG signal sample, the amplitude a(h) and the mean power frequency f(h) have been calculated:

- a(h) has been obtained as in [20] by rectification and low-pass filtering of the signal, with adaptive filter length determined as proposed in [39,40];

- f(h) has been calculated as in [21] by iteratively estimating the complex covariance function on a moving window, which for this study has been set at 2 seconds. The window length has been chosen as the best tradeoff between time resolution and variance of estimation.

The mean pedalling cycle for each phase has been considered in order to obtain the mean amplitude envelope of sEMG signal and to compare it to the force profile obtained by the biomechanical model.

Quantitative comparison between the amplitude envelopes of sEMG signals and the force profiles has been carried on as explained in the following. For the different phases of the training session two time series have been extracted: they are constituted by the mean values of both envelopes (ME(n)) and force profiles (MF(n)) calculated for each pedalling cycle. Two different curves, obtained by a cubic polynomial interpolation, have been estimated for both ME(n) and MF(n). The similarity between the two curves has been assessed by using the Pearson's correlation test.

Moreover the mean spectral frequency has been calculated for each phase of the training session. This value, together with the one related to the signal amplitude, has been used to code the muscular status as in [19], by using the following coding:

- the simultaneous increase of both amplitude and mean spectral frequency is coded as a force increase;
- the simultaneous decrease of both amplitude and mean spectral frequency is coded as a force decrease;
- the increase of the amplitude and the decrease of the mean spectral frequency is coded as muscular fatigue;
- the increase of the mean spectral frequency and the decrease of the amplitude are coded as recovery.

2.2 Results and discussion

Results are provided for a single experimental case in order to show the feasibility of the approach. Statistical purposes are outside the scope of this work.

In Fig. 2 a sample of recorded signals is provided for the warm-up phase of the training session. The sEMG signals of RF, BF, TA and SO are drawn together with the two components of the force exerted on the pedal and the two angles θ_P and θ_C. In Fig. 3 a sample (5 seconds) of muscular forces estimated by the model is provided for the same phase as shown in Fig. 2.

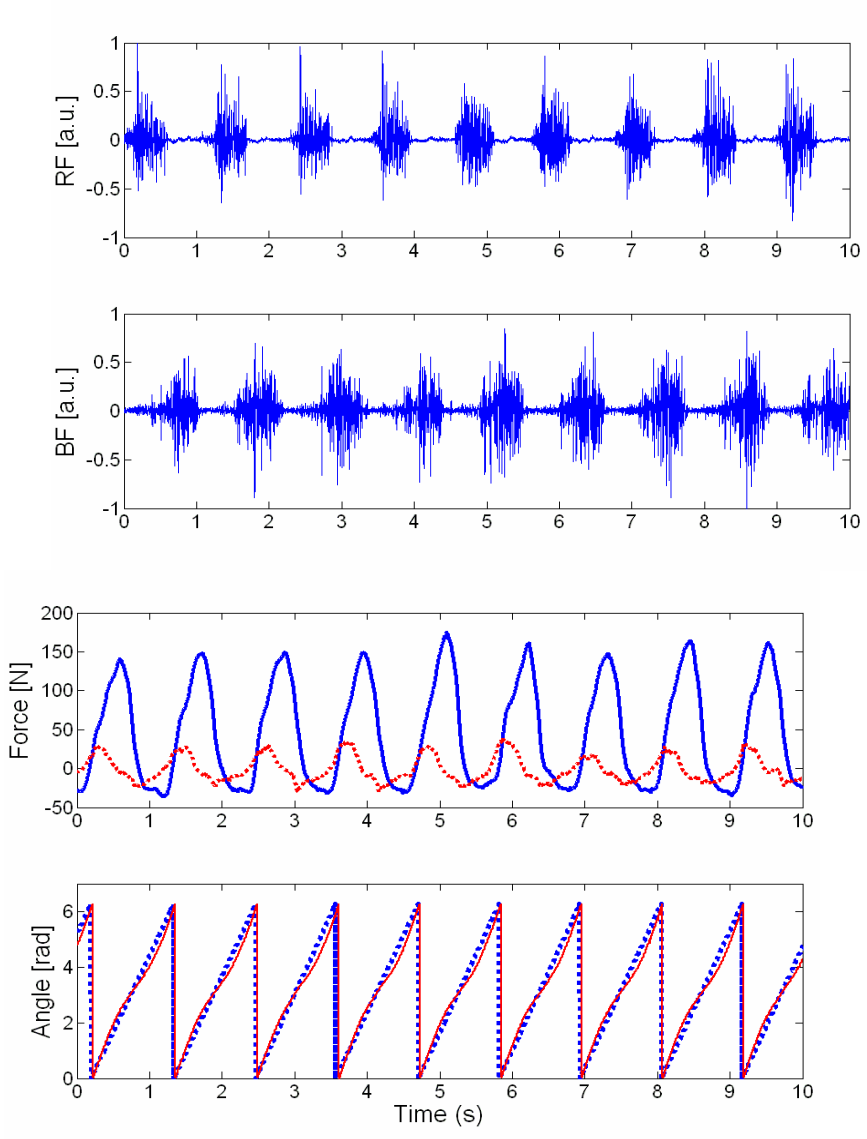

Fig.2: Recorded signals during the warm-up phase of the training session: from the top, normalized raw sEMG of RF, BF vertical (solid line) and horizontal (dotted line) pedal force components, crank angle θ_C.(dotted line) and pedal angle θ_P (sold line)

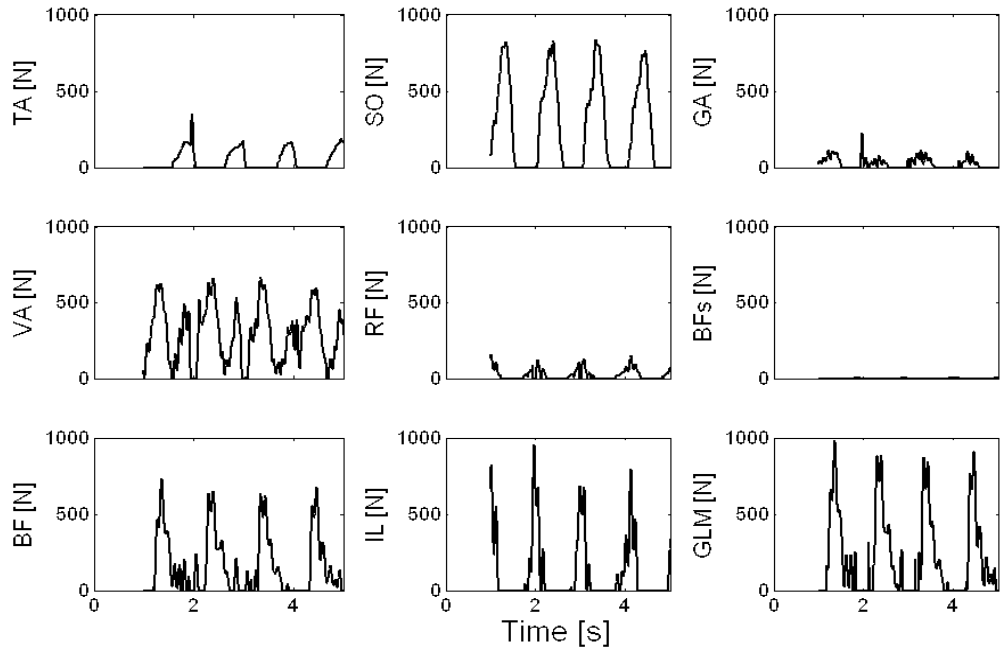

Fig.3: Muscular forces estimated by the model for the nine muscles.

From now on the results will be presented for BF and RF muscles.

In Fig. 4, the force profiles provided by the biomechanical model and the corresponding mean envelopes of sEMG signals for the BF muscle are presented with reference to the five exercise phases described in the previous paragraph.

The trends are drawn with respect to a normalized pedalling cycle. Since BF and RF activate in an antagonistic way, the choice of a single reference cycle would hinder the visualization of one of the profiles (on the same cycle BF presents the maximum activation about at the 40% while RF presents its activation pattern across the 0% of the cycle). Fig.5 reports the two reference systems chosen to describe the pedalling cycle of the BF and RF muscles respectively.

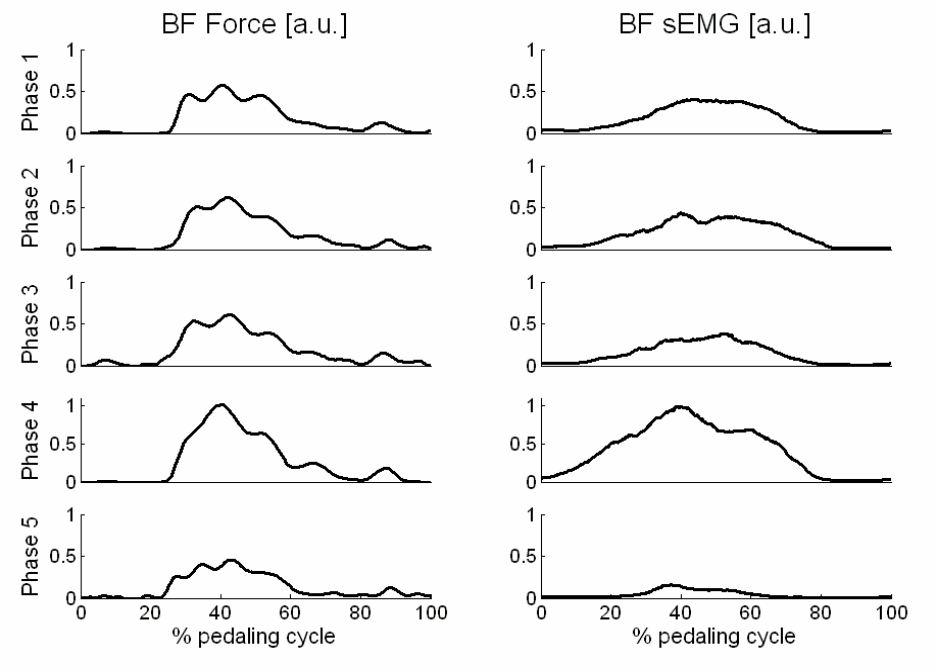

Fig. 4: Force profiles and sEMG envelopes for the BF muscle.

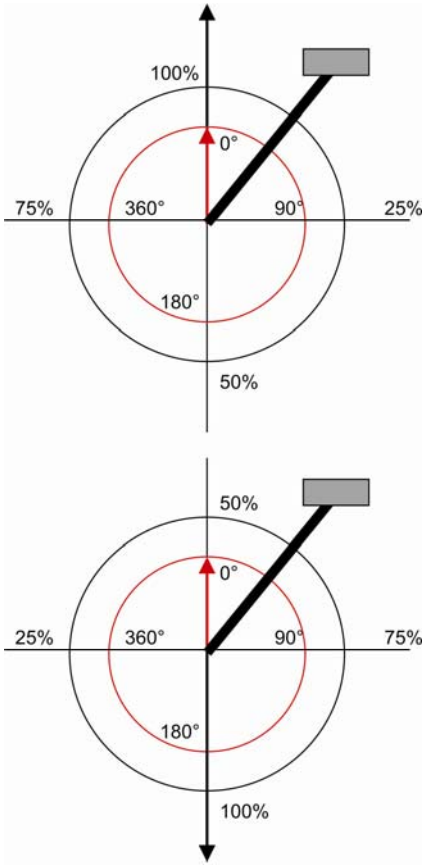

Fig. 5: Reference systems for pedalling cycle: BF (top) and RF (bottom).

In Fig. 6 the force profiles provided by the biomechanical model and the corresponding mean envelopes of sEMG signals for the RF muscle are presented with reference to the five exercise phases, as in Fig.4.

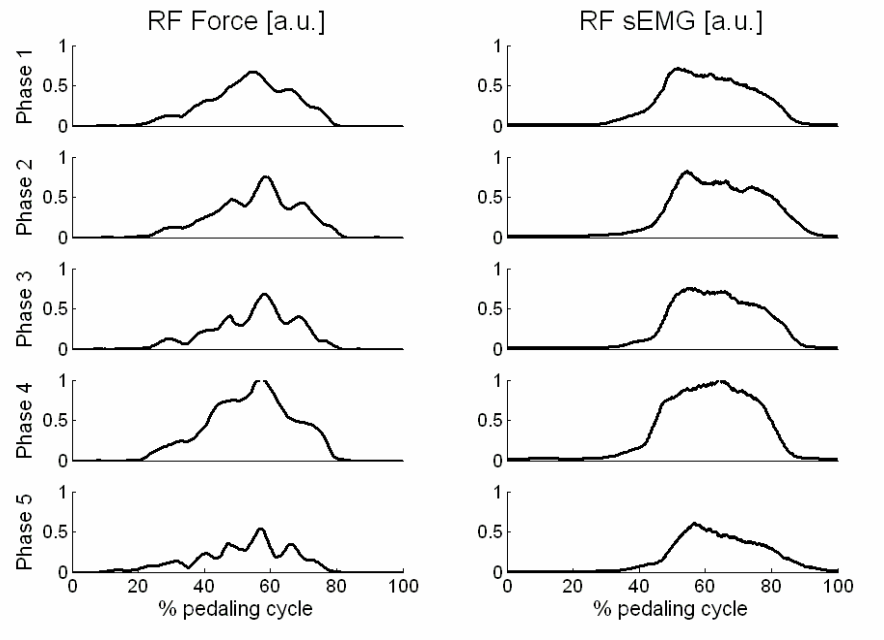

Fig. 6: Force profiles and sEMG envelopes for the RF muscle.

In Table 1, the mean values of the force profiles are provided.

	Muscular force (N)	
	RF	**BF**
Phase 1	32.4	139.0
Phase 2	32.0	140.5
Phase 3	26.6	159.0
Phase 4	49.7	225.5
Phase 5	21.4	112.5

Table 1 – Mean values of the muscular force for RF and BF muscles obtained by the biomechanical model, for the different phases of the training session. Values are expressed in newton.

The mean envelopes of sEMG compared to the muscular force profiles show a good agreement with special reference to the modifications in the amplitude occurring in the different exercise phases.

The quantitative comparison between the amplitude envelopes of sEMG signals and the force profiles obtained by the biomechanical model can be expressed in terms of correlation coefficients provided by the Pearson's test. In Table 2, the correlation coefficients are reported for each phase and for the RF and BF muscles.

Pearson's correlation coefficient		
	RF	**BF**
Phase 1	0.66	0.88
Phase 2-3	0.99	0.98
Phase 4	0.94	0.91
Phase 5	0.8	0.99

Table 2 –Pearson's correlation coefficient obtained by comparing the cubic polynomial curves obtained by ME(n) and MF(n) for each phase of the training session and RF and BF muscles respectively.

A good agreement between electrical and mechanical profiles is shown in Fig.7, where ME(n) and MF(n) are drawn together with the respective cubic polynomial approximations, for a trial corresponding to the phase 3 of a training session.

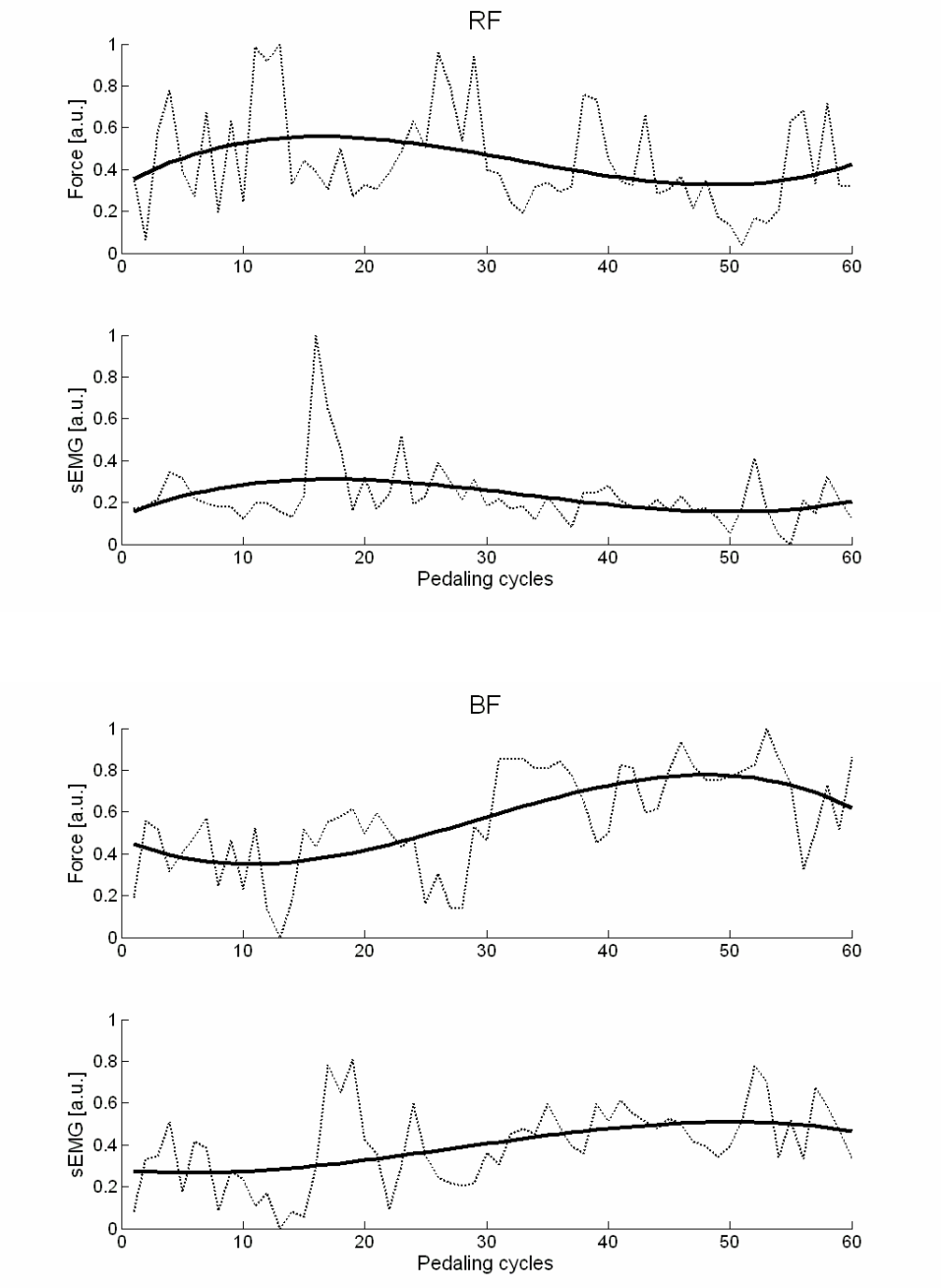

Fig. 7: From the top to bottom: MF(n) and ME(n) with the respective cubic polynomial approximations, for RF and BF muscles. Data are referred to a trial corresponding to the phase 3 of a training session.

The values of the mean spectral frequency and the mean values of the sEMG amplitude envelopes are provided in Table 3.

Muscular Activity				
	Mean Frequency (Hz)		Amplitude (A.U.)	
	RF	**BF**	**RF**	**BF**
Phase 1	83.3	80.6	0.7	0.4
Phase 2	85.4	85.5	0.8	0.4
Phase 3	83.5	86.5	0.7	0.3
Phase 4	83.3	90.8	1.0	1.0
Phase 5	81.1	80.8	0.5	0.1

Table 3 – Values of the mean power frequency (Hz) and of the mean value of the amplitude for a mean pedalling cycle (Arbitrary Units) for the different phases of the training session.

In order to validate the muscular activity coding provided by the electrical indicators, the profiles of muscular force estimated by the biomechanical model have to be considered.

Looking at Table 2, it is worth to outline how the electrical indicators (i.e. mean spectral frequency and amplitude) code the muscular status, especially for phases 4 and 5 related to the sprint and the recovery. In phase 4 the muscular code provides a force increase (simultaneous increase of amplitude and mean spectral frequency) for BF, while in phase 5 both muscles can be coded in the force decrease status (simultaneous decrease of amplitude and mean power frequency). This result is confirmed by the muscular forces estimated by the biomechanical model, as it is shown in Fig. 4 and in Table 1 (phase 4 presents the highest force values, phase 5 presents the lowest force values).

2.3 Conclusions

In this work a preliminary study on the contribution of lower limb muscles to cycling has been presented. Particular attention has been devoted to the analysis of changes in muscular synergies due to kinematic, kinetic and physiological modifications. To this purpose a time-varying analysis has been carried on, by analyzing different temporal phases of a pedalling training session.

A classical inverse dynamic approach has been implemented and different patterns of muscular forces have been estimated for all the modelled muscles and for different phases of the cycling exercise. At the same time, sEMG signals have been processed in order to estimate the muscular status and to compare this "electrical estimate" to the muscular forces obtained from the biomechanical model. The processing of sEMG signals has been carried on by using optimized adaptive algorithms.

Preliminary results show the effectiveness and the feasibility of the approach. In particular, the correlation between the force exerted and the sEMG envelope has been put in evidence, together with substantial agreement of the biomechanical model with the muscular code obtained by electrical indicators estimated from sEMG signals. This conclusion opens a wide field of applications as sEMG signals allow to have information on muscular force and to assess motor performance by means of a non-invasive approach.

Temporal analysis of the force and of the sEMG amplitude profiles appears a valid investigation line in order to better understand the changes in muscular strategies. However, future work must be directed toward a wide experimental campaign aiming at the statistical validation of the approach which the first results declare very promising.

3. Muscular fatigue from electromyographic recordings: real-time monitoring during exercise training

Standard definition of localized muscular fatigue relies on mechanical deficit occurring as a consequence of prolonged or exhausting body exercises. In facts, as stated in [41], muscular fatigue can be described as "any exercise-induced reduction in the maximal capacity to generate force or power output". Then, the occurrence of muscular fatigue can be monitored by measuring force or power output.

However, the mechanical deficit is the consequence of physiological modifications connected to muscles metabolism. Many activities, related to rehabilitation, ergonomics and athletes training could greatly profit from a timely indication of physiological modifications driving to muscular fatigue. The most common indication is provided by blood lactate measurements: these are invasive and typically imply the stop of the exercise execution.

Surface electromyography (sEMG) provides an indirect measurement of muscular fatigue: in fact, the amplitude and the mean spectral frequency of sEMG signal can be considered as electrical indicators of the physiological modifications preceding fatigue.

Several studies showed that these indicators provide valuable information during fatiguing protocols characterized by isometric and force-constant contractions (i.e. static conditions). The modifications of the electrical parameters associated to muscular fatigue are the following: the signal amplitude increases [42÷46] and the signal spectrum shifts toward the low frequency band [47÷54]. In these conditions each parameter provides a proper indication of fatigue.

When the force production during the exercise cannot be kept constant, even if the variation is slow such as in semi-static conditions, the parameters loose their reliability because they do not only depend on fatigue state, but also on the force production. Thus, it becomes mandatory to control the current level of force production together with the fatigue signs.

Since muscular status depends on both force and fatigue, the electrical parameters have to be simultaneously monitored. Luttmann and coworkers [55,56,57], proposed a protocol,

called Joint Analysis of EMG Spectrum and Amplitude (JASA) aiming at coding muscular status on the basis of simultaneous modification of electrical parameters. They applied JASA protocol in essentially static protocols (i.e. ergonomic studies) giving rise to the following coding: 1) simultaneous increase of amplitude and mean frequency: force increase; 2) simultaneous decrease of amplitude and mean frequency: force decrease; 3) decrease of mean frequency and increase of amplitude: fatigue; 4) increase of mean frequency and decrease of amplitude: recovery.

However the detection of muscular status from sEMG signal [58,59,60] during dynamic protocols is an unsolved problem. Possible solutions are related to the availability of techniques working in real-time (i.e. during exercise execution) and in an adaptive way with respect to the statistical nature of the signal. In fact, sEMG signal recorded during movement is characterized by sources of non-stationarities mainly resulting from the time-varying relationship between force and length of muscles, and from the typical displacement of the sensor with respect to the underlying muscle fibres.

Objective of this study is the analysis of muscular fatigue during dynamic protocols. The study has been carried on by developing a real-time monitor for fatigue detection, based on the simultaneous estimation of mean frequency and amplitude of sEMG signal. The estimation is based on processing adaptive techniques purposely developed by some of the authors [20,21], whose implementation has been modified in order to work in real-time.

The monitor performance have been tested in a field condition, by analyzing signals recorded during spinning sessions in order to assess the approach during extended, sub-maximal training events.

3.1 Materials and Methods

The real-time monitor for muscular fatigue is mainly based on:

- the simultaneous estimation of amplitude and mean spectral frequency (i.e. the electrical indicators of muscular status) of sEMG signal;

- the evaluation of the modifications occurring in the indicators with respect to reference values corresponding to the warm-up period.

The amplitude estimation in dynamic conditions is provided by the algorithm presented in [20], where the authors proposed a technique to extract the envelope of sEMG signal by using filters chosen adaptively according to the time-varying signal characteristics.

In particular, the estimator consists of a whitening block, a detector (order ν) and a smoothing filter, and sEMG signal is modelled as $s(h) = \alpha^{\xi}(h)n(h)$, where $\alpha(h)$ is a modulating waveform representing muscular activity related by ξ to the electrical signal, and n(h) is a member of an ergodic gaussian process.

All the estimator parameters are obtained by minimizing the mean square error of the estimation [40],

$$\varepsilon^2(h) = E\{(\alpha(h) - a(h))^2\} \qquad (1)$$

where a(h) is the estimate of the amplitude $\alpha(h)$.

In [39], the authors demonstrated that the minimization of (1) provides the optimal value of the smoothing filter length. In [39,40] for the case of a symmetrical (non-causal) smoothing filter, the optimal value of the filter length in correspondence to the h-th sample of the signal is given by:

$$M(h) = \left[\frac{9\varphi(\xi,\nu)}{(\xi\nu - 1)^2}\right]^{1/5}\left[\frac{a(h)}{\dot{a}(h)}\right]^{4/5} \qquad (2)$$

where $\dot{a}(h)$ represents the estimate of the first derivative of a(h), and

$$\varphi(\xi,\nu) = \frac{1}{\xi\nu^2}\left[\frac{\sqrt{\pi}\Gamma(\nu + 0.5)}{\Gamma^2(\nu + 0.5)} - 1\right] \qquad (3)$$

with Γ(.) the Euler gamma function.

The optimal filter length is obtained by an iterative procedure whose convergence has been theoretically demonstrated in [20].

The mean spectral frequency estimation is provided by the algorithm presented in [21] where the authors used the derivatives of the complex covariance function to obtain the moments of the signal spectrum.

In particular, the mean spectral frequency is calculated as:

$$f(h) = \frac{1}{2\pi j}\frac{\dot{C}(h)}{C(h)}\bigg|_{h=0} = \dot{\theta}(h)\big|_{h=0} \qquad (4)$$

where

$$C(h) = |C(h)|e^{j2\pi\theta(h)} = \frac{1}{2N+1}\sum_{k=-N}^{N} s^{+}(h)(s^{+}(h+k))^{*} \qquad (5)$$

is the complex covariance function estimated on a window (2N+1) samples long, with $s^{+}(h)$ being the analytical signal of s(h).

The mean spectral frequency for every signal sample (i.e. h-th sample) is obtained by using an iterative procedure for the complex covariance function estimation:

$$\tilde{C}(h) = R(h) + P(h) + F(h) \qquad (6)$$

where:

$$\begin{aligned} R(h) &= s^{+}(h)(s^{+}(h-1))^{*} \\ P(h) &= \sum_{i=1}^{N} w^{i} R(h-i) = \\ &= w(P(h-1) + R(h-1)) - w^{N+1} R(h-N-1) \\ F(h) &= \sum_{i=1}^{N} w^{i} R(h+i) = \\ &= w^{-1} F(h-1) - R(h) + w^{N} R(h+N) \end{aligned} \qquad (7)$$

represent respectively the contributions of the samples in the window preceding and

following the h-th sample. w=(N-1)/N is a weight factor, depending on the number N of signal samples contributing to the covariance estimate.

The monitor evaluates muscular modifications by comparing the percentage variation of the indicator pair {a(h),f(h)} (i.e. Δa%, Δf%) with respect to reference values representative of a no fatigued muscular status. The latter has been considered as that occurring during the warm-up period preceding the exercise session.

The working status of the muscle has been coded as in the following:

if Δa%, Δf% are both positive the muscle increases the exerted force;

if Δa%, Δf% are both negative the muscle decreases force;

if Δa% is negative and Δf% is positive the muscle is recovering;

if Δa% is positive and Δf% is negative the muscle is going into fatigue.

Spinning training sessions have been used to test the approach. Ten able bodied subjects, with different training levels, volunteered for a spinning session, around 50 minutes long. The exercise session is composed of several tasks characterized by different combinations of body posture and percent resistance of the flying wheel (RFW%), referred to the maximum resistance offered by the brake.

sEMG signals have been acquired by using a movement analysis system (StepPC©, DEM-Italy), also used to record simultaneously cardiac activity and angular displacement at knee joint. Signals were acquired at 2000 samples/s and digitized by means of a 12 bit A/D converter.

Sensors positioning on the dominant leg is drawn in Figure 1. Circular sEMG electrodes (6 mm diameter and 20 mm electrode spacing, centre-to-centre) have been positioned on rectus femoris of the dominant leg, while ECG probes were positioned by using Lead I configuration (positive electrode on the left arm, negative electrode on the right arm). Double differential active probes have been used to record sEMG and ECG activity. The electrogoniometer, positioned on the knee of the dominant leg, can measure angles in range (–170°÷170°).

The percentage of Heart Rate (HR%) with respect to the Maximal HR (MHR=220-age) has been calculated from ECG signal. The cycling frequency is obtained by the angular signal as a Revolutions Per Minute (RPM) value.

The fatigue monitor, running simultaneously to the signal acquisition, provides the experimenter with on-line information on muscular status, cardiac frequency and cycling speed. Data were hidden to the exerciser to prevent biofeedback that was not in the aims of the present work.

3.2 Results

The real-time monitor has been tested on signals acquired during spinning exercises sessions.

Muscular activity is represented on a "work-plane" where any of the four quadrants (covered anti-clockwise) is representative of the following conditions: force increase, recovery, force decrease and fatigue. Every point that will be drawn on the plane will represent the muscular status ($\Delta a\%(h)$, $\Delta f\%(h)$) at the time h.

Results are presented by using a panel, which is shown in Figure 2, where muscular status on the work-plane (sub-panel (a)) sEMG signal (sub-panel (b)), RPM time series (sub-panel (c)), and HR% time series (sub-panel (d)), are simultaneously drawn. The background of sub-panels (b), (c) and (d) presents different textures related to the different quadrants of the work-plane. Moreover, in sub-panel (a) each point is drawn by using a gray-scale (black to white) to code temporal information (black is the starting point, white is the ending point).

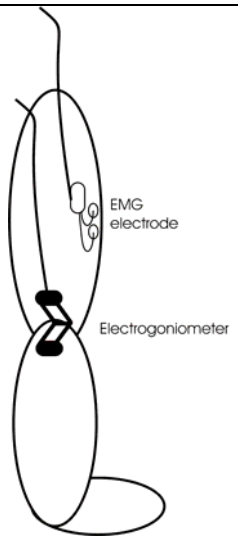

Figure 1: Positioning of sEMG electrodes and of the electrogoniometer

Figure 2 reports the analysis of a spinning session portion (i.e. 110 seconds long) characterized by a transition from a "jump on the hill" to a "running" task, when subject pedals in standing position. The task transition can be described by using the nominal values of the exercise variables: velocity 90-100 RPM in task 1 9, 55-60 RPM in task 2, HR% 85% in task 1, 70% in task 2, flying wheel resistance 70 RFW% in the final end of task 1, 30 RFW% in task 2. The analysis provides the following results:

sub-panel a: muscle status evolves through all the four conditions. At the beginning of

the first task, the subject increases the force exerted as it is shown by the percent increase of both amplitude and mean frequency up to respectively 60% and 9%. Going on with the first task, a fatigue status is reached, even if mixed with some force decrease symptoms: mean frequency decreases up to 5%. At the task transition, the muscle starts exerting less force due to the recovery time which divides the two tasks, and both signal amplitude and mean frequency decrease respectively by the 60% and the 10%. After the 75-th second of the observation period, the muscle goes into recovery before exerting force at the beginning of the second task.

- sub-panel b: sEMG signal changes its structure according to the physiological muscular status. In both tasks where muscular status is coded as force increase (initial and final epochs of the signal) the signal structure presents high bursts continuous through time. When muscular status is coded as fatigue, mean frequency decreases by the 10% of the value of the warm-up, and bursts structure appears discontinuous. In force decrease status bursts are small and short. The recovery status shows an increase of both duration and amplitude of the bursts.

- sub-panel c: cycling speed decreases from 100 RPM to 55 RPM, at around 35 seconds. At this stage the flying wheel resistance is diminished by the subject in order to recover from the first task thus justifying a force decrease status.

- sub-panel d: HR% is high during first task (about 85%) but it starts decreasing at the exercise transition when flying wheel resistance decreases and less force is required by the motor task. At the end of the force decrease status, HR% is about 77% and reaches a plateau until the force generation status is reached again when HR% starts increasing.

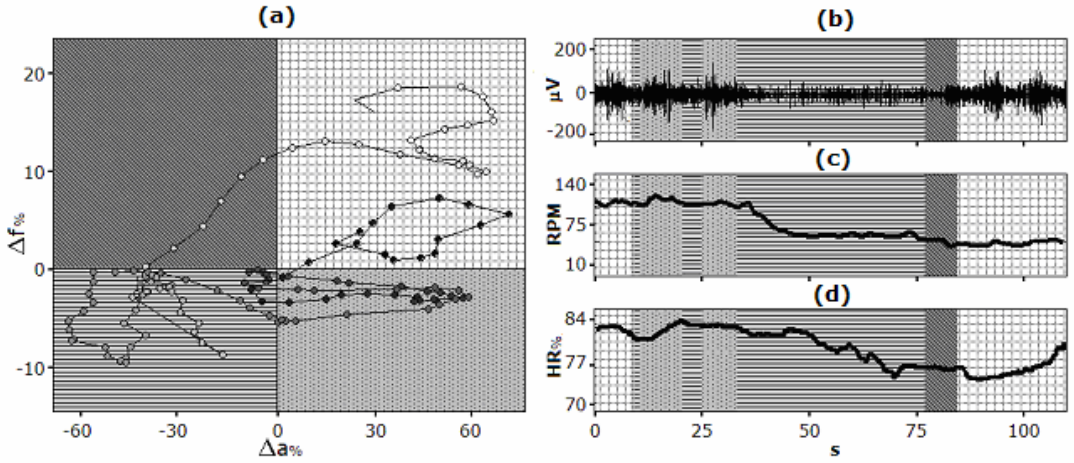

Figure 2 Report of exercise monitoring: A) sEMG signal, B) RPM value, C) HR%, D) muscular status on the work plane.

3.3 Discussion and conclusions

Preliminary results obtained with the proposed monitor appear encouraging for muscular monitoring during prolonged exercise training.

Since the computational complexity of the algorithms is limited, the monitor provides real-time information related to localized muscle fatigue. The properness of the estimation techniques, already demonstrated in previous works, guarantees the consistency of results. Moreover, the possibility of monitoring simultaneous changes of frequency and amplitude of sEMG signals guarantees the use of the monitor in on-field situations, without controlled force conditions.

The obtained results show the effectiveness of the approach in real exercise situations, and the monitoring of HR and RPM data confirms the validity of the indications on muscular status provided by the monitor. In fact, it clearly emerges that insights on muscular conditions are in agreement with both cardiovascular trends and training conditions.

In conclusion, this study proposes a new way of monitoring muscular fatigue from experimental myoelectric signals recorded during dynamic protocols.

The importance of such an approach is related to the prevention and management of muscle failure due to fatigue. In fact, muscle failure prevents force to be produced as needed and alters the precision of the movement. Then, indication of muscular fatigue is needed to quantify the time for performing a certain activity without reaching the state of immoderate fatigue and preventing the person to continue the activity.

For all these reasons the fatigue processor becomes an interesting tool for a wide range of activities, such as the follow-up of sports training efficiency, but also for ergonomic analyses, and monitoring of therapeutic methods' efficiency in rehabilitation.

4. The pedal force measure as a mean to reliably estimate maximal muscle power

4.1 Context

Maximal muscle power is a relevant physiological measurement to provide valid information on the training status of individuals as well as the ability to perform physically demanding activities [61]. To his aim, it is generally estimated during an all-out pedalling action lasting a few seconds.

Maximal power is a variable closely related to athletic performance and many athletes are trained to increase muscle power to enhance performance. In addition, there are general fitness benefits and rehabilitation advantages from increasing maximal muscle power. It has indeed been shown that improvements in maximal muscle power are accompanied with an increase in functional ability in elderly women [62,63].

Maximal muscle power can be measured through a variety of techniques. For example, established methods of measuring maximal power are vertical jumps and Nottingham Power Rigs. All of them, though, restricted the ability of the subject to produce maximal power since they make use of either body weight or a flywheel with a fixed inertia, which can restrict the ability of the muscle to operate at the optimal force and velocity for maximal power output [64]. Other instruments include friction braked cycle ergometers, which have the advantage that the load can be adjusted to allow the muscle to work at its optimal force and speed for maximal power production [65]. However, the latter ones suffer from a main flaw, that is that they require the use of instrumented flywheels [66], which are not commercially available. Another technique uses stereophotogrammetry to measure the acceleration of a flywheel of a friction braked cycle ergometer [67].

The availability of an instrumented pedal to measure forces exerted by the athlete at the foot level, unveils the possibility to measure maximal muscle power from the force information. Following this end, the purpose of the work here presented is to test the reliability and validity of this new method based on a direct measure of power, and comparing it against a kinematic based indirect estimation based un stereophotogrammetric recordings. The same comparison was made for the torque components.

4.2 Materials and methods

The experimental campaign of this portion of the work has been done in collaboration with the Sport and Exercise Science laboratory of the Strathclyde Institute of Pharmacy and Biological Sciences, University of Strathclyde, Glasgow, Scotland.

In the following details on the participants recruitment, the equipment used, and the acquisition procedure are provided, together with information on the analysis of data, and on the statistics.

4.2.1. Participants

In this campaign, eight healthy men (age 28.5 ± 5.2 years; stature 1.78 ± 0.04 m; body mass 77.0 ± 11.5 kg; mean ± SD) and eight healthy women (age 23.1 ± 3.4 years; stature 1.65 ± 0.06 m; body mass 60.4 ± 5.0 kg; mean ± SD) volunteered for the study. They were free from any current muscular or joint injury and cardiovascular or metabolic disease.

Participants were required to be exercising at least three times per week and advised not to alter their current training program during the course of the study. Every effort was made to ensure that they attended the laboratory at the same time of day. The study was approved by the Ethics Committee of the University of Strathclyde in Glasgow. The participants read a description of the background, procedures and risks of the experiment and then provided written consent to participate, with them being free to withdraw from the experiment at any time.

Both genders were taken into account, since in literature it is acknowledged that gender differences will influence performance of physical tasks. To take into account gender differences in the model, several researchers investigated techniques to normalise for fat free mass (FFM), for dynamic strength and for percentage fat or a combination of these. As a corollary to the study, it will be possible to check if gender differences are present.

4.2.2. Stereophotogrammetry

To indirectly estimate the power from motion capture data, three reflective markers were placed equidistance around the edge of the flywheel of a Monark ergometer. A reference marker was placed midway between these markers to allow subsequent identification and consistency to be kept between the labelling of markers. Two further markers were placed on the pedal and the centre of the crank, to obtain both flywheel speed and pedal angle. All markers were 1cm in diameter and placed on the left hand side of the bike. Kinematic data were collected using a five camera system (Vicon M2 California, USA) at 250Hz. This system was calibrated both statically and dynamically on a daily basis, setting

the thresholds not to repeat the calibration at 1.5mm for mean residual and at 0.5% for static reproducibility, respectively. A two dimensional sagittal plane analysis was performed on the data. Power (W) was calculated from 3d kinematics of each marker, after low pass filtering (Butterworth, 4th order, cut-off frequency 8 Hz), digital double differentiation and post-acquisition digital low pass filtering (cut-off 20 Hz).

4.2.3. Instrumented pedal

The instrumented pedal described in Chapter 1 was used to collect 2 components of the reaction force vector. Details on calibration are shown in the same Chapter. For this experimental campaign, the sampling rate was set at 1000 samples/s, and data were low pass filtered at 20 Hz, thus maintaining the same post-acquisition scheme of 3d kinematics.

4.2.4. Experimental procedure

Participants were required to attend the laboratory on three occasions, each lasting approximately one hour, the first session was used for familiarisation. Four to six days elapsed between sessions. Five minute warm up of sub-maximal cycling (100-150W) and six second sprints against frictional loads of 0.25 and 0.75 N.kg-1 were followed by a five minute rest, participants then were tested for the maximal resistance to complete two pedal revolutions, which will be referred to as 2-revolution maximum (2RM). Starting from the load at which the participants could not move the pedals, the load was reduced by 0.5 kg decrements until the participants were able to complete two pedal revolutions, using only

their right leg. Then, in order to ensure that the selected load was the actual maximum, the participants were required to perform further attempts increasing the load by 0.5 kg increments. Three minutes of rest were allowed between each attempt during the strength trials.

After five minutes of rest period, the participants performed 30 seconds of continuous cycling at 30% of their 2RM at 60 rpm. This trial was repeated three times with at least three minutes rest between trials.

After another five minute rest period, individuals then performed a series of six second sprints against two resistances (20% and 50% of 2RM). Three trials were performed at each load with at least three minutes rest between trials. These trials were administered in a random order.

4.2.5. Data processing

Power calculations through motion analysis

The inertial properties of the flywheel were obtained from the manufactures manual. The two components that made up the actual load on the flywheel were calculated from the method proposed by Lakomy (1986), these are:

1) the frictional load applied to the flywheel;
2) the excess/inertial load that must be overcome to accelerate the flywheel.

The frictional load was given by the weights placed in the basked on the Monark ergometer.

The excess load was calculated by placing a known resistance against the flywheel (ranging from 1 to 3 kg) and accelerating the flywheel up to 120rpm. The time taken for the flywheel to stop (deceleration of the flywheel) was plotted against the frictional load and a regression equation was obtained (Chart 1). The product of the frictional load and excess load yields the actual load being applied to the flywheel.

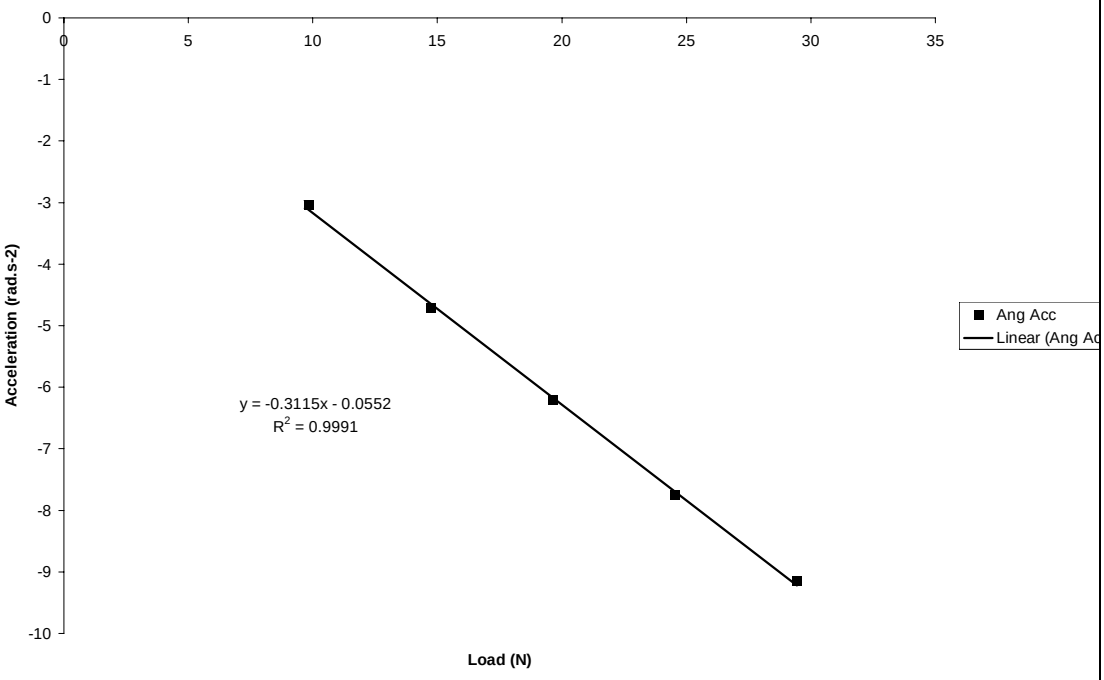

Chart 1: Flywheel deceleration as a function of frictional load

Power calculations through force transducers

Force data were projected on to the crank reference system, as described in Chapter 1. The force component which is tangential to the crank was taken into account to determine the torque with respect to the chain driver.

From the crank angle data, also the power at the crank level was estimated, according to the equation:

$$P = T \cdot \omega$$

Where T is the torque at the chain driver and ω is the angular velocity of the chain driver.

Both torque and power were then transformed into their equivalent at the flying wheel level by considering the gear ratio.

4.2.6. Data analysis and statistics

From both the torque and the power time series, selected parameters were extracted. Those were the mean value of the power and of the torque, averaged over 3 seconds, and 6 seconds, respectively, and the peak of both the torque and the power.

These latter ones were checked for skewness and kurtosis to choose whether to use parametric or non-parametric tests. As data were normally distributed (all values less than $|2|$), validity was assessed using paired Student's t-tests (two tailed) and associated 95%

confidence intervals (95% CI) was used to examine systematic bias between the two different methods of mechanical power measurement.

Reliability was assessed using Coefficient of Variation and Intraclass Correlation Coefficient.

4.3 Experimental results

In the following, selected results on the comparison between the different methods of maximal muscle power and torque are shown.

During constant speed trials (figs 1+2), motion analysis recorded higher power outputs than force transducers on average by 11.7 W ± 1.2 on day 1 in male subjects. This difference was 14.7 W ± 0.8 on day 2 in male subjects. For female subjects during constant speed trials, motion analysis recorded higher power outputs than force transducers on average by 5 W ± 0.4 on both day 1 and 2.

Pearson's correlation co-efficient was on average 0.904 ± 0.09 in males and 0.959 ± 0.03 in females.

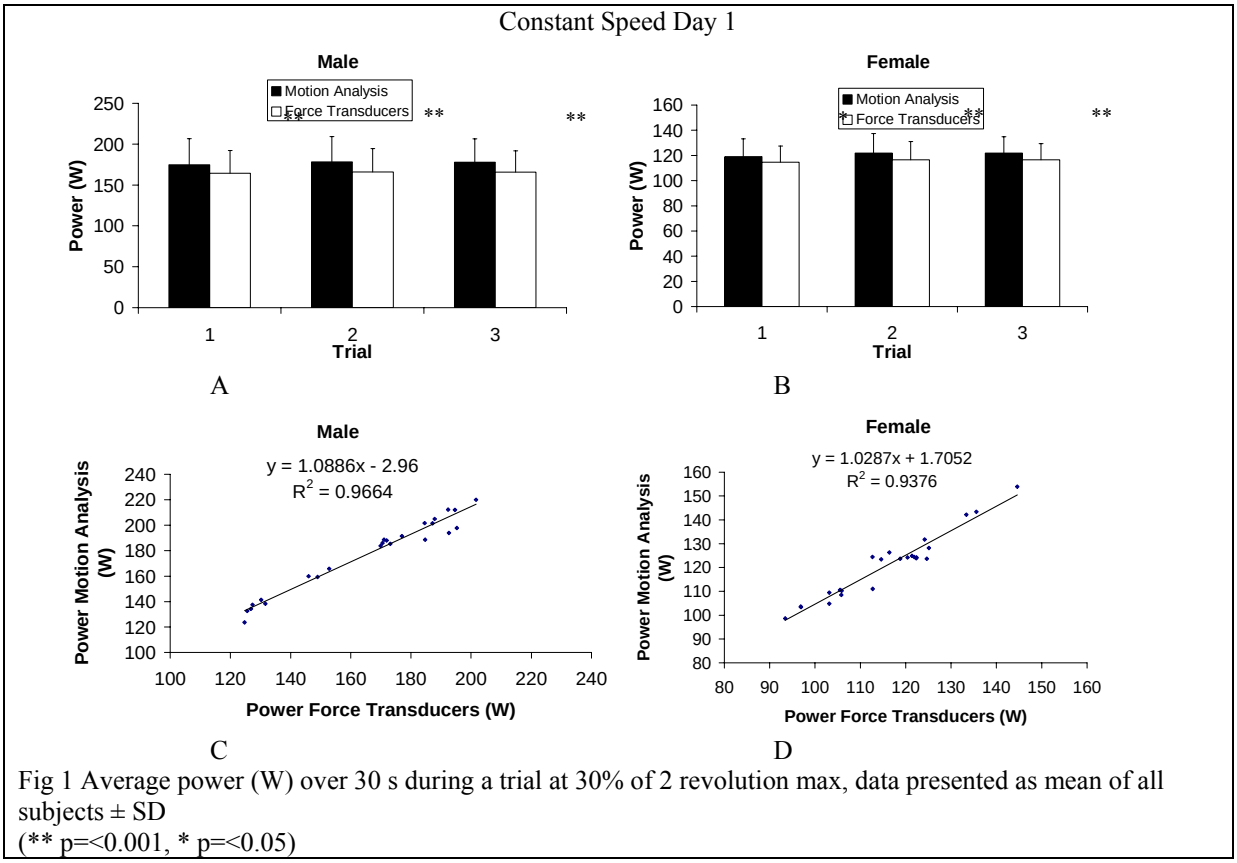

Fig 1 Average power (W) over 30 s during a trial at 30% of 2 revolution max, data presented as mean of all subjects ± SD
(** p=<0.001, * p=<0.05)

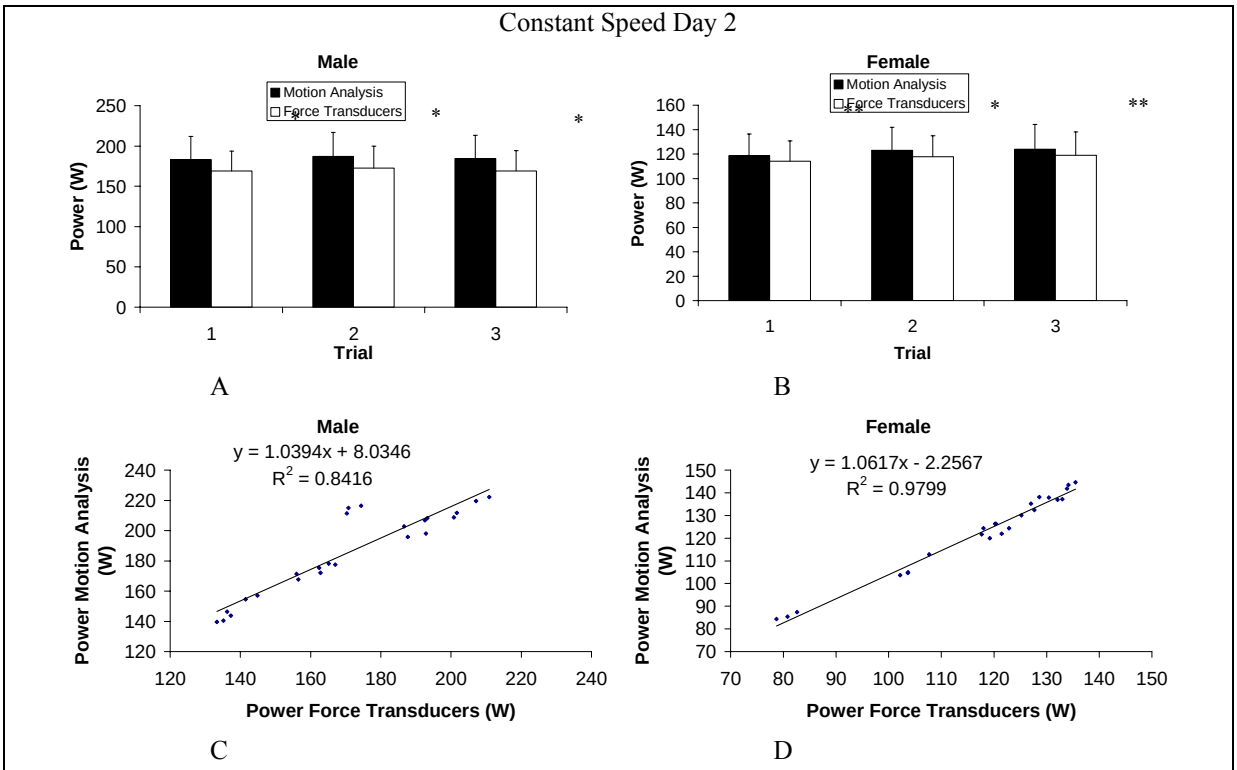

Fig 2 Average power (W) over 30 s during a trial at 30% of 2 revolution max, data presented as mean of all subjects ±.SD (** p=<0.001, * p=<0.05).

During trials at 20% of 2RM when data was averaged over 6 seconds (figs 3+4), motion analysis recorded higher power outputs than force transducers on average by 32W ± 2.4 on day 1 and by 37.2 ± 2.1 on day 2 in male subjects. For female subjects during trials at the same load, motion analysis was on average 15 W ± 0.3 and 13.7 W ± 0.9 higher than force transducers on day 1 and 2 respectively.

Pearson's correlation co-efficient was on average 0.917 ± 0.01 and 0.987 ± 0.01 in males and females respectively

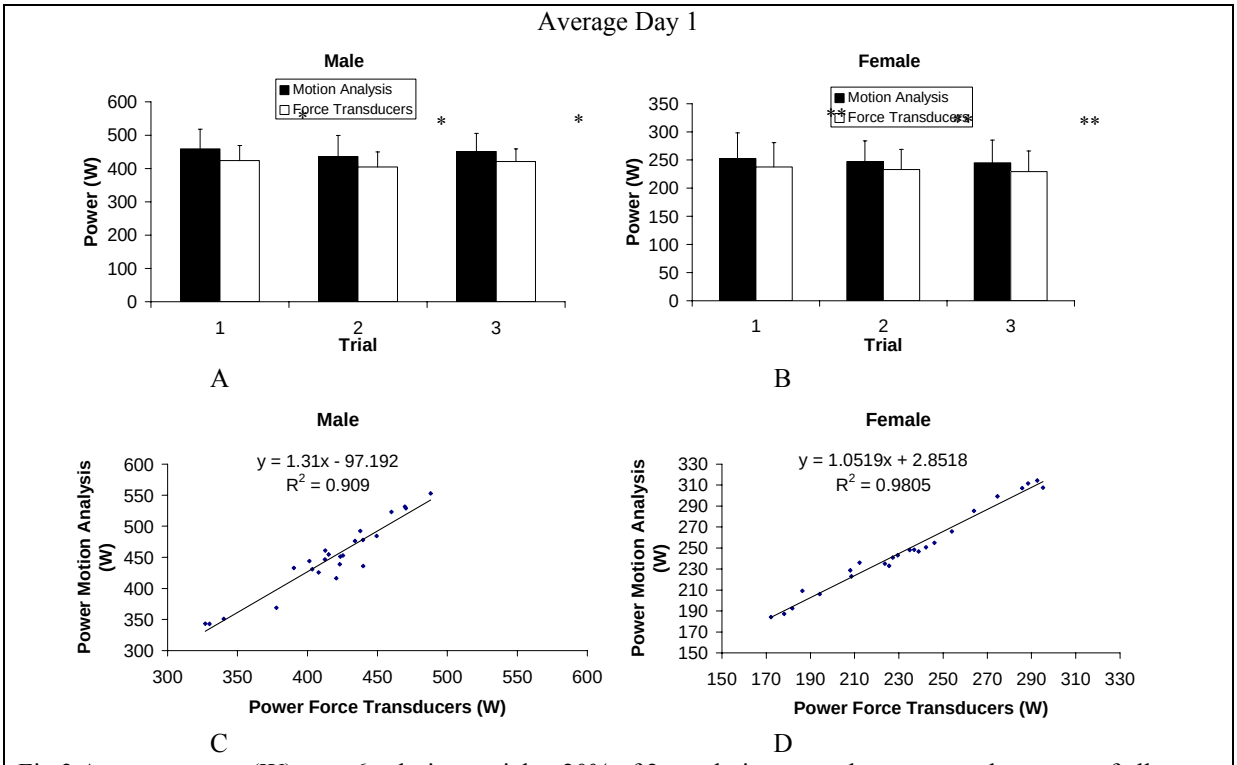

Fig 3 Average power (W) over 6 s during a trial at 20% of 2 revolution max, data presented as mean of all subjects ± SD (** p=<0.001, * p=<0.05)

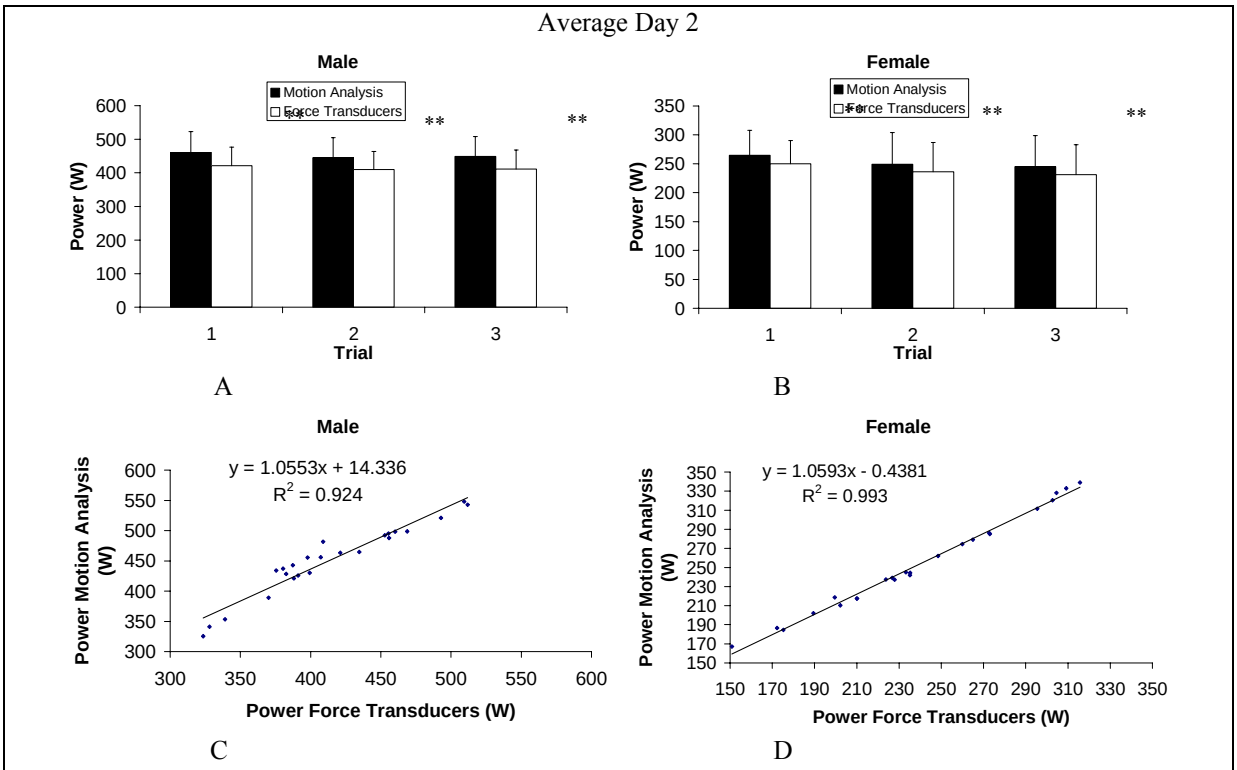

Fig 4 Average power (W) over 6 s during a trial at 20% of 2 revolution max, data presented as mean of all subjects ± SD (** p=<0.001, * p=<0.05)

When power was averaged over the 3 highest peaks and the load was 20% of 2RM (figs 5+6), motion analysis recorded higher power outputs than force transducers on average by 48.7 W ± 2.4 and by 55.3 W ± 3.5 on day 1 and 2 respectively in male subjects. Motion analysis recorded higher values than force transducers on average by 22.6 W ± 2.1 and 21 W ± 1.5 on day 1 and 2 respectively in female subjects.

Pearson's correlation co-efficient was on average 0.951 ± 0.004 and 0.971 ± 0.01 in males and females respectively.

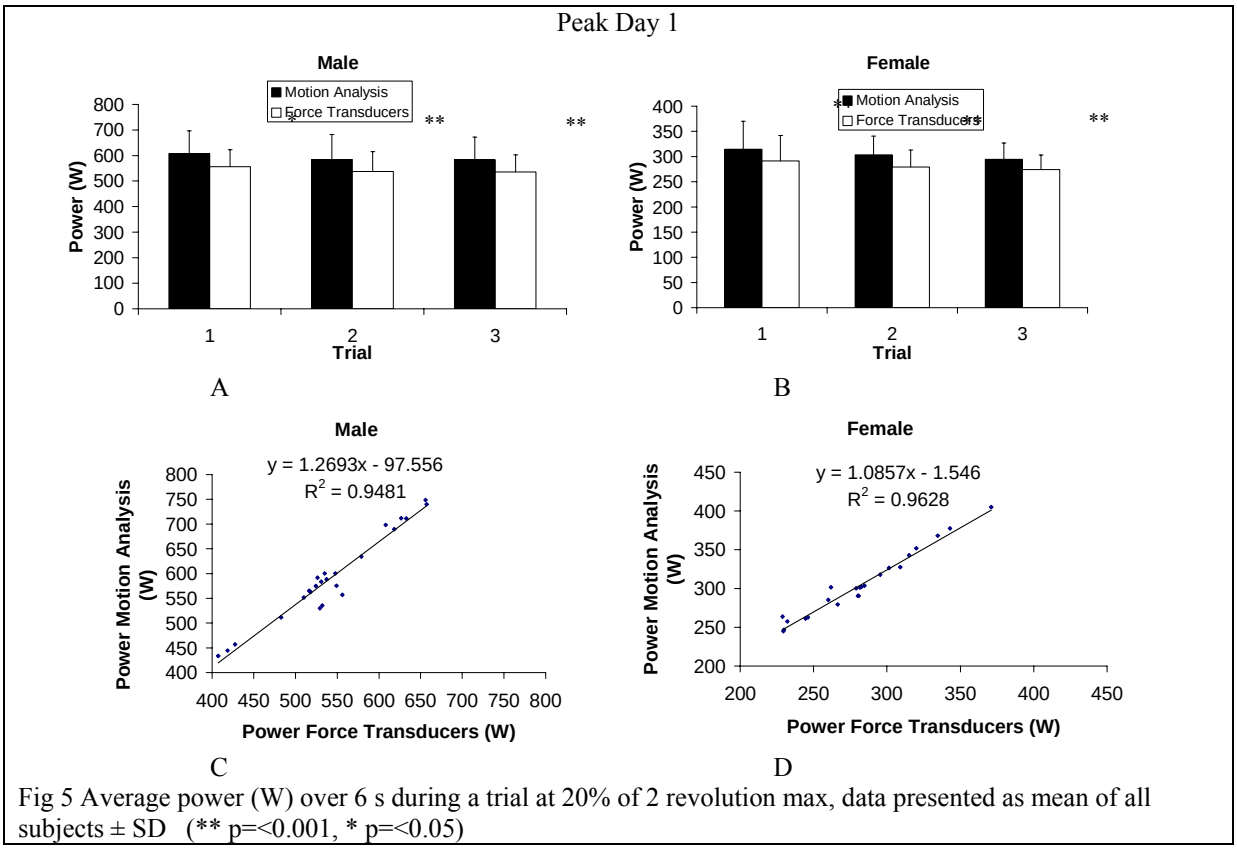

Fig 5 Average power (W) over 6 s during a trial at 20% of 2 revolution max, data presented as mean of all subjects ± SD (** p=<0.001, * p=<0.05)

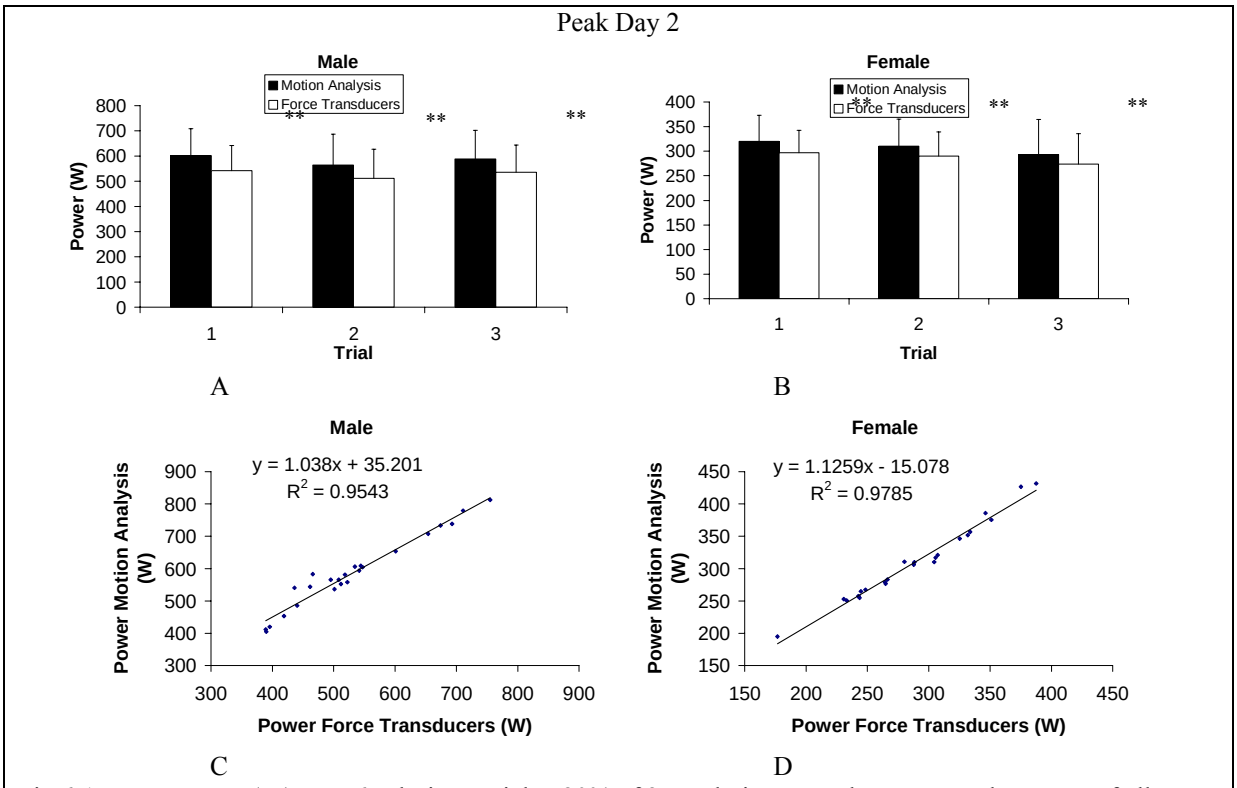

Fig 6 Average power (W) over 6 s during a trial at 20% of 2 revolution max, data presented as mean of all subjects ± SD (** p=<0.001, * p=<0.05)

During trials at 50% of 2RM when data was averaged over 6 seconds (figs 7+8), motion analysis recorded higher power outputs than force transducers on average by 43.4 W ± 0.6 on day 1 and by 39.9 ± 1.6 on day 2 in male subjects. For female subjects during trials at the same load, motion analysis was on average 15.6 W ± 0.4 and 13.4 W ± 0.6 higher than force transducers on day 1 and 2 respectively.

Pearson's correlation co-efficient was on average 0.956 ± 0.02 in males and 0.989 ± 0.01 in females.

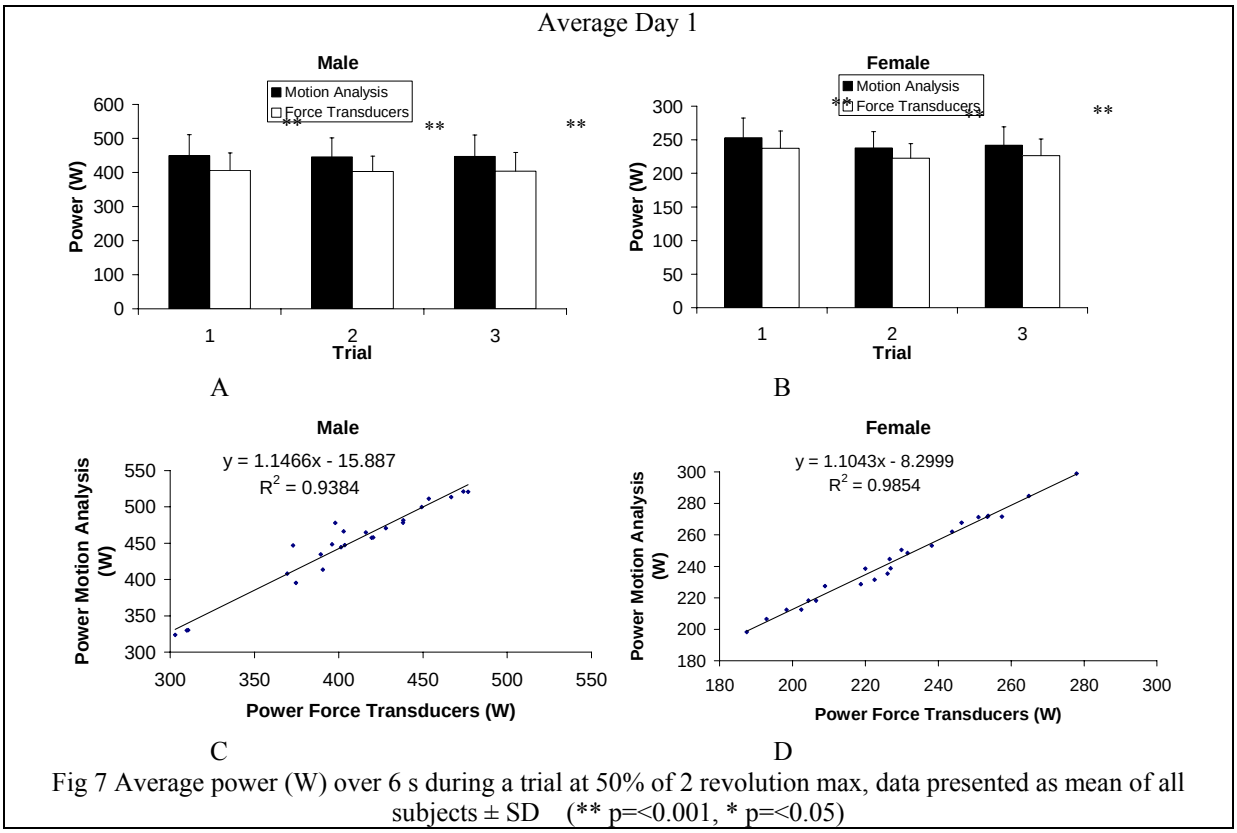

Fig 7 Average power (W) over 6 s during a trial at 50% of 2 revolution max, data presented as mean of all subjects ± SD (** p=<0.001, * p=<0.05)

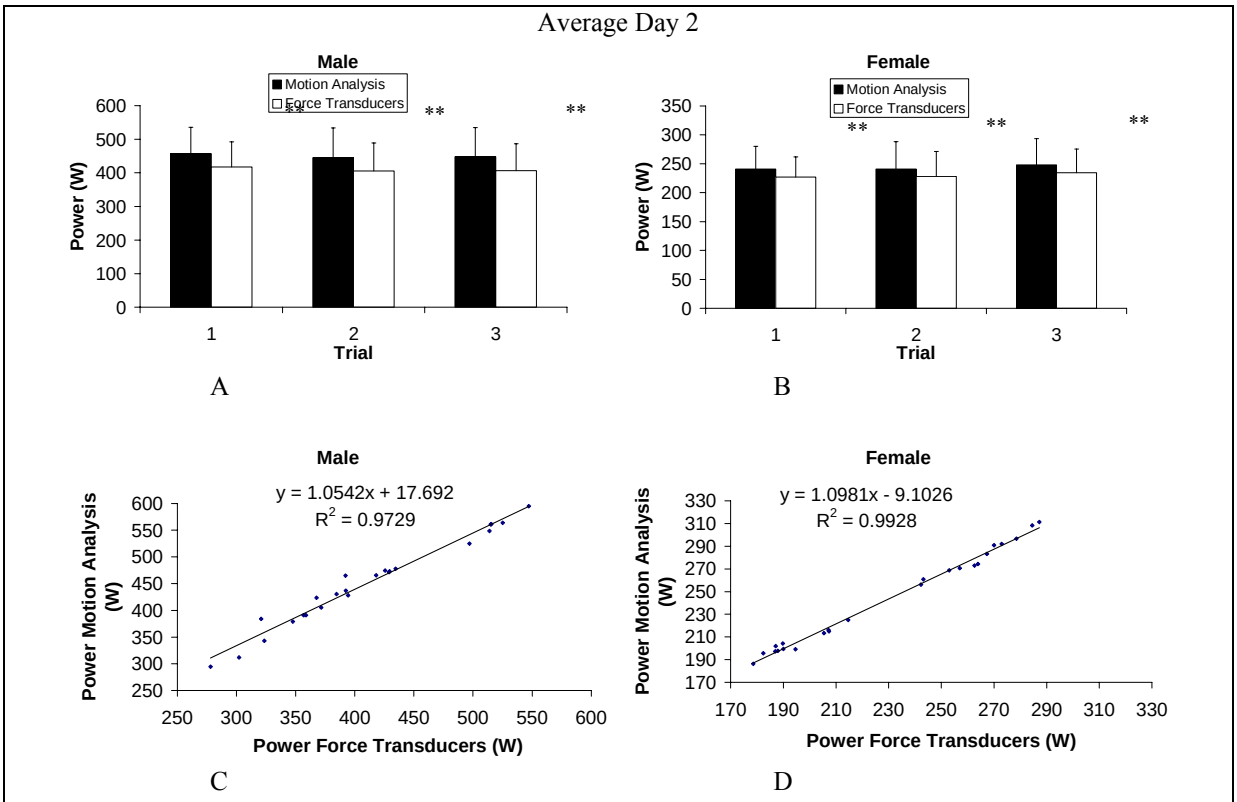

Fig 8 Average power (W) over 6 s during a trial at 50% of 2 revolution max, data presented as mean of all subjects ± SD (** p=<0.001, * p=<0.05)

When power was averaged over the 3 highest peaks and the load was 50% of 2RM (figs 9+10), motion analysis recorded higher power outputs than force transducers on average by 65.7 W ± 1.3 and by 60.7 W ± 1.4 on day 1 and 2 respectively in male subjects. Motion analysis recorded higher values than force transducers on average by 22.6 W ± 0.5 and 20.3 W ± 0.6 on day 1 and 2 respectively in female subjects.

Pearson's correlation co-efficient was on average 0.959 ± 0.02 and 0.985 ± 0.01 in males and females respectively.

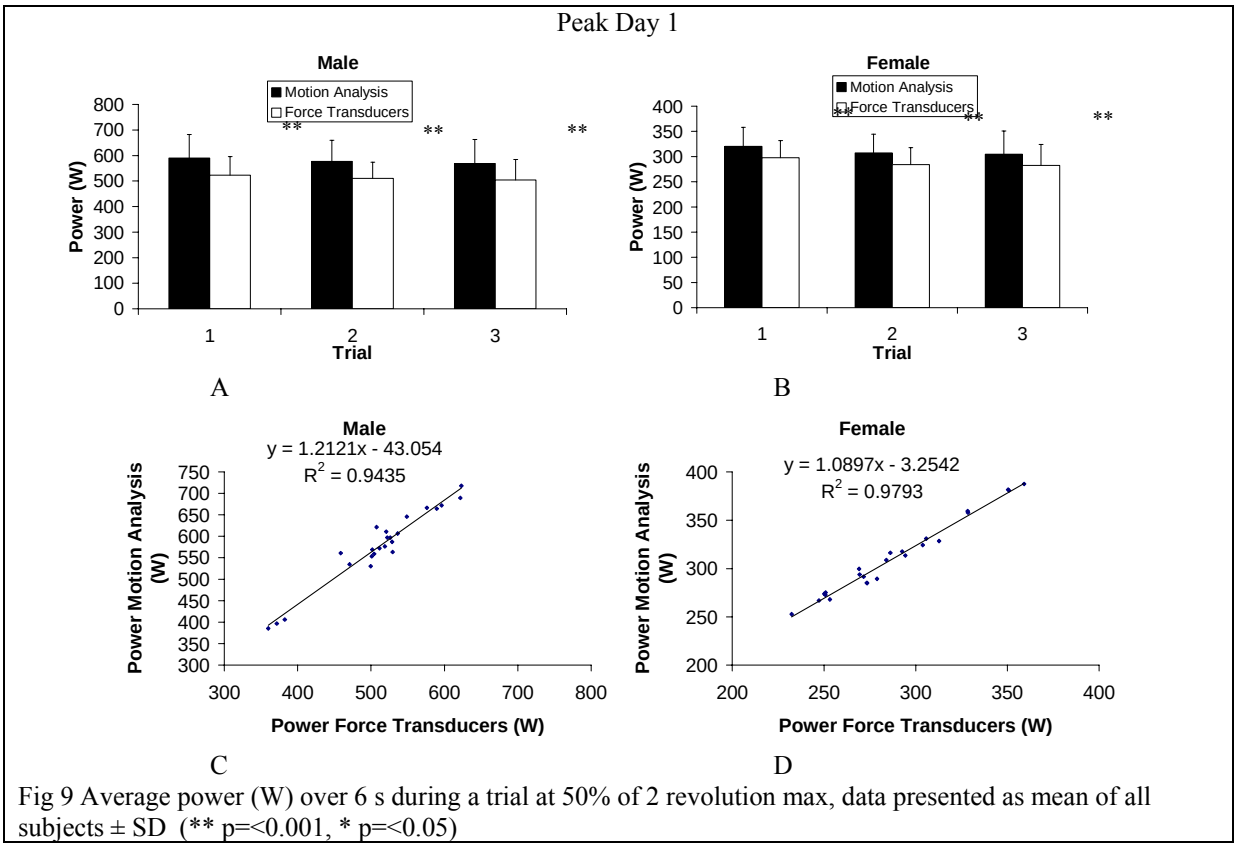

Fig 9 Average power (W) over 6 s during a trial at 50% of 2 revolution max, data presented as mean of all subjects ± SD (** p=<0.001, * p=<0.05)

Peak Day 2

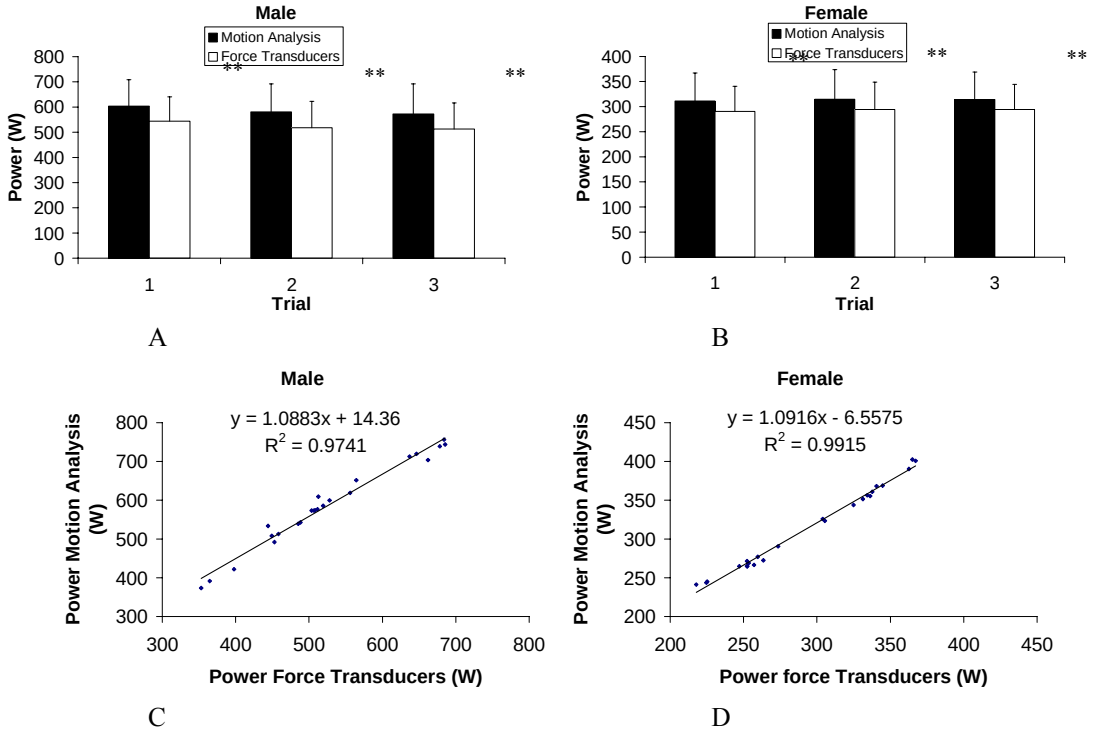

Fig 10 Average power (W) over 6 s during a trial at 50% of 2 revolution max, data presented as mean of all subjects ± SD (** p=<0.001, * p=<0.05)

A mean intraclass coefficient (ICC) of 0.948 ± 0.051 between motion analysis trials in males suggests an excellent degree of reciprocity between trials and days during constant speed trials (table 1). This degree of reciprocity was also demonstrated by females with a mean ICC of 0.893 ± 0.102 during trials at the same intensity and duration (table 2).

Constant Speed Male

Data presented as mean of all subjects ± SD on motion analysis (MA) and force transducers (FT)

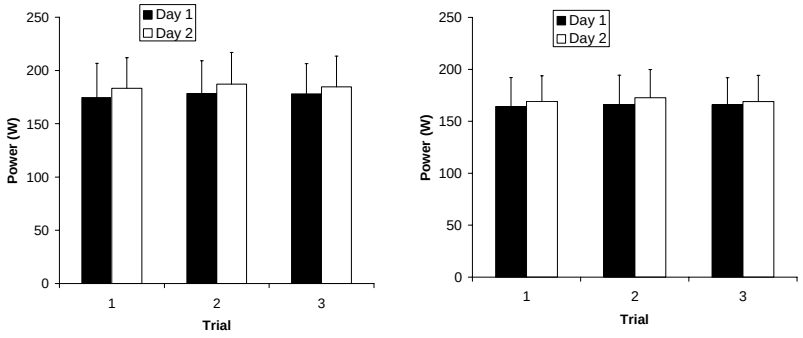

Fig 11 A: MA B: FT

	R	ICC	CV %
MA inter-day	0.904 (± 0.178)	0.890 95% CI 0.749-0.973	5.3 (± 1.9)
FT inter-day	0.908 (± 0.173)	0.904 95% CI 0.777-0.976	4.8 (± 1.2)
MA intra-day 1	0.985 (± 0.016)	0.979 95% CI 0.933-0.995	2.3 (± 2.0)
MA intra-day 2	0.978 (± 0.023)	0.976 95% CI 0.925-0.995	2.3 (± 1.0)
FT intra-day 1	0.985 (± 0.009)	0.984 95% CI 0.948-0.996	2.0 (± 0.7)
FT intra-day 2	0.980 (± 0.024)	0.974 95% CI 0.918-0.994	2.3 (± 0.8)

Table 1. *Statistical comparisons of power (W) per each of the measuring systems (Motion Analysis, MA, or Force Transducers, FT), in males performing 30-s sprints at 30% of 2 revolution maximum (2RM). Data is an average of power over 30-s. Inter-day reliability is presented as the average of all 3 trials in day 1 compared to the average of all 3 trials in day 2. Intra-day reliability is presented as the comparison of trials 1-3 in the same day (either day 1 or day 2). Table reports mean Pearson's inter-item correlation (± range), intraclass correlation coefficient (one way random model) and coefficient of variation (mean ± SD).*

Constant Speed Female

Data presented as mean of all subjects ± SD on motion analysis (MA) and force transducers (FT)

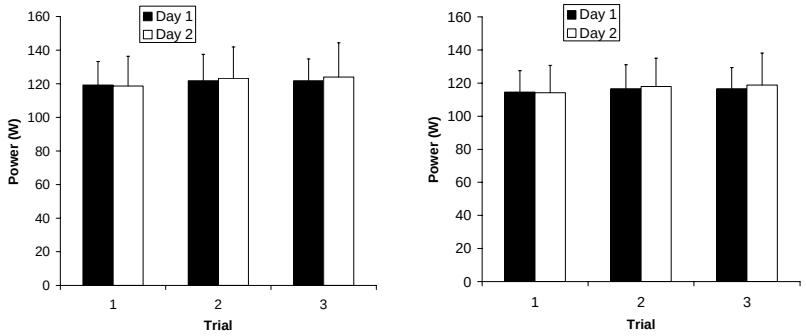

Fig 12 A : MA B: FT

	R	ICC	CV %
MA inter-day	0.787 (±0.422)	0.776 95% CI 0.548-0.939	5.7 (± 4.3)
FT inter-day	0.738 (± 0.587)	0.740 95% CI 0.494-0.928	6.3 (± 4.5)
MA intra-day 1	0.965 (± 0.022)	0.950 95% CI 0.851-0.989	2.0 (± 1.5)
MA intra-day 2	0.977 (± 0.026)	0.954 95% CI 0.862-0.990	2.6 (± 2.1)
FT intra-day 1	0.909 (± 0.033)	0.910 95% CI 0.745-0.979	25.8 (± 9.2)
FT intra-day 2	0.973 (± 0.035)	0.951 95% CI 0.853-0.989	25.7 (± 13.3)

Table 2 *Statistical comparisons of power (W) per each of the measuring systems (Motion Analysis, MA, or Force Transducers, FT), in females performing 30-s sprints at 30% of 2 revolution maximum (2RM). Data is an average of power over 30-s. Inter-day reliability is presented as the average of all 3 trials in day 1 compared to the average of all 3 trials in day 2. Intra-day reliability is presented as the comparison of trials 1-3 in the same day (either day 1 or day 2). Table reports mean Pearson's inter-item correlation (± range), intraclass correlation coefficient (one way random model) and coefficient of variation (mean ± SD).*

When individual's power output was measured at 20% of their 2RM and averaged over 6 seconds by motion analysis, similar high correlation was found with an average ICC of 0.874 ± 0.039 and 0.883 ± 0.033 demonstrated by males (table 3) and females (table 4) respectively.

20% Average Male

Data presented as mean of all subjects ± SD on motion analysis (MA) and force transducers (FT)

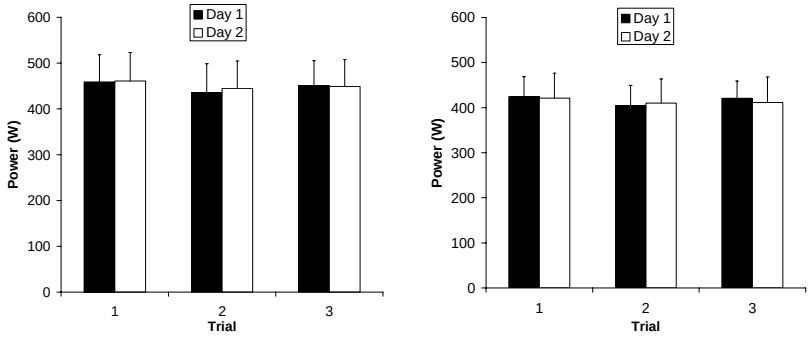

Fig 13 A: MA B: FT

	R	ICC	CV %
MA inter-day	0.854(± 0.236)	0.846 95% CI 0.666-0.961	4.9 (± 1.9)
FT inter-day	0.854 (± 0.219)	0.836 95% CI 0.648-0.957	4.5 (± 1.6)
MA intra-day 1	0.885 (± 0.065)	0.857 95% CI 0.619-0.966	4.3 (± 2.7)
MA intra-day 2	0.930 (± 0.045)	0.919 95% CI 0.768-0.982	3.7 (± 1.5)
FT intra-day 1	0.862 (± 0.098)	0.817 95% CI 0.536-0.956	3.8 (± 2.4)
FT intra-day 2	0.955 (± 0.026)	0.948 95% CI 0.844-0.988	2.9 (± 1.1)

Table 3 *Statistical comparisons of power (W) per each of the measuring systems (Motion Analysis, MA, or Force Transducers, FT), in males performing 6-s sprints at 20% of 2 revolution maximum (2RM). Data is an average of power over 6-s. Inter-day reliability is presented as the average of all 3 trials in day 1 compared to the average of all 3 trials in day 2. Intra-day reliability is presented as the comparison of trials 1-3 in the same day (either day 1 or day 2). Table reports mean Pearson's inter-item correlation (± range), intraclass correlation coefficient (one way random model) and coefficient of variation (mean ± SD).*

20% Average Female

Data presented as mean of all subjects ± SD on motion analysis (MA) and force transducers (FT)

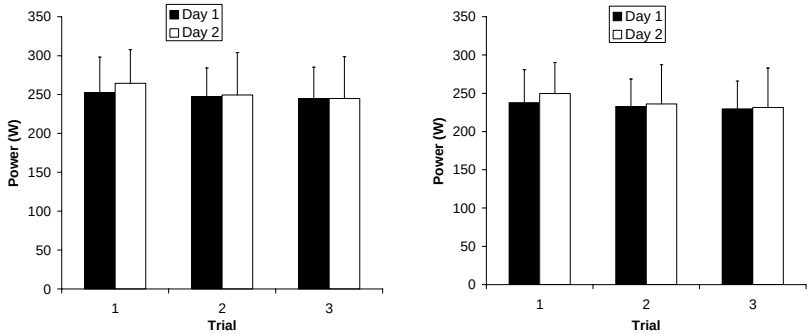

Fig 14 A : MA B: FT

	R	ICC	CV %
MA inter-day	0.897(±0.170)	0.864 95% CI 0.699-0.966	7.0 (± 2.2)
FT inter-day	0.883 (± 0.190)	0.850 95% CI 0.672-0.961	7.3 (± 2.4)
MA intra-day 1	0.932 (± 0.017)	0.922 95% CI 0.775-0.982	4.2 (± 2.4)
MA intra-day 2	0.903 (± 0.097)	0.864 95% CI 0.636-0.968	7.5 (± 4.3)
FT intra-day 1	0.916 (± 0.009)	0.906 95% CI 0.735-0.978	4.7 (± 2.6)
FT intra-day 2	0.911 (± 0.086)	0.871 95% CI 0.651-0.970	7.3 (± 4.4)

Table 4 *Statistical comparisons of power (W) per each of the measuring systems (Motion Analysis, MA, or Force Transducers, FT), in females performing 6-s sprints at 20% of 2 revolution maximum (2RM). Data is an average of power over 6-s. Inter-day reliability is presented as the average of all 3 trials in day 1 compared to the average of all 3 trials in day 2. Intra-day reliability is presented as the comparison of trials 1-3 in the same day (either day 1 or day 2). Table reports mean Pearson's inter-item correlation (± range), intraclass correlation coefficient (one way random model) and coefficient of variation (mean ± SD).*

During trials at 20% of 2RM and averaging of the 3 highest peaks occurring during the 6 second trial, mean ICC's of 0.983 ± 0.021 and 0.759 ± 0.059 were demonstrated by motion analysis in male (table 5) and female (table 6) subjects respectively.

20% Peak Male

Data presented as mean of all subjects ± SD on motion analysis (MA) and force transducers (FT)

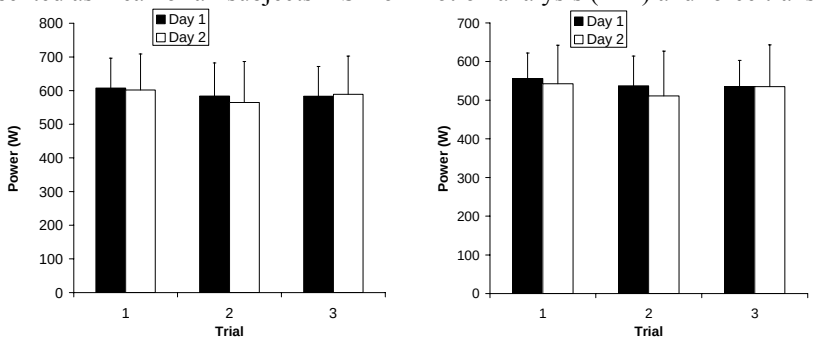

Fig 15 A :MA B: FT

	R	ICC	CV %
MA inter-day	0.907(±0.190)	0.883 95% CI 0.735-0.971	5.5 (± 2.6)
FT inter-day	0.879 (± 0.206)	0.826 95% CI 0.631-0.955	6.4 (± 3.0)
MA intra-day 1	0.933 (± 0.099)	0.918 95% CI 0.765-0.981	3.7 (± 2.9)
MA intra-day 2	0.894 (± 0.109)	0.879 95% CI 0.668-0.971	5.7 (± 3.5)
FT intra-day 1	0.926 (± 0.084)	0.906 95% CI 0.734-0.978	3.4 (± 2.4)
FT intra-day 2	0.896 (± 0.077)	0.884 95% CI 0.681-0.973	5.5 (± 3.9)

Table 5 *Statistical comparisons of power (W) per each of the measuring systems (Motion Analysis, MA, or Force Transducers, FT), in males performing 6-s sprints at 20% of 2 revolution maximum (2RM). Data is an average of power of the 3 highest peaks during the 6-s. Inter-day reliability is presented as the average of all 3 trials in day 1 compared to the average of all 3 trials in day 2. Intra-day reliability is presented as the comparison of trials 1-3 in the same day (either day 1 or day 2). Table reports mean Pearson's inter-item correlation (± range), intraclass correlation coefficient (one way random model) and coefficient of variation (mean ± SD).*

20% Peak Female

Data presented as mean of all subjects ± SD on motion analysis (MA) and force transducers (FT)

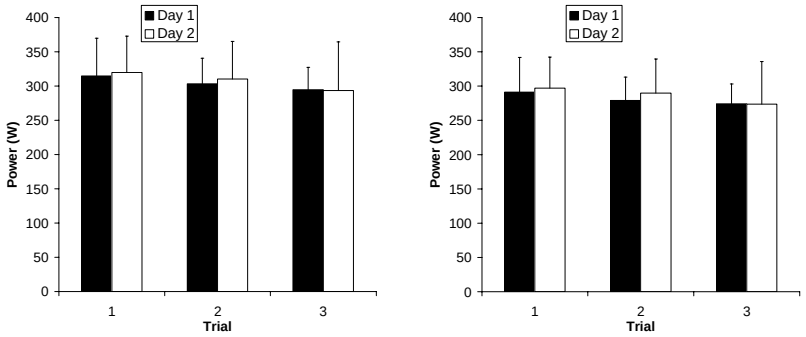

Fig 16 A : MA B: FT

	R	ICC	CV %
MA inter-day	0.796(±0.410)	0.752 95% CI 0.512-0.932	7.8 (± 3.7)
FT inter-day	0.772 (± 0.391)	0.732 95% CI 0.483-0.925	8.1 (± 3.4)
MA intra-day 1	0.781 (± 0.140)	0.704 95% CI 0.338-0.923	6.3 (± 4.2)
MA intra-day 2	0.867 (± 0.095)	0.821 95% CI 0.544-0.957	7.0 (± 6.6)
FT intra-day 1	0.749 (± 0.148)	0.678 95% CI 0.298-0.915	6.5 (± 4.4)
FT intra-day 2	0.855 (± 0.111)	0.810 95% CI 0.523-0.954	6.8 (± 6.8)

Table 6 *Statistical comparisons of power (W) per each of the measuring systems (Motion Analysis, MA, or Force Transducers, FT), in females performing 6-s sprints at 20% of 2 revolution maximum (2RM). Data is an average of power of the 3 highest peaks during the 6-s. Inter-day reliability is presented as the average of all 3 trials in day 1 compared to the average of all 3 trials in day 2. Intra-day reliability is presented as the comparison of trials 1-3 in the same day (either day 1 or day 2). Table reports mean Pearson's inter-item correlation (± range), intraclass correlation coefficient (one way random model) and coefficient of variation (mean ± SD).*

When individual's power output was measured at 50% of their 2RM and averaged over 6 seconds by motion analysis, similar high correlation was found with an average ICC of 0.900 ± 0.048 and 0.878 ± 0.045 demonstrated by males (table 7) and females (table 8) respectively.

50% Average Male

Data presented as mean of all subjects ± SD on motion analysis (MA) and force transducers (FT)

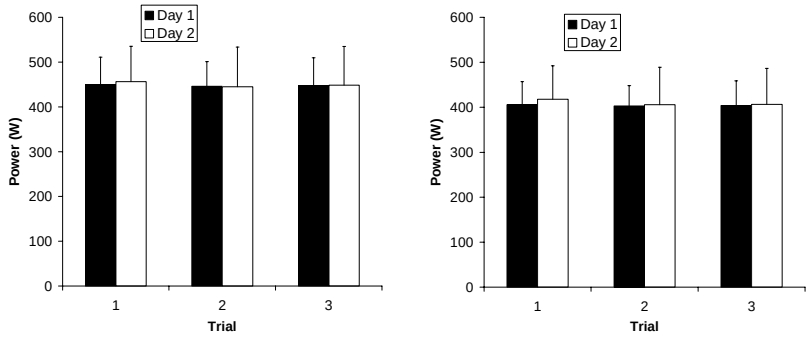

Fig 17 A: MA B: FT

	R	ICC	CV %
MA inter-day	0.860 (±0.311)	0.846 95% CI 0.665-0.960	5.6 (± 2.8)
FT inter-day	0.842 (± 0.377)	0.816 95% CI 0.613-0.952	6.0 (± 3.0)
MA intra-day 1	0.932 (± 0.054)	0.937 95% CI 0.814-0.986	2.6 (± 2.0)
MA intra-day 2	0.914 (± 0.066)	0.917 95% CI 0.761-0.981	5.3 (± 2.8)
FT intra-day 1	0.908 (± 0.064)	0.913 95% CI 0.753-0.980	3.0 (± 2.1)
FT intra-day 2	0.925 (± 0.046)	0.925 95% CI 0.782-0.983	5.2 (± 2.9)

Table 7 *Statistical comparisons of power (W) per each of the measuring systems (Motion Analysis, MA, or Force Transducers, FT), in males performing 6-s sprints at 50% of 2 revolution maximum (2RM). Data is an average of power over 6-s. Inter-day reliability is presented as the average of all 3 trials in day 1 compared to the average of all 3 trials in day 2. Intra-day reliability is presented as the comparison of trials 1-3 in the same day (either day 1 or day 2). Table reports mean Pearson's inter-item correlation (± range), intraclass correlation coefficient (one way random model) and coefficient of variation (mean ± SD).*

50% Average Female

Data presented as mean of all subjects ± SD on motion analysis (MA) and force transducers (FT)

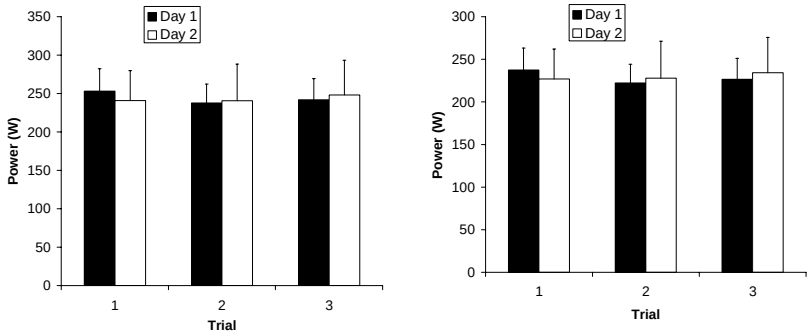

Fig 18 A : MA B: FT

	R	ICC	CV %
MA inter-day	0.910 (±0.162)	0.840 95% CI 0.654-0.959	5.7 (± 2.3)
FT inter-day	0.904 (± 0.156)	0.830 95% CI 0.637-0.956	5.7 (± 2.0)
MA intra-day 1	0.947 (± 0.033)	0.866 95% CI 0.641-0.968	3.8 (± 1.7)
MA intra-day 2	0.938 (± 0.055)	0.928 95% CI 0.791-0.984	4.1 (± 2.8)
FT intra-day 1	0.947 (± 0.032)	0.856 95% CI 0.617-0.966	3.8 (± 1.6)
FT intra-day 2	0.938 (± 0.049)	0.926 95% CI 0.786-0.983	4.0 (± 2.7)

Table 8 *Statistical comparisons of power (W) per each of the measuring systems (Motion Analysis, MA, or Force Transducers, FT), in females performing 6-s sprints at 50% of 2 revolution maximum (2RM). Data is an average of power over 6-s. Inter-day reliability is presented as the average of all 3 trials in day 1 compared to the average of all 3 trials in day 2. Intra-day reliability is presented as the comparison of trials 1-3 in the same day (either day 1 or day 2). Table reports mean Pearson's inter-item correlation (± range), intraclass correlation coefficient (one way random model) and coefficient of variation (mean ± SD)*

During trials at 50% of 2RM and averaging of the 3 highest peaks occurring during the 6 second trial, mean ICC's of 0.899 ± 0.036 and 0.894 ± 0.054 were demonstrated by motion analysis in male (table 9) and female (table 10) subjects respectively.

50% Peak Male

Data presented as mean of all subjects ± SD on motion analysis (MA) and force transducers (FT)

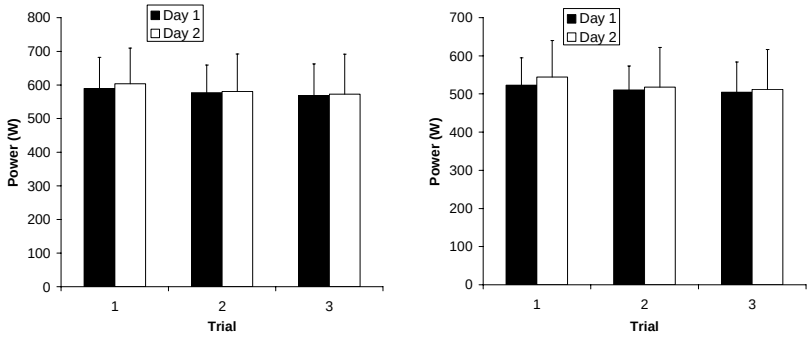

Fig 19 A : MA B: FT

	R	ICC	CV %
MA inter-day	0.899 (±0.168)	0.881 95% CI 0.730-0.970	5.7 (± 2.0)
FT inter-day	0.894 (± 0.157)	0.852 95% CI 0.676-0.962	6.0 (± 1.9)
MA intra-day 1	0.953 (± 0.013)	0.941 95% CI 0.826-0.987	3.3 (± 1.5)
MA intra-day 2	0.882 (± 0.045)	0.875 95% CI 0.660-0.971	6.1 (± 3.9)
FT intra-day 1	0.923 (± 0.029)	0.906 95% CI 0.733-0.978	3.8 (± 2.0)
FT intra-day 2	0.892 (± 0.040)	0.878 95% CI 0.667-0.971	6.1 (± 4.0)

Table 9 *Statistical comparisons of power (W) per each of the measuring systems (Motion Analysis, MA, or Force Transducers, FT), in males performing 6-s sprints at 50% of 2 revolution maximum (2RM). Data is an average of power of the 3 highest peaks during the 6-s. Inter-day reliability is presented as the average of all 3 trials in day 1 compared to the average of all 3 trials in day 2. Intra-day reliability is presented as the comparison of trials 1-3 in the same day (either day 1 or day 2). Table reports mean Pearson's inter-item correlation (± range), intraclass correlation coefficient (one way random model) and coefficient of variation (mean ± SD).*

50% Peak Female

Data presented as mean of all subjects ± SD on motion analysis (MA) and force transducers (FT)

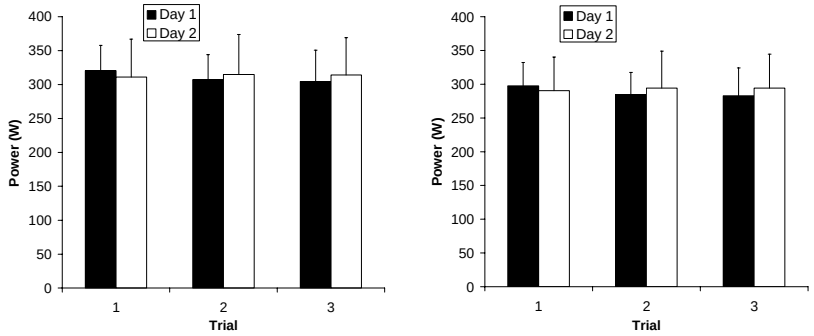

Fig 20 A: MA B: FT

	R	ICC	CV %
MA inter-day	0.862 (±0.278)	0.838 95% CI 0.652-0.958	5.6 (± 3.7)
FT inter-day	0.838 (± 0.328)	0.814 95% CI 0.610-0.951	5.9 (± 3.9)
MA intra-day 1	0.947 (± 0.052)	0.898 95% CI 0.715-0.976	3.8 (± 2.3)
MA intra-day 2	0.941 (± 0.024)	0.946 95% CI 0.839-0.988	3.2 (± 2.4)
FT intra-day 1	0.946 (± 0.055)	0.893 95% CI 0.704-0.975	3.8 (± 2.2)
FT intra-day 2	0.956 (± 0.031)	0.948 95% CI 0.845-0.988	3.2 (± 2.1)

Table 10 *Statistical comparisons of power (W) per each of the measuring systems (Motion Analysis, MA, or Force Transducers, FT), in females performing 6-s sprints at 50% of 2 revolution maximum (2RM). Data is an average of power of the 3 highest peaks during the 6-s. Inter-day reliability is presented as the average of all 3 trials in day 1 compared to the average of all 3 trials in day 2. Intra-day reliability is presented as the comparison of trials 1-3 in the same day (either day 1 or day 2). Table reports mean Pearson's inter-item correlation (± range), intraclass correlation coefficient (one way random model) and coefficient of variation (mean ± SD).*

5. Pedalling efficiency evaluation using pedal force measure

The aim of this work was to develop a method useful to optimize the posture on the bicycle during cycling, finalized to improve the force exertion of the leg to the pedal. As a matter of fact, the issues related to the body posture are somewhat complex because they are tightly related to the configuration of each bicycle. The latter has to be considered as an instrument that permits a lot of regulations (saddle, pedals and handle bar) depending on the physical athlete's characteristics, on the branch and on the adaptation's ability. The best position on the bicycle is acknowledged to be the one to which the athlete is most familiar with [15], but the correct regulation of each component of the bicycle could modify the kinematic chain of lower limbs, with positive effect on the performance. In this context, the regulation of the saddle's position plays an important role, in terms of height and fore-aft position. These parameters are strictly connected to the efficiency of the gesture and the wrong regulation could give problems of overloading on the lower limbs [3].

In literature there are many studies on the cycling efficiency that is defined on a bioenergetics point of view, as the relationship between the work expressed on a trail and the energetic cost of the exercise [4, 68].

In this study, a method to define an index to evaluate the efficiency from a biomechanical point of view is presented. Some biomechanical indexes have already been defined and used to evaluate efficiency in cycling, but these were never calculated in real time to obtain a feedback useful to athlete to modify his ability to execute the gesture.

5.1 Context and Importance of the study

Using the instrumented pedal, it is possible to measure the force applied to the pedal and the relative angle between the pedal and the crank. With these data, it is possible to calculate the forces applied to the crank that can be used to evaluate the efficiency of the gesture.

The resultant force applied on the pedal can be expressed as the vector sum of the two components: perpendicular and parallel to the crank's axis. The perpendicular is the component used to win the resistance to the forwarding while the parallel is the dissipated component. The optimal situation should be if for every instant of the cycle the resultant force was directed along the perpendicular to the crank, but this situation is not achievable. Only a portion of the resultant force, variable in the pedalling cycle, is used in a useful way, so it is possible to define the efficiency as the relationship between the force perpendicular to the crank and the resultant to the pedal.

5.1.1. The Proposed Approaches

There are two main ways of defining the efficiency of pedalling, both based on the ratio between the effective force FT, perpendicular to the crank, and the resultant force FTOT, obtained as sum of the two component measured by the pedal. The difference between the two definitions is based on the period on which the index is calculated.

The first definition of the index is given considering the instantaneous percent of the total force that contribute to the prevail of the pedalling resistance [7,13,69]:

$$IE\left(t\right) = \frac{F_T\left(t\right)}{F_{TOT}\left(t\right)} \qquad 5.1$$

Instead the second approach considers the forces in a defined time slot so the index results a mean percent of the resultant force in a period $\Delta t=(ti-t0)$ [13,70,71]:

$$IE_{\Delta t} = \frac{\int_{t_0}^{t_i} F_T(t)\,dt}{\int_{t_0}^{t_i} F_{TOT}(t)\,dt} \qquad 5.2$$

The time support over which this index can be calculated can be chosen in 3 different ways: by considering the entire revolution of the crank IE360o, only the pushing phase IE180oDesc, or only the pulling phase IE180oAsc.

$$IE_{360^0} = \frac{\int_{0}^{2\pi} F_T(\theta)\,d\theta}{\int_{0}^{2\pi} F_{TOT}(\theta)\,d\theta} \qquad 5.3$$

$$IE_{180^0\,Desc} = \frac{\int_{0}^{\pi} F_T(\theta)\,d\theta}{\int_{0}^{\pi} F_{TOT}(\theta)\,d\theta} \qquad 5.4$$

$$IE_{180^0\,Asc} = \frac{\int_{\pi}^{2\pi} F_T(\theta)\,d\theta}{\int_{\pi}^{2\pi} F_{TOT}(\theta)\,d\theta} \qquad 5.5$$

The optimal performance in the execution of the gesture could be obtained if the athlete applies a force to the pedal that is all directed along the normal to the crank: in this case, the instantaneous value of the index would be 1.

5.2 The pedalling movement

5.2.1. The pedalling style

A first model of pedalling is called “round pedalling” and consists in exerting the force during the whole cycle so that the power is almost equally distributed in the two phases of pushing and pulling [72]. Starting from the top dead centre (TDC), to obtain a propulsive force dorsiflexion is needed. Then it is necessary to apply a vertical force pointing downwards up to the bottom dead centre (BDC) and then a vertical force pointing upwards in the pulling phase. At the same time it is necessary to exert a horizontal force directed forward in the firsts 90°, backward in the range 90°-270° and forward from 270° to the end of cycle. This kind of pedalling needs a coordinate muscular activation to make the foot bending in a correct way, that is necessary to apply the force as described above.

Another model of pedalling is the one called “piston-like” in which the power is mostly exerted in the pushing phase. In this model, the exerted force is very variable on the whole cycle, and the maximum value is reached around the middle of the pushing phase. The features of this pedalling mode are an increased value of dissipated force, a high instantaneous value of torque to the chain driver, and a diminished portion of the entire pedalling cycle over which the force is exerted.

5.2.2. The role of the foot

Understanding the role of the foot in cycling is necessary, if the aim of the work is to optimize the body posture. The foot transmits the action from the muscular chains of the lower limb on the point of resistance constituted by the pedal, so its position is critical for the maximization of the transmitted force. This transfer happens by continuously varying the ankle orientation, by way of plantarflexion and dorsiflexion with a range of motion of around 15° (ankling). The force transfer to the pedal is mainly conveyed in the front part of the foot corresponding to the metacarpo-phalangeal joint position, where the clipless shoe are mounted. .

Theoretically the maximum efficiency condition is verified when the pedal receives a push perpendicular to the axis of the crank. In every phase of the pedalling cycle therefore the function of the foot is to efficiently transfer the propulsive force of the leg on the pedal. The foot position is modified to maximize the push force component that is perpendicular to

the crank, during the entire pedalling cycle, according to the range of motion of ankle plantar and dorsiflexion.

The regulation of the saddle position influences the action of the foot in the execution of the gesture. With a saddle too much high there is an excessive high extension of the foot so there is a slowing down at the Bottom Dead Centre (BDC) while with a saddle too much low there is an excessive flexion of the foot so there is a slowing down at the Top Dead Centre (TDC). Moreover a wrong regulation of the fore-aft position gives similar problems.

5.3 The body posture of the cycling gesture: the position on the saddle

A "correct" posture of the body on the bicycle is necessary to enhance the ability of each athlete to optimize the action of the leg during pedalling and to prevent pathology to muscular-skeletal system. On the other hand, an "incorrect" body posture reduces the efficiency of pedalling and introduces tensions to lower limbs that could induce functional overload pathology [3].

The two most useful parameters to determine the correct body posture during cycling are the height and fore-aft position of the saddle, strictly related each other so that the modification of one gives the variation of the other. This is due to the geometry of the bicycle, in fact because of the seat tube's inclination if the saddle's height is modified, there is a consequently variation of the antero-posterior position.

The saddle's height is defined as the distance between the centre of the chain driver and the saddle's anatomic centre, placed at 12 cm from the back side of it.

The fore-aft position is the distance between the vertical line, passing for the centre of the chain driver, and the saddle. There are two definitions depending on considering the anatomic centre or the point of the saddle. (Figure 5.1).

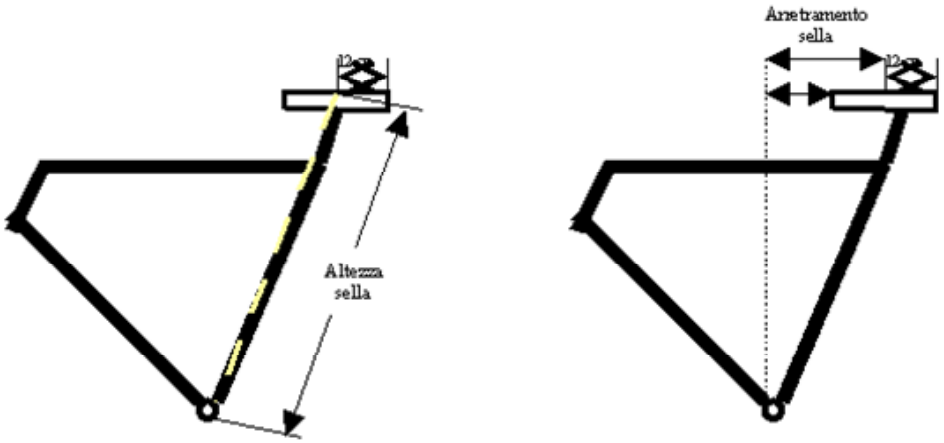

Figure 5.1: *height and fore-aft position regulations of the saddle*

The method used to evaluate the optimal body posture on the saddle during cycling is based on following criteria:

- The ranging of the patella and the pedal's bolt whit the crank's angle at 90° (crank parallel to the ground in the forward direction) and the pedal's flat surface parallel to the floor. This condition is known as the KOPS technique (Knee Over Pedal Spindle) and it is the most used to control the antero-posterior displacement on the saddle;

- Knee's angle, defined by the femur and the tibia, with the pedal parallel to the floor and the crank at bottom death point. This method is used to check the optimal height.

These two criteria are used to optimize the the exertion of force in both phases of pushing and pulling. An optimum height's regulation permits to maximize muscular efficiency while an optimum antero-posterior regulation 'minimizes relative variations of exerted force during the entire pedalling cycle' (in informal terms this feature is generally called 'roundness'), still maintaining a correct distribution of the stress between agonistic and antagonistic muscles.

If the body posture is optimized, at the beginning of the pushing phase the leg flexion and the knee position will allow minimizing the effort to start-up in the easiest way. During

the whole cycle the two conditions described above should be maintained, but this can not be verified in a dynamic condition.

If, on the other hand, the position of the saddle does not determine an optimized body posture, the pedalling efficiency can be clearly affected. If the saddle is too high, the hip would be excessively abducted, and in the final phase of pushing the knee would be hyper extended. In this way, the push is not effective, taking place a considerable slowing down to the passage of the BDC. Due to the knee hyperextension, there is a consequent pelvis tilting in the final phase of pushing.

With a too low saddle position, there are difficulties in the overcoming of TDC, with a consequent limited pushing phase. Moreover there is a dispersion of energy in the final phase as a result of both the difficulty of overcoming the TDC and from the limited knee extension in the final phase of pushing.

With a saddle positioned too much backward, the knee joint position would be behind the perpendicular to the axis of the pedal in the central phase of pushing. This position determines an increased activity of the posterior muscles of the leg with a smaller involvement of the quadriceps group. In the passage to the BDC the movement is slowed down and, therefore, there is less fluidity in the recovery of the leg. In the phase of pulling, the greater distance of the hip joint projection on to the ground falls further apart from the pedal, thus causing greater resistance in the pulling phase.

If the saddle is positioned too much forward, on the other hand, the knee joint position would fall too close to the pedal, thus impeding an optimal transfer of the exerted force in terms of effective component to the crank; the knee joint, in the central part of the pushing, is ahead to the perpendicular to the axis of the pedal so there is an excessive work of the rectus femoris and vastii compared to the posterior muscles of the thigh, a s the bicep femoris.

5.4 The pedalling efficiency evaluation

5.4.1. The Experimental Setup

An experimental campaign was executed in order to evaluate differences in pedalling with the saddle in different positions, evaluating the efficiency of the gesture.

Seven subjects of different gender and age in the range 28 to 40 were asked to pedal in different conditions. The subjects had different athletic skill and technical ability in cycling.

The tests have been done altering some parameters of the gesture, such as the frequency of pedalling and the position on the saddle, in terms of height and fore-aft position, and maintaining constant the power of pedalling.

The frequency and the power of pedalling have been checked with the use of the cycle simulator that presents an aerodynamic brake: the power is set by fixing the frequency of pedalling and the gear ratio between the chain driver and the cog wheel. Besides, opportunely varying these two parameters, it is possible to keep on working to the same power, but with different frequency, planning different conditions of execution of the exercise.

The cycle simulator works with a free wheel system. This mechanism allows the wheel to freely turn for the inertia in the sense of the motion without dragging the pedals, unlike what happens in the so-called fixed release, in which there is a direct transmission of the motion from the pedals to the wheel and stopping pedalling or pedalling contrarily the wheel is braked. The blades present on the wheel, to which the motion is transmitted, give a resistance to the motion and therefore the breaking action. The aerodynamic braking effect of the blades allows establishing a relationship between the speed of the wheel and the power.

The position of the saddle has been valued making some changes to the optimal one, defined according to the KOPS method, described above, which is a consolidated method both in the context of athletic work-out programs, and in clinical sport programs [73].

After a 10 minutes of warm-up, each trial was executed in the following way:

- A 5 minutes trial with the saddle in the optimal position;
- A 5 minutes trial with the height of the saddle increased of 3% in comparison to the optimal position and consequently behind;
- A 5 minutes trial with the height of the saddle decreased of 3% in comparison to the optimal position and consequently advanced.

This set of trials was repeated for each athlete at two different frequency of pedalling (50-60, 80-90 RPM) maintaining the power constant, that could be done changing the ratio of transmission of the cyclosimulator in order to make the resistant wheel moving at the same velocity.

5.4.2. Instruments

The forces and the pedal angle were measured using the instrumented pedal described above in this thesis. As described above, the pedal is based on the use of Shimano Pedalling Dynamics (SPD) clipless fastening and it maintains the geometry and the weight of a commercial pedal. The clipless fastening required the use of special shoe provided of a metallic cleat that fixed the foot to the pedal. In this way while a leg pushes downward the other one can pull in the opposite verse making active all the phases of pedalling.

The signal related to the angular position was also acquired to perform the complete spatial reconstruction of the loads applied on the crank and to evaluate the frequency of pedalling. Measuring the two components Fz and Fx of the resultant force applied to the pedal, in direction respectively normal and parallel to the plane of the pedal, and knowing the relative angle between pedal and crank it is thus possible to reconstruct the force's components applied to the crank.

5.5 Signal processing

From the measure of the force components applied on the plan of the pedal in parallel direction Fx and in orthogonal direction Fz, and of the pedal angle, the components Ft, effective component, and Fn, component dissipated, are calculated.

The resultant force Ftot is given by the vectorial sum of the two components in one of the two systems of reference RSp or RSc (Figure 5.2).

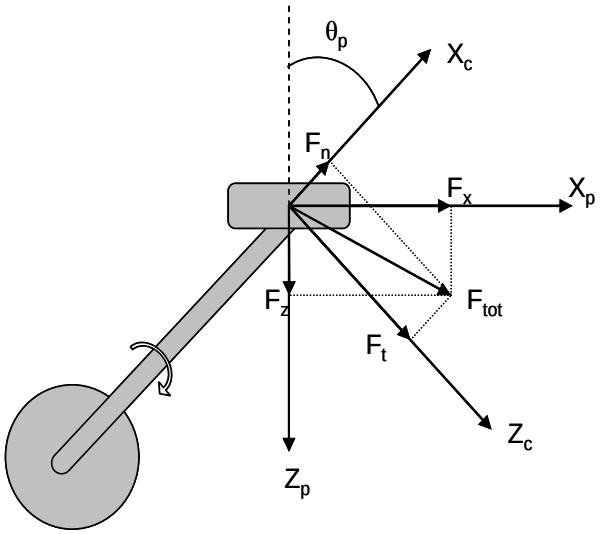

Figure 5.2: *Force components on the pedal and on the crank.*

To evaluate the forces on the crank the following equations have been used:

$$F_t = F_z \times sen\theta_p + F_x \times \cos\theta_p \qquad 5.6$$

$$F_n = -F_z \times \cos\theta_p + F_x \times sen\theta_p \qquad 5.7$$

$$F_{tot} = \sqrt{F_x^{\,2} + F_z^{\,2}} = \sqrt{F_t^{\,2} + F_n^{\,2}} \qquad 5.8$$

For the evaluation of the pedalling efficiency, four indexes have been defined. These

are different among them for the considered computational period.

The indexes are obtained by comparing the effective force Ft to the total force Ftot. The first index, as described above, is defined as the instantaneous percentage of the vector of total load that contributes to the positive work:

$$IE_{ist}(t) = \frac{F_t(t)}{F_{tot}(t)} \times 100$$

To obtained an integral measure of the efficiency, three new indexes were defined as the ratio between the effective force's integral and the resultant force's integral in three different periods: complete revolution IErev, phase of push or descending IEpush and phase of pull or ascending IEpull:

$$IE_{rev} = \frac{\int_0^{2\pi} F_t(\theta_p)d\theta}{\int_0^{2\pi} F_{tot}(\theta_p)d\theta} \times 100 \qquad 5.9$$

$$IE_{push} = \frac{\int_0^{\pi} F_t(\theta_p)d\theta}{\int_0^{\pi} F_{tot}(\theta_p)d\theta} \times 100 \qquad 5.10$$

$$IE_{pull} = \frac{\int_{\pi}^{2\pi} F_t(\theta_p)d\theta}{\int_{\pi}^{2\pi} F_{tot}(\theta_p)d\theta} \times 100 \qquad 5.11$$

The acquired signals have been processed by the use of a LabVIEW application that can work in real time.

5.5.1. The LabVIEW monitor

The application used to analyze data in real time was developed in LabVIEW 8.0 (National Instruments™) with the aim to give a real time feedback to the athlete during the execution of the gesture.

The scheme of the LabVIEW application is:

- acquisition, calibration and filtering of the signal;
- extraction of the crank force components using the formulas previously defined;
- extraction of the efficiency indexes;
- graphic representation of results.

After the acquisition, the signals are calibrated and filtered (Figure 3.13). For the force signals a lowpass filter with cut-off frequency equal to 40 Hz has been used, and the equations of calibration described in chapter 1 have been used.

For the angle of pedal, instead, a median filter with n=5 samples window and a function for the conversion of the angle in radiant and subsequently in degrees have been used. The use of the median filter allows having a signal filtered with minimum distortion in comparison to the real course (distortions are smaller in comparison to those obtained with a linear moving average lowpass filter). The median filter lowpass filtration, because it works on a window of samples, that are ordered in increasing way and than the centre of the window is taken as mean value. Subsequently the window is translated of 1 sample and the operation is repeated for the whole signal. In this way the presence of discontinuity due to the transition among the end of the cycle and the beginning of the following one, is preserved. Using a normal pass-low filter the discontinuity would be altered, with consequent loss of information on the signal.

From the time series of the calibrated signals it is possible to determine, by simply applying the formulas defined above, the components Fn and Ft and therefore the total force Ftot. From the latter ones, the instantaneous index IEist time series, and the integral values IE_{rev}, IE_{push}, IE_{pull}, which were extracted by locating the time instances of each phase of the pedalling cycle.

The front panel of the LabVIEW virtual instrument presents some displays on which the values of the calculated indexes, as well as the time trends of these during the test, the forces' profiles the angle of pedal and the frequency of pedalling are updated in real time.

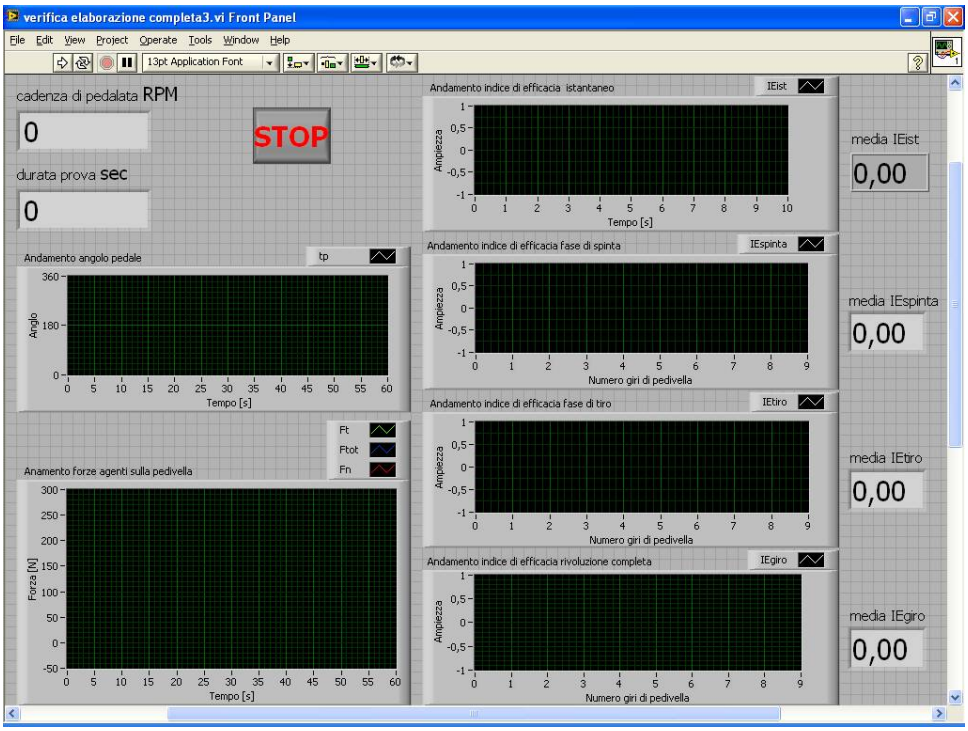

a)

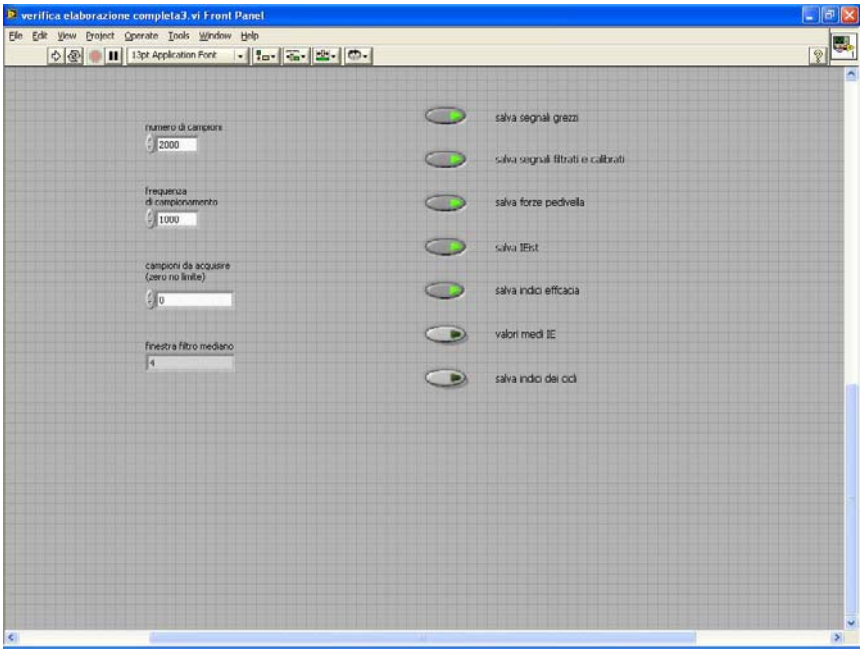

b)

Figure 5.3*: LabView front panel: a) Signals control and results displaced b)Settings section.*

In this way it is possible to provide in real time to the athlete all the information about his performance. In this way it would be possible to timely make the athlete modify the pedalling strategy, by asking him to maintain the indexes of efficiency as high as possible.

5.6 Results and discussion

5.6.1. Pedal forces measures

In Figure 5.4 the time trends of the Fx and Fz force components acquired during the experimental tests are shown. In the figure two different pedalling conditions are compared: the first (A) with phase of pull active and the second one (B) with the passive pulling.

A

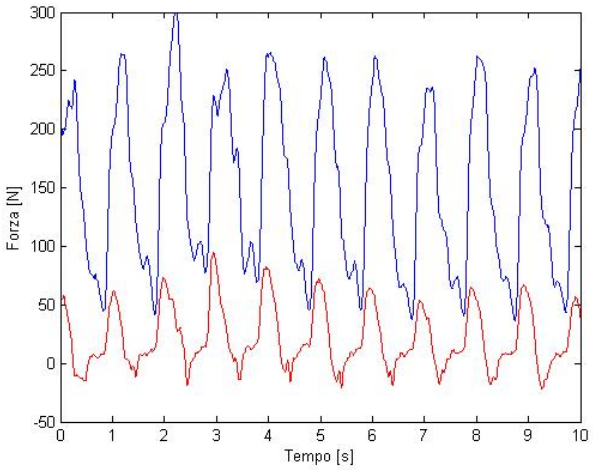

B

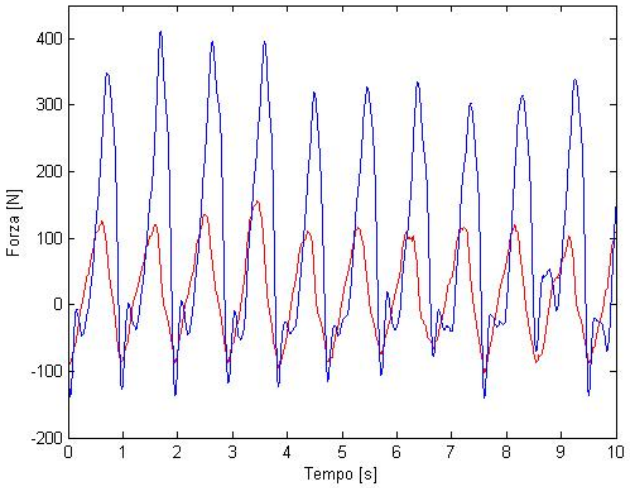

Figure 5.4: *Time series of the Fx (red line) and Fz (blue line) force components: (A) with the phase of pull active, (B) with the phase of pull passive.*

By observing the time series of these forces in the situation A, the Fz is always positive, so it is hypothesized that it doesn't give any active contribution to the pulling phase, while in the situation B there is a contribution to the pull that makes this phase active. As per Fx, it is fairly smaller in the condition A as compared to B. It is important to outline that, in order to optimize pedalling, Fz has to be positive for the first 180°, corresponding to the phase of push, and negative for the following 180°, that correspond to the pulling phase, while Fx should be positive for the first 90° then should become negative in the range 90° to 270° and finally positive again in the last 90° of the pulling phase. Observing the figure, in the situation A this condition is clearly not verified while in the case B the behaviour is closer to the ideal situation.

A confirmation about what observed on the time trends of the forces Fx and Fz could be found by analysing the time series of Ftot, Ft and Fn (Figure 5.5). In the condition A, the Ft is almost negative for all the pulling phase and it means that the foot of the examined limb is actually pushed upwards by the other; on the other side in the case B it happens that Ft is always positive for the whole cycle, because the athlete pushes in the descending phase and pulls in the ascending one.

A

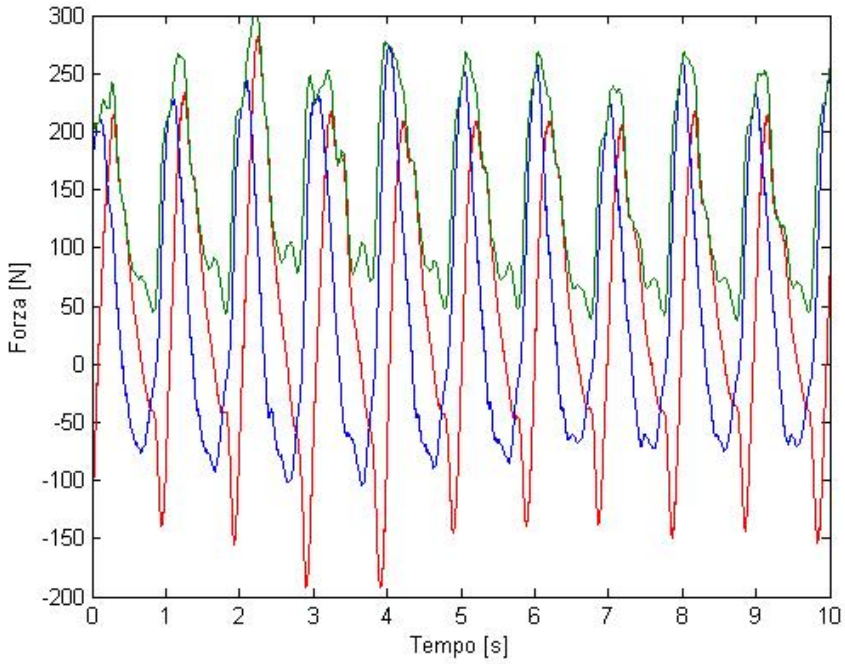

B

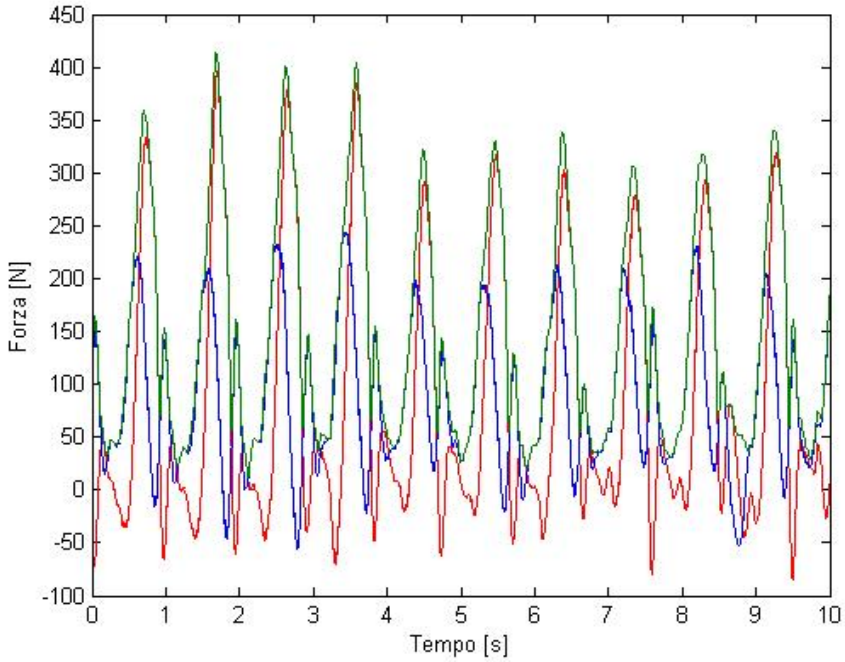

Figure 5.5: *Time series of the F_{tot} (green line), F_t (blue line) and F_n (red line) force components: (A) with the phase of pull active, (B) with the phase of pull passive.*

5.6.2. The efficiency index

In the following, the charts with the percentage values of the indexes of efficiency are shown, with the mean values over the entire test.

For a more detailed analysis over the time, the graphs related to the mean profiles of the effective force and of the total force over the entire cycle are also displayed. The profiles of the instantaneous indexes of efficiency, and the average over the entire cycle both the instantaneous and the mean on the cycle are also shown. The latter ones were calculated on the whole cycle, on the pushing phase and on the pulling phase.

In

Chart ***5.1***, Figure 5.6, Figure 5.7 and *Figure 5.8* the results of the analysis for one of the subject during the trial with low pedalling frequency are shown, while Chart 5.2, Figure 5.9, Figure 5.10 Figure 5.11 show the results for the same subject during the trial with high pedalling frequency.

Regarding the trial with the lowest RPM value, tests performed with the saddle in optimal position are those with the highest indexes values. In fact, both the instantaneous indexes and the average ones over the entire revolution, the pushing phase, and the pulling phase result greater in comparison to the other tests with different saddle's positions described above. In this case, the pulling in the phase of recovery of the pedal is completely absent as it is shown by the value percentage negative of IEpull. The negative value of the index is due to the fact that the effective force, normal to the crank, is negative, while under conditions of optimal pedalling it should be always positive. The negative value of the force is explained by the fact that the athlete does not apply a force of pulling during the corresponding phase, so the foot and the leg analyzed are "carried on" by the other limb, which, in turns, is in the pushing phase. Besides, the negative contribution on the cycle results to be smaller with the saddle in optimal position in comparison to the other tests and this means that in this condition during the phase of recovery also if the athlete is not optimizing the use of muscles, he has to carry on less weight with the active limb. In this trial there was no feedback so the athlete was free to choose his strategy of pedalling, obtaining the illustrated trends and values for the efficiency indexes.

Similar results have been obtained for the other examined subjects in the same conditions of executing the tests.

Subject 1 60 RPM	IErev	IEpush	IEpull	IEist
Step 1	45 %	70 %	-29 %	12 %
Step 2	32 %	67 %	-52 %	0 %
Step 3	32 %	66 %	-47 %	1 %

Chart 5.1: Efficiency indexes for the subject 1 @low RPM.

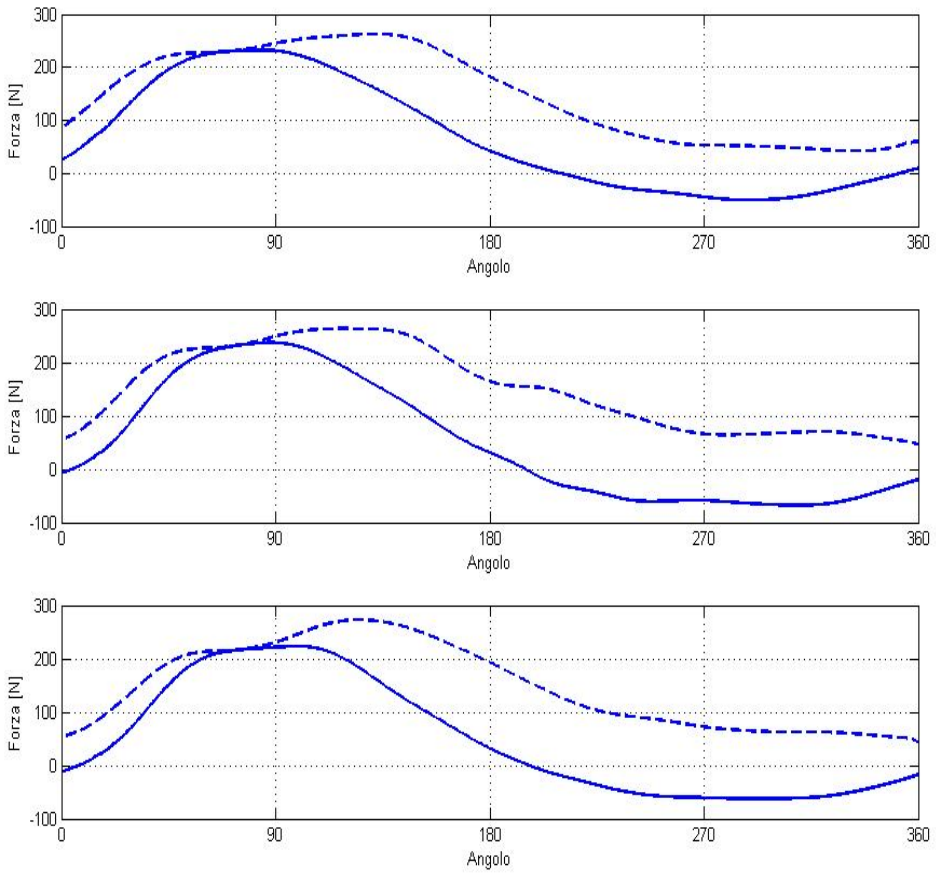

Figure 5.6*: Time trend of the mean force in the cycle @low RPM: Ft (solid line) and Ftot (dash line). From the top: optimal, high and behind and low and advanced saddle positions.*

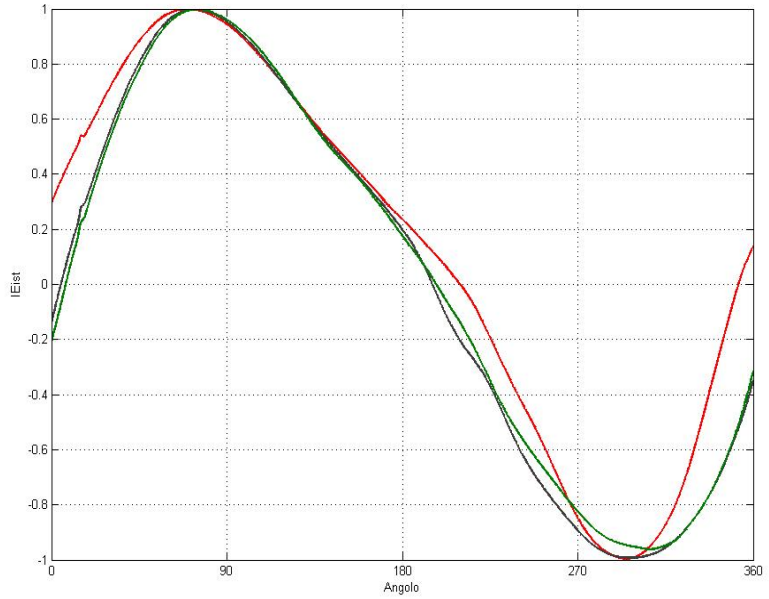

Figure 5.7*: Time trend of the* IEist *for the 3 saddle position @low RPM: optimal (red line), high and behind (grey line) and low and advanced (green line) positions.*

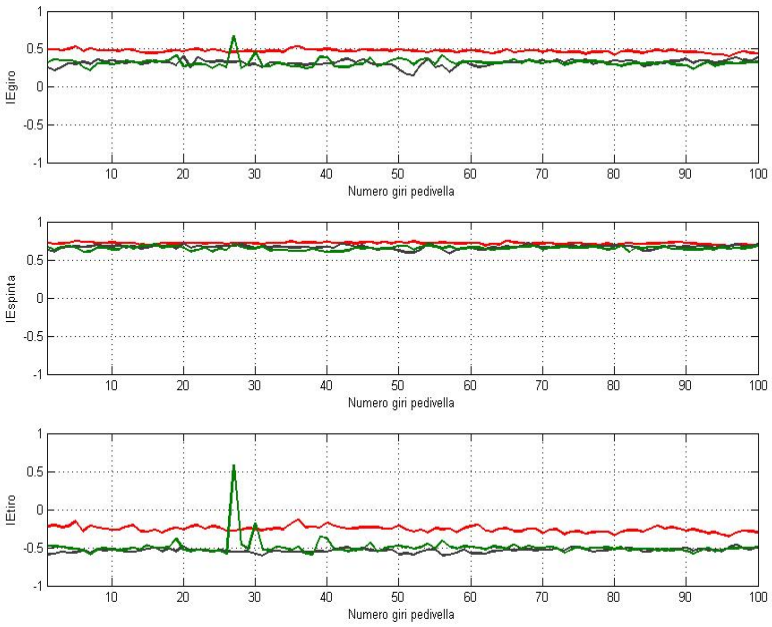

Figure 5.8: time trends for the 3 index Irev, Ipush and Ipull for the 3 saddle position @low RPM: optimal (red line), high and behind (grey) and low and advanced (green) positions.

Increasing the frequency, there is a general decrease of the indexes. This is due to the difficulty of optimizing the muscular activation to maximize the effective force. The increased execution velocity is associated to the difficulty of coordinating the muscular activations, that are necessary to flex the foot to optimize the force transmitted to the crank. Therefore in these conditions it has been observed that each subject adopts a specific strategy, by choosing one of the two phases that results to be the pushing in natural way. So the index describing the efficiency in pulling presents lower values as compared to the trial at low frequency.

This can also be highlighted by looking at the average on the cycle trends of the effective and total forces. In the firsts 90° degrees of the cycle the two time series are almost overlapped. This means that the total force is almost whole transferred along the direction of the effective forces whit values of the indexes near to the unity, , while in the subsequent part of the cycle are different, outlining an increase of the dissipated force.

Subject 1 90 RPM	IErev	IEpush	IEpull	IEist
Step 1	32 %	67 %	-37 %	16 %
Step 2	18 %	62 %	-56 %	-2 %
Step 3	13 %	57 %	-55 %	-1 %

Chart 5.2: Efficiency indexes for the subject 1 @high RPM.

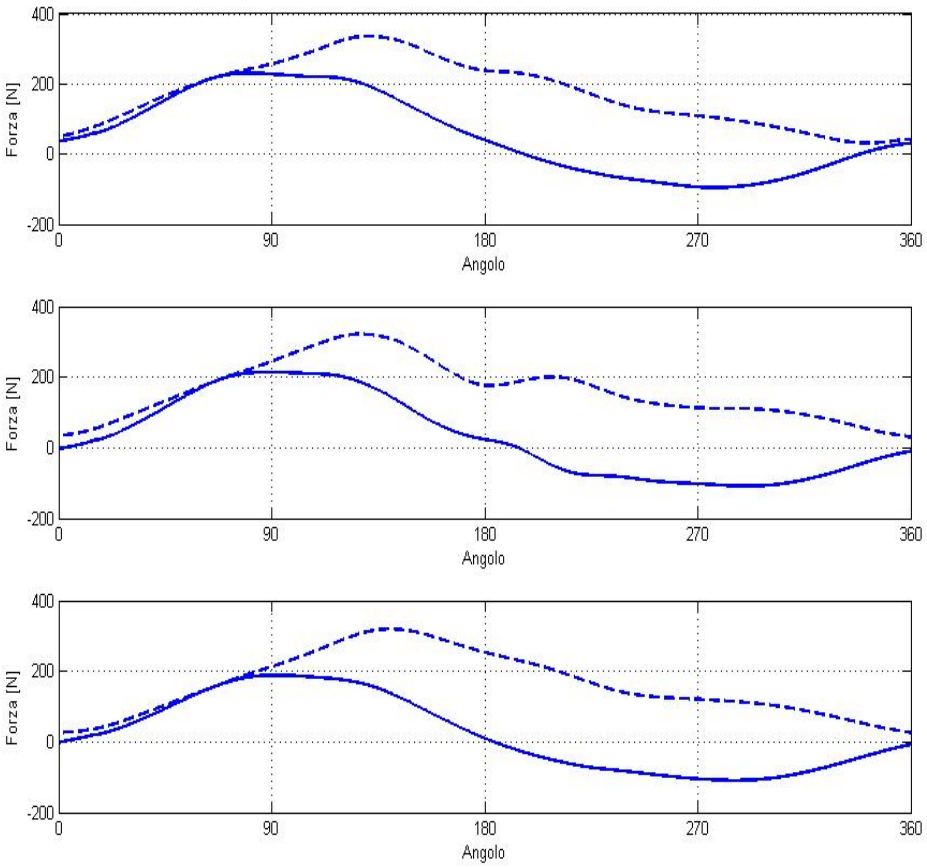

Figure 5.9: Time trend of the mean force in the cycle @high RPM: Ft (solid line) and Ftot (dash line). From the top: optimal, high and behind and low and advanced saddle positions.

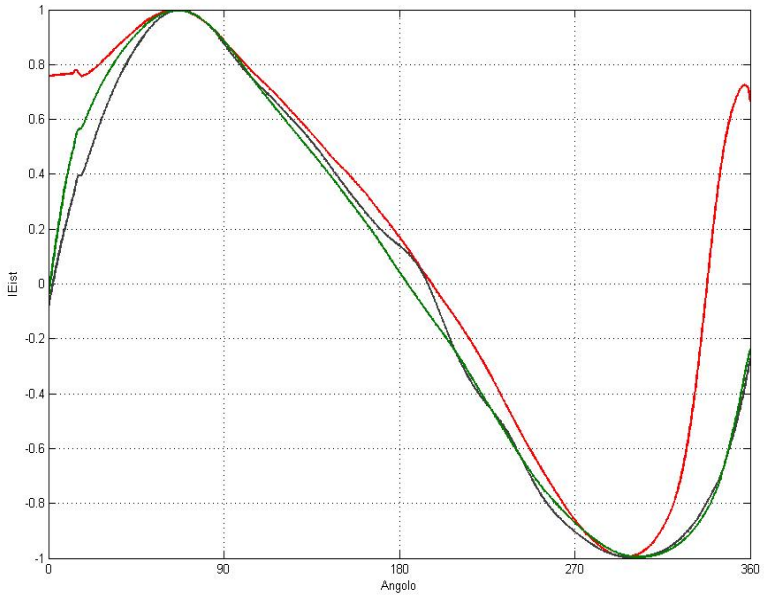

Figure 5.10: Time trend of the IEist for the 3 saddle position @high RPM: optimal (red line), high and behind (grey line) and low and advanced (green line) positions.

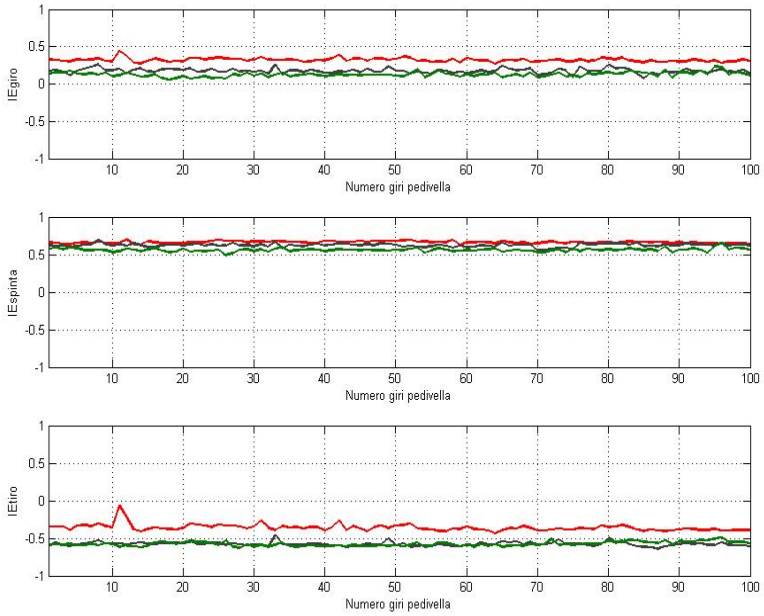

Figure 5.11: *time trends for the 3 index* Irev, Ipush *and* Ipull *for the 3 saddle position @high RPM: optimal (red line), high and behind (grey) and low and advanced (green) positions.*

In the following figures the results for a test at low frequency of pedalling (Chart 5.3, Figure 5.12, Figure 5.13, Figure 5.14) and a test at high frequency of pedalling (Chart 5.4, Figure 5.15, Figure 5.16, Figure 5.17) are illustrated. In this condition, though, the subject has been provided with a bio-feedback regarding his way of pedalling. In this test the athlete has tried to improve the performance in the phase of pulling on the basis of the values of the indexes. In fact after a training it is possible to understand how to make the indexes increasing, so the indexes monitor could be a guide to learn how to pedal in the way that the efficiency is the highest possible.

Also in this case there are some differences in the tests between low and high frequency of pedalling. Again, there is a general decreasing of the indexes' values related with the increasing the frequency. The pulling phase is neglected, as it can be observed from the efficiency indexes values, respect to pushing one, that in some cases results more accurate than at low RPM.

Subject 4 60 RPM	IErev	IEpush	IEpull	IEist
Step 1	59 %	59 %	57 %	57 %
Step 2	44 %	54 %	10 %	42 %
Step 3	45 %	55 %	11 %	39 %

Chart 5.3: Efficiency indexes for the subject 4 @low RPM.

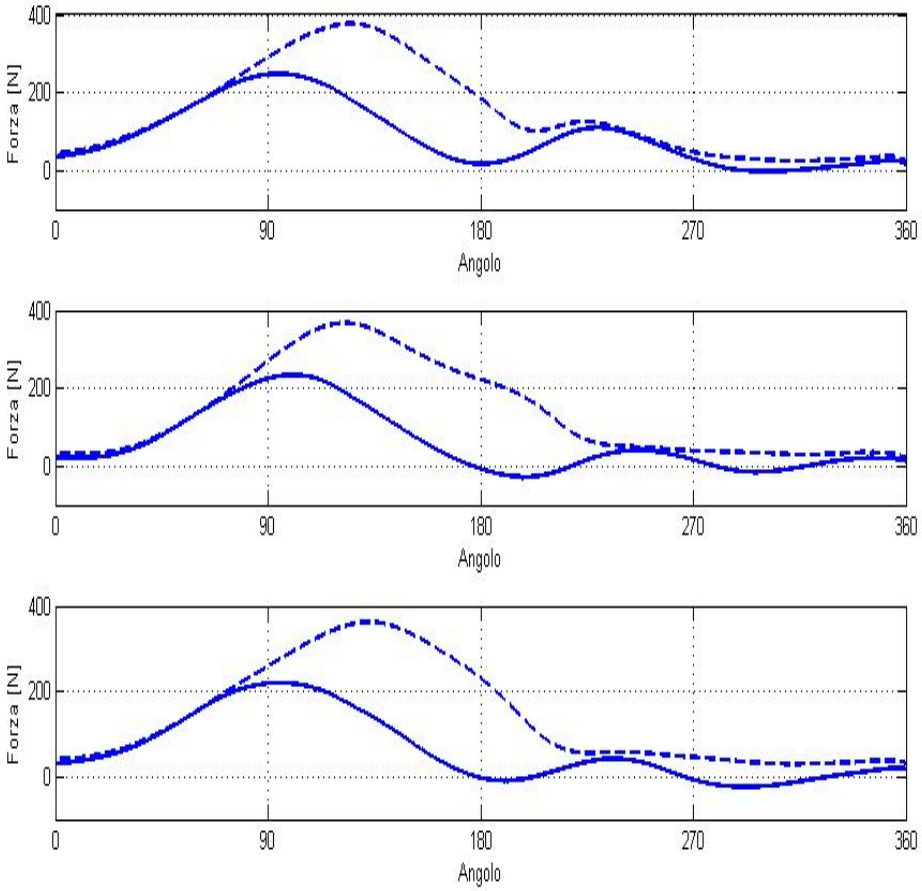

Figure 5.12: Time trend of the mean force in the cycle @low RPM: Ft (solid line) and Ftot (dash line). From the top: optimal, high and behind and low and advanced saddle positions.

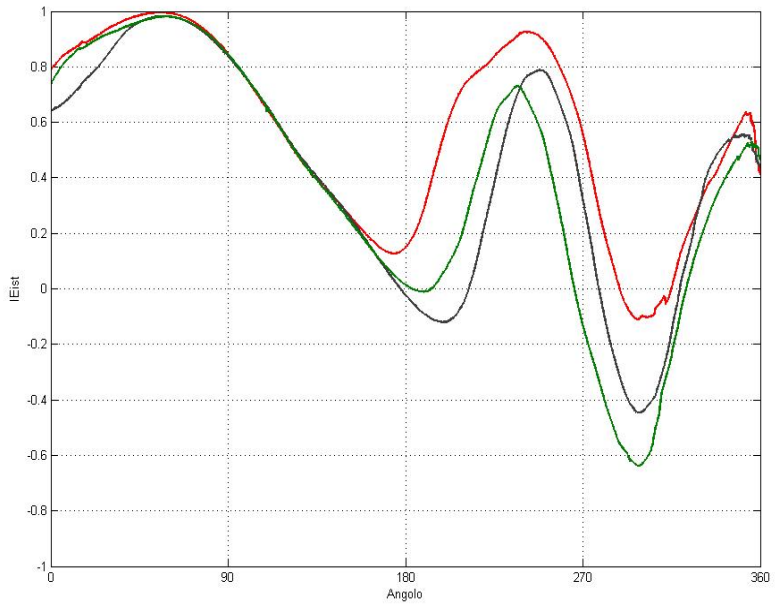

Figure 5.13: Time trend of the IEist for the 3 saddle position @low RPM: optimal (red line), high and behind (grey line) and low and advanced (green line) positions

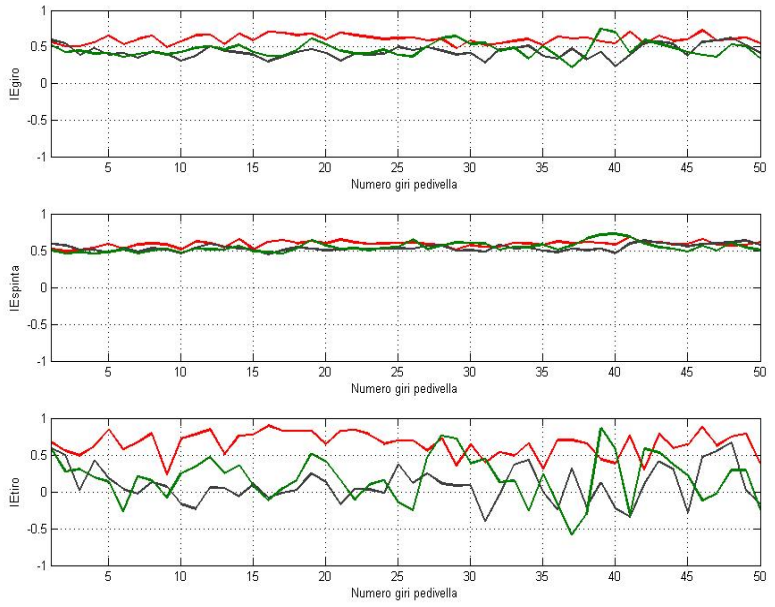

Figure 5.14: *time trends for the 3 index* Irev, Ipush *and* Ipull *for the 3 saddle position @low RPM: optimal (red line), high and behind (grey) and low and advanced (green) positions.*

Subject 4 80 RPM	IErev	IEpush	IEpull	IEist
Step 1	21 %	57 %	-44 %	12 %
Step 2	16 %	63 %	-60 %	-1 %
Step 3	14 %	59 %	-59 %	-2 %

Chart 5.4: Efficiency indexes for the subject 4 @high RPM.

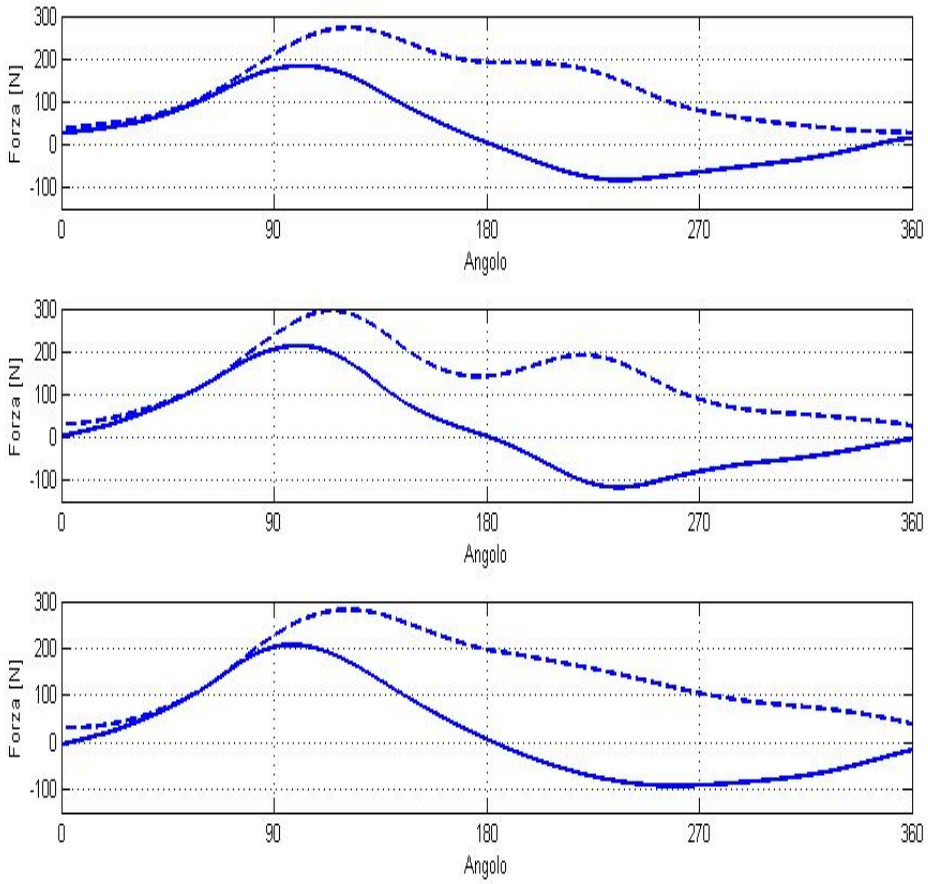

Figure 5.15: Time trend of the mean force in the cycle @high RPM: Ft (solid line) and Ftot (dash line). From the top: optimal, high and behind and low and advanced saddle positions.

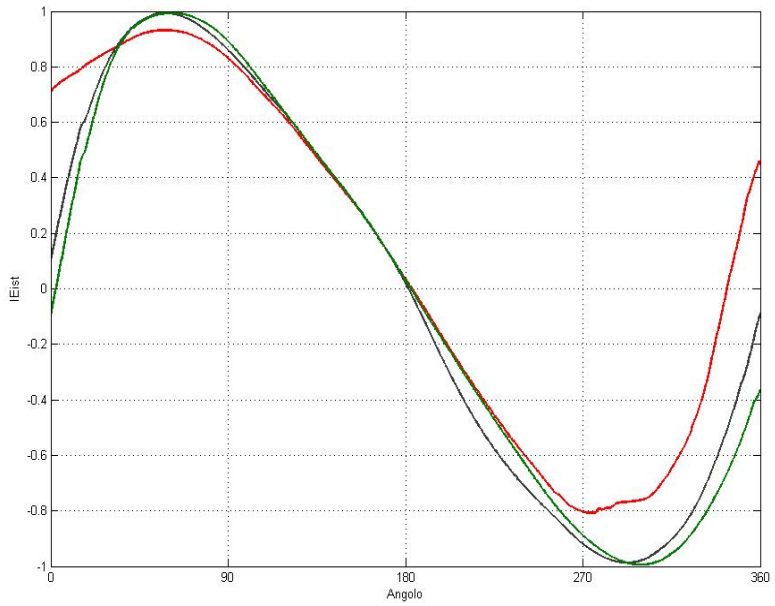

Figure 5.16: Time Time trend of the IEist for the 3 saddle position @high RPM: optimal (red line), high and behind (grey line) and low and advanced (green line) positions

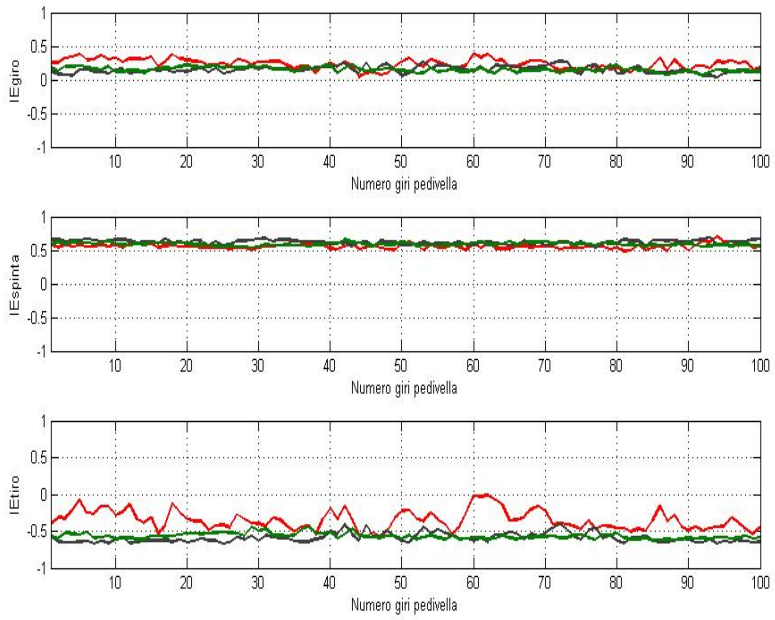

Figure 5.17: *time trends for the 3 index* Irev, Ipush *and* Ipull *for the 3 saddle position @high RPM: optimal (red line), high and behind (grey) and low and advanced (green) positions.*

In conclusion, moving the athlete from the optimal position causes a decrease of the efficiency indexes, which can be thus considered as performance descriptors. Changing the position determines changes to the kinematic chain of the lower limbs, including the end effector, i.e. the foot, which transmits the force to the pedal. If the foot is in a sub-optimal position, a higher dissipation of the exerted power occurs, and this leads also to greater difficulties in pulling the pedals in the recovery phase.

5.7 Conclusions

From the preliminary results obtained with the real-time monitor realized in LabVIEW it is possible to conclude that the real-time dynamic analysis of pedalling allows both to evaluate the performance during the test and to improve it individualizing the causes of the sub-optimal efficiency. Such causes can be associated with two different factors.

I. The first one resides in the wrong movement of plantarflexion-dorsiflexion at the ankle level during the turn of the crank. The developed monitor allows to underline and to quantify such wrong movements by means of the analysis of the differences between the two curves that represent the resultant force Ftot applied on the pedals and the effective force Ft applied in perpendicular direction to the crank. A correct movement would correspond to force vector as close to orthogonal to crank as possible, with the aim of minimizing the component parallel to the crank, which will be dissipated. In this way Ft and Ftot would have the tendency to match. This event would correspond to maximum efficiency in the transmission from the foot to the crank.

II. The second one consists of passively execution of the phase of pull. The monitor underlines this error in pedalling through the determination of the effective force, which, in the case of passive pulling, exhibits negative values. To prevent these condition to occur, both a correct movement of plantarflexion-dorsiflexion at the ankle level and the application of a force directed in the verse of pedalling are needed, so that the foot in this phase at least does not impede the push phase execution.

From the analysis of the preliminary results it has been possible to draw some interesting conclusions:

- The optimal position is indeed the one corresponding to the maximum value of the efficiency index, both for the instantaneous values, and for the values averaged over the entire revolution, the push phase, and the pull phase; by lowering or lifting the saddle in comparison to the optimal position, a diminution of all the four indexes used for describing the test occurs.

- In the tests in which the pull phase is entirely passive, the value of the index that characterizes the turn falls down, even if the performance is high during the phase of push. In this case the foot in phase of recovery is “carried” from the other one that is performing the push phase on the other pedal. In this condition, a negative value of the efficiency index in the phase of pulling is obtained, since the foot is exerting a force that results in the opposite verse; vice versa in the tests in which the pull phase is

active, the value of the efficiency index, in turns, increases.

- The indexes averaged over the complete revolution IErev, the pushing phase IEpush, and the pulling phase IEpulls are good indicators of the pedalling strategy that the athlete is executing and these gives information about the recovery phase, giving information on either a pulling strategy or a passive one.
- Providing the athlete with the real time feedback helps the athlete changing the pedalling strategy. Moreover, the use of the indexes is a useful way to determine the optimal body posture on the saddle, which, in turns, will improve the performance.

Through the real time evaluation of the efficiency indexes it is possible to think about the realization of an innovative device that can provide both athletes and trainers information on the gesture, so that opportune changes to optimize the movement of pedalling can be done, with consequent increase of the performances and delay of the muscular fatigue.

The obtained preliminary results encourage continuing the experiments on this field in order to give a statistic validation to the method.

The developed device, since the instrumented pedal can be fitted on any kind of bicycle, can be used during the execution of tests in the laboratory with athletes that use their own bicycles. Moreover, by using a wireless data transmitter system, the prototype can be used for tests on tracks or on the road.

Another future application is the integration of the information obtained with this device with dynamic, metabolic and postural information to be able to optimize the gesture relating it to the useful force and the metabolic consumptions. To this purpose, it will result useful to undertake an analysis with the contemporary use of the instrumented pedal, for the dynamic data, the surface electromyography, for the study of the muscular synergies, and a system that analyze metabolic parameters with the purpose of simultaneously obtaining the efficiency of the gesture, the evolution of the muscular fatigue condition and the variations in the strategies of muscular activation, both with the progress of the exercise and with the variation of the position on the saddle.

References

[1] Bonsignore D.,Gallozzi C.,Scaramuzza V.,"Il tiro con l'arco",Medicina Dello Sport, 56 n.1, 2003.

[2] Di Prampero P.E., Antonutto G., Capelli C., Mognoni P., "Costo energetico e fattori limitanti le massime prestazioni nel ciclismo", in Bioingegneria della postura e del movimento, 571-591, Patron 2003.

[3] Gallozzi C., Rodano R., Sacchi M., Squadrone R., "La sella al posto giusto", La Bicicletta, n. 222, pp. 81-86, 2002.

[4] Di Prampero P.E., "Cycling on Earth, in space, on the Moon", Eur J Appl Physiol; 82: 345 – 360, 2000.

[5] Di Prampero P.E., "The energy cost of Human locomotion on land and in water", Int. Journal of Sports Medicine; 7: 55 – 72, 1986.

[6]Soden P.D., Adeyefa B.A., "Force applied to a bicycle during normal cycling", J.biomechanics Vol.12 pp.527-541, 1979.

[7] Hull M.L., Davis R.R., "Measurement of pedal loading in bicycling: I. Instrumentation, II. Analysis and results", J. Biomechanics, 14n°12: 843-872, 1981.

[8] Boyd T., Hull M.L., Wootten D., "An improved accuracy six-load component pedal dynamometer for cycling", J. Biomechanics, 29: 1105-1110, 1996.

[9] Stone C., Hull L., "The effect of rider weight on rider-induced loads during common cycling situations" J.biomechanics Vol.28 No.4 pp.363-375, 1995.

[10] Hull M.L. et al.,"A method for biomechanical analysis of bicycle pedalling", J.Biomechanics Vol.18 pp.631-644, 1985.

[11] Newmiller et al., "A mechanically decoupled two force component bicycle pedal dynamometer", J.Biomechanics Vol.21 pp.375-386, 1988.

[12] Sanderson D. J., Black A., "The effect of prolonged cycling on pedal forces", J. Sport Sciences, 21: 191-199, 2003.

[13] Lucchetta M., Petrone N., "Progetto di un pedale dinamometrico per l'acquisizione di carichi su biciclette fuoristrada", XXVII° convegno nazionale AIAS, Perugia, 1998.

[14] Orsingher I. et al., "Acquisizione su strada dei carichi su bicicletta da corsa per la definizione di standard di prova a fatica", XXX Convegno Nazionale AIAS, Alghero 12-15, 2001.

[15] Petrone N., Milan G., Orsingher I., Sawacha Z., "Sviluppo di un sistema integrato per l'ottimizzazione della postura di pedalata", Associazione Italiana per l'Analisi delle Sollecitazioni (AIAS) XXXI Convegno Nazionale, Parma, 2002.

[16] Sanderson et al., "Use of augmented feedback for the modification of the pedalling mechanics of cyclist", Canadian journal of sports sciences Vol.15 pp.38-42, 1989.

[17] Sanderson et al., "The influence of cadence and power output on force application and in-shoe pressure distribuition during cycling by competitive and recreational cyclist" Journal of sports Sciences Vol.18 pp.173-181, 2000.

[18] V. Basmajian, C.J. De Luca, "*Muscles Alive*" Baltimore MD: 1985, Williams and Wilkins.

[19] S. Conforto, D. Bibbo, M. Schmid, T. D'Alessio, "Muscular Fatigue from Electromyographic Recordings: Real-Time Monitoring during Exercise Training", 3rd European Medical and Biological Engineering Conference IFMBE Proceedings Praha, Czech Republic 2005.

[20] T. D'Alessio, S. Conforto, "Extraction of the envelope from surface EMG signals: an adaptive procedure for dynamic protocols", IEEE Engineering in Med. and Biol. Magazine, vol. 6, pp. 55-61, 2001.

[21] S. Conforto, T. D'Alessio, "Real time monitoring of muscular fatigue from dynamic surface myoelectric signals using a complex covariance approach", Medical Engineering and Physics, vol. 21, 1999, pp. 225-234.

[22] S. Bouisset, F. Lestienne, B. Maton, "The stability of synergy in agonists during the execution of a simple voluntary movement, Electroence", Clin. Neurophysiol., vol. 42, 1977, pp. 543-551.

[23] C.J. De Luca, Z. Erim, “Common Drive in Motor Units of a Synergistic Muscle Pair”, The Journal of Neurophysiology, vol. 87, n. 4, 2002, pp. 2200-2204.
[24] P.Crenna, C.Frigo, J.Massion, A.Pedotti, “Forward and backward axial synergies in man”, Experimental Brain Research, vol. 65, n. 3, 1987, pp. 538-548.
[25] N. Yoshida, K. Domen, Y. Koike, M. Kawato, “A method for estimating torque-vector directions of shoulder muscles using surface EMGs”, Biological Cybernetics, vol. 86, n. 3, 2002, pp. 167-177.
[26] A.M. Sabatini, “Identification of neuromuscular synergies in natural upper-arm movements”, Biological Cybernetics, vol. 86, n. 4, 2002, pp. 253–262.
[27] J. Kutch, T.S. Buchanan, “Human elbow joint torque is linearly encoded in electromyographic signals from multiple muscles”, Neuroscience Letters, vol. 311, 2001, pp. 97–100.
[28] R. Holdefer, L. Miller, “Primary motor cortical neurons encode functional muscle synergies”, Experimental Brain Research, vol. 146, n. 2, 2002, pp. 233-243.
[29] J.P. Scholz, G. Schöner, “The uncontrolled manifold concept: identifying control variables for a functional task”, Experimental Brain Research, vol. 126, n. 3, 1999, pp. 289-306.
[30] B.I. Prilutsky, “Coordination of two- and one-joint muscles: Functional consequences and implications for motor control”, Motor Contr., vol. 4, 2000, pp. 1–44.
[31] Frigo C., Pavan E., “La stima di forze interne al sistema muscolo scheletrico”, in Bioingegneria della postura e del movimento, 257-277, Patron 2003.
[32] Glitsch U, Baumann W., “The three-dimensional determination of internal loads in the lower extremity”, J.Biomechanics, vol. 30, n. 11-12, 1997, pp. 1123-1131.
[33] P. de Leva, “Adjustament to Zatsiorsky-Seluyanov’s segment inertia parameters”, J.Biomechanics, vol. 29, n. 9, 1996, pp. 1223-1230.
[34] V. M. Zatsiorsky, V. N. Seluyanov, and L. G. Chugunova, “Methods of determining mass-inertial characteristics of human body segments,” in Contemporary Problems of Biomechanics, G. G. Chernyi and S. A. Regirer, Eds. /Boca Raton, FL: CRC, 1990, pp. 272–291.
[35] B.I. Prilutsky, R.J. Gregor, “Strategy of muscle coordination of two- and one-joint leg muscles in controlling an external force”, Motor Contr., vol. 1, 1997, pp. 92–116.
[36] R. D. Crowninshield and R. A. Brand, “A physiologically based criterion of muscle force prediction in locomotion”, J. Biomechanics, vol. 14., 1981, pp. 793–801.
[37] J. Dul, G. E. Johnson, R. Shiavi, and M. A. Townsend, “Muscular synergism— II. A minimum-fatigue criterion for load sharing between synergistic muscles”, J. Biomechanics, 1984, vol. 17, pp. 675–684.
[38] D. Bibbo, M. Schmid, S. Conforto, “A wireless instrumented pedal to measure force during cycling”, ISEK Conference 2006.
[39] T. D’Alessio, “Some results on the optimization of a digital processor for surface EMG signals” Electromyography and Clinical Neurophysiology, vol. 24, 1984, pp. 625-643.
[40] T. D’Alessio, “Analysis of a digital EMG signal processor in dynamic conditions”, IEEE Transactions on Biomedical Engineering, vol. BME-32, n. 1, 1985, pp. 78-82.
[41] Vollestad N.K. (1997): “Measurement of human muscle fatigue”, Journal of Neuroscience Methods, 74, pp. 219-227.
[42] Arendt-Nielsen L., Mills K.R. (1988): “Muscle fibre conduction velocity, mean power frequency, mean EMG voltage and force during submaximal fatiguing contractions and human quadriceps”, Eur. J. Appl. Physiol., 58, pp. 20-25.
[43] Bigland-Ritchie B., Cafarelli E., Vollestad, N.K. (1986): “Fatigue of submaximal static contractions”, Acta Physiol. Scand. (Suppl.), 128, pp. 137-148.
[44] De Vries H.A. (1968): “Efficiency of electrical activity as a physiological measure of the functional state of muscle tissue”, Am. J. Phys. Med., 47, pp. 10-21.
[45] Maton B. (1981): “Human motor unit activity during the onset of muscle fatigue in submaximal isometric isotonic contractions”, Eur. J. Appl. Physiol., 46, pp. 271-277.
[46] Petrofsky J.S., Glaser R.M., Philips C.A., Lind A.R., Williams C. (1982): “Evaluation of the amplitude and frequency components of the surface EMG as an index of muscle fatigue”, Ergonomics, 25, pp. 213-223.
[47]Biedermann J., Shanks G.L., Forrest W., Inglis V. (1991): “Power spectrum analysis of myoelectric activity: discriminators in the differential assessment of patients with chronic low back pain”, Spine, 16, pp. 1179-1184.

[48] De Luca C.J. (1993): "Use of the surface EMG signal for performance evaluation of back muscle", Muscle and Nerve, 16, 210-216.
[49] Klein A.M., Snyder-Macler L., Roy S.H., De Luca C.J. (1991): "Comparison of spinal mobility and isometric trunk extensor forces with electromyographic spectral analysis in identifying low back pain", *Physical Therapy,* 71*,* pp. 445-454.
[50] KNAFLITZ M., MERLETTI R., DE LUCA C.J. (1990): "Inference of motor unit recruitment order in voluntary and electrically elicited contractions", *J. Appl. Physiol.,* 68, pp. 1657-1667.
[51] KNAFLITZ M., BALESTRA G., ANGELINI C., CATALDINI M. (1996): "Muscle fatigue evaluation in the follow-up of children affected by Duchenne muscular dystrophy", *Basic and Applied Myology,* 6*,* pp. 115-123.
[52] LINSSEN W.H.J.P., STEGEMAN D.F., JOOSTEN E.M.G., BINKHORST R.A., MERKS M.J.H., LAAK H.J., NOTERMANS S.L.H. (1991): "Fatigue in type I fiber predominance: a muscle force and surface EMG study on the realtive role of type I and type II muscle fibers", *Muscle and Nerve,* 14, pp. 829-837.
[53] MANNION A.F., DOLAN P. (1994): "Electromyographic median frequency changes during isometric contraction of the back extensors to fatigue", *Spine,* 19*,* pp. 1223-1229.
[54] PRIEZ A., DUCHENNE J., GOUBEL F. (1992): "Duchenne muscular dystrophy quantification: a multivariate analysis of surface EMG", *Med & Biol & Eng & Comput,* 30*,* pp. 283-291.
[55] LUTTMANN A., JÄGER M., SÖKELAND J., LAURIG W. (1996): "Electromyographical study on surgeons in urology, Part II: Determination of muscular fatigue", *Ergonomics,* 39, pp. 298-313.
[56] LUTTMANN A., JÄGER M., LAURIG W. (2000): "Electromyographical indication of muscular fatigue in occupational field studies", *Int. J. Industr. Ergonomics,* 25, pp. 645-660.
[57] HÄGG G.M., LUTTMANN A., JÄGER M. (2000): "Methodologies for evaluating electromyographic field data in ergonomics", *J. Electromyogr. Kinesiol.,* 10, pp. 301-312.
[58] HORITA T., ISHIKO T. (1987): "Relationships between muscle lactate accumulation and surface EMG activities during isokinetic contractions in man", *Eur. J. Appl. Physiol.,* 56*,* pp. 18–23.
[59] ELERT J., GERDLE V. (1989): "The relationship between contraction and relaxation during fatiguing isokinetic shoulder flexions: An electromyographic study", *Eur. J. Appl. Physiol.,* 59*,* pp. 303–309.
[60] Potvin J.R., Bent L.R. (1997): "A validation of techniques using surface EMG signals from dynamic contractions to quantify muscle fatigue during repetitive tasks", J. Electromyogr. Kinesiol., 7(2), pp. 131–139.
[61]Komi, P., & Hakkinen, K. (1988). "Strength and power". In A. Drix, H. Knuttgen, & K. Tittel (Eds.), Encyclopaedia of sports medicine: Vol. 1. The Olympic book of sports medicine (pp. 181-193). Boston: Blackwell Scientific.
[62] Rahmani, A., Viale, F., Dalleau, G., & Lacour, J-R. (2001) "Force/velocity and power/velocity realtionships in squat exercise". Eur. J. Appl. Physiol. 84: 227-32.
[63]Macaluso, A., Young, A., Gibb, K.S., Rowe, D.A., & De Vito G. (2003). "Cycling as a novel approach to resistance training increases muscle strength, power, and selected functional abilities in healthy older women". J. Appl. Physiol. 95: 2544-53.
[64]Sargeant, A.J., Hoinville, E., & Young, A. (1981). "Maximum leg force power output during short-term dynamic exercise". J. Appl. Physiol. 51: 1175-82..
[65]Franklin, K.L., Gordon, R.S., Baker, J.S., & Davies, B. (2005). "Mechanics of a rope-braked cycle ergometer flywheel and its use for physiological measurement". Res. Sports Med. 13: 331-44.
[66]Arsac, L.M., Belli, A., & Lacour, J.R. (1996). "Muscle function during brief maximal exercise: accurate measuments on a friction loaded cycle ergometer". Eur. J. Appl. Physiol. 74: 100-106.
[67] Duffy, C.R. (2006). "Optimal load for maximal power output during a 6 second all out cycling effort in older women". Annual symposium of the Royal Society of Edinburgh.
[68] Zameziati, K.; Mornieux, G.; Rouffet, D.; Belli, A. (2006). "Relationship between the increase of effectiveness indexes and the increase of muscular efficiency with cycling power". Eur J Appl Physiol; 96: 274 - 281.
[69] Sanderson, D.J.; Cavanagh, P.R. (1985). "An investigation of the effectiveness of force application in cycling" Medicine and Science in Sport and Exercise; 17: 222.

[70] Coyle, E.F.; Feltner, M.E.; Kautz, S.A.; Hamilton, M.T.; Montain, S.J.; Baylor, A.M.; Abraham, L.D.; Petrek, G.W. (1991). “Physiological and biomechanical factors associated with elite endurance cycling performance”. Med Sci Sports Exerc; 23: 93-107.
[71] Lafortune, M.A.; Cavanagh, P.R. (1983). “Effectiveness and efficiency during bicycle riding”. In: Matsui H, Kobayashi K (eds) Biomechanics VIIB: International Series on Sports Science 4B. Human Kinetics, Champaign, pp 928-936.
[72] Fagioli F., “L’analisi della pedalata”, La Bicicletta, ottobre 1999.
[73] Bontrager K., “The Myth of "KOPS": An Alternative Method of Bike Fit”, published online on http://www.sheldonbrown.com/kops.html